Dipoles, conjugation and molecular electronics

Kovalchuk, Andrii

Dipoles, Conjugation and Molecular Electronics

Andrii Kovalchuk

Dipoles, Conjugation and Molecular Electronics

Andrii Kovalchuk
University of Groningen, Netherlands

ISBN: 978-94-034-0754-8 (printed)
978-94-034-0753-1 (electronic)

This project was carried out in the research group Chemistry of (Bio) Molecular Materials and Devices which is part of Stratingh Institute for Chemistry and Zernike Institute for Advanced Materials, University of Groningen, The Netherlands.
This work was funded by European Research Council, ERC Starting Grant 335473 (MOLECSYNCON).

Printed by: GVO drukkers & vormgevers B.V

Front & Back: The cover art is an artistic representation of the Fermi level and the subsequent Fermi level shift. Design by Xinkai Qiu. Original image courtesy flora-silve.deviantart.com.

An electronic version of this dissertation is available at
http://www.rug.nl/research/portal.

university of groningen / faculty of science and engineering

university of groningen

Dipoles, Conjugation and Molecular Electronics

PhD Thesis

to obtain the degree of PhD at the
University of Groningen
on the authority of the
Rector Magnificus Prof. E. Sterken
and in accordance with
the decision by the College of Deans.

This thesis will be defended in public on

Friday 29 June 2018 at 12.45 hours

by

Andrii Kovalchuk

born on 3 January 1990
in Dnieprodzerzhinsk, Oekraïne

Supervisors

Prof. R.C. Chiechi
Prof. J.C. Hummelen

Assessment Committee

Prof. F.C. Grozema
Prof. S.S. Faraji
Prof. M.A. Stöhr

Contents

1 Introduction **1**
- 1.1 The field of Molecular Electronics . . . 2
- 1.2 Large-area molecular junctions and SAMs . . . 3
- 1.3 Eutectic Ga-In alloy as the top electrode . . . 5
- 1.4 Mechanism of charge transport . . . 8
- 1.5 Thesis outline . . . 9
- Bibliography . . . 10

2 Synthetic control over transition voltages **15**
- 2.1 Introduction . . . 16
- 2.2 Results and discussion . . . 17
  - 2.2.1 J/V Measurements . . . 17
  - 2.2.2 Transition Voltage Measurements . . . 19
  - 2.2.3 Level Alignment . . . 20
  - 2.2.4 DFT Calculations . . . 20
  - 2.2.5 Trends in Transition Voltages . . . 23
- 2.3 Conclusions . . . 24
- 2.4 Experimental details . . . 25
- Bibliography . . . 27

3 Dipole-induced asymmetric conduction **33**
- 3.1 Introduction . . . 34
- 3.2 Results and discussion . . . 34
- 3.3 Conclusions . . . 40
- 3.4 Experimental details . . . 41
- Bibliography . . . 42

4 In-place switching of rectification **47**
- 4.1 Introduction . . . 48
- 4.2 Results and discussion . . . 48
- 4.3 Conclusions . . . 54
- 4.4 Methods . . . 55
- Bibliography . . . 57

5 Surprising substituted oligo(*p*-phenylene ethynylene)s **61**
- 5.1 Introduction . . . 62
- 5.2 Results and discussion . . . 62
- 5.3 Conclusions . . . 67
- 5.4 Synthesis . . . 67
- Bibliography . . . 73

Summary **75**

Nederlandse Samenvatting **77**

Acknowledgements **79**

Curriculum Vitæ **81**

1

INTRODUCTION

1

1.1. THE FIELD OF MOLECULAR ELECTRONICS

The invention of the transistor has revolutionized the world like nothing else laying foundation to the information age. What used to fill a room is now a 10-nm circuit element. The device traveled the road of 6 orders of magnitude in size and does not show the signs of slowing down. However, back in the 1950s some researchers were skeptical about the miniaturization of a transistor. Thus, people were looking at different ways of scaling down circuits. The concept of molecular engineering, introduced by von Hippel,[1] has led to the first notion of "molecular electronics". If a single molecule can play a role of a *p*-*n* junction, a diode, or even a logic element, then all such elements will be inherently at the molecular scale. Assuming we could effectively wire the molecules, the vision of a new molecular computer was born. Pioneering work was done by Mahn and Kuhn in 1971, who measured electron charge transport through a monolayer of fatty acid salts.[2] This was the first experimental measurement of the current through a one-molecule thick layer. Later, in 1974, Aviram and Ratner proposed the structure of their famous rectifier—a hypothetical molecule that could act as a diode inducing asymmetric current-voltage output.[3] These two works inspired by the idea of molecular computing laid the foundation of the field of Molecular Electronics.

Nowadays, 40 years later, the cutting edge Si-based technology aims at sub-10-nm feature size, but their molecular counterparts are nowhere to be found. At this point it is clear that the vision of molecular computing was too ambitious. However, the journey was not all in vain, as many discoveries were made and many tools were developed along the way. One of the most eye-catching achievements was the ability to measure electron charge transport through a single molecule. By means of scanning tunneling microscope (STM) break-junctions or mechanically-controllable break-junctions (MCBJ) a single molecule can be trapped between two macroscopic metal electrodes. This spectroscopic approach enables the acquisition of fundamental insight into electron transport through organic molecules. However, integration of single-molecule junctions into a device architecture is an almost impossible task, due to stability and reproducibility as the major issues. An approach that circumvents most of these problems and is already a basis for existing technology ("musical molecules" by McReery *et al.*[4]) is the large-area junction technique. This approach is based on covering large areas of an electrode with a molecular layer via chemical modification or by means of self-assembly. The latter is more popular, as it allows the formation of well-defined self-assembled monolayers (SAM) of molecules of interest. Once the top electrode is placed on top of the molecular layer a molecular junction is formed.

Molecular Electronics is now a dynamic, highly interdisciplinary field where theoretical physicists and quantum chemists work on the ways to describe charge transport through molecules, organic chemists design, synthesize and measure various molecules and surface scientists, applied physicists and engineers develop measurement tools and device architectures. The field has redefined itself; no-one claims to be building molecular computers anymore. Yet, the acquired knowledge suggests that molecules are capable of performing many specific functions that can be complementary to or even outperform classical Si-based technology.

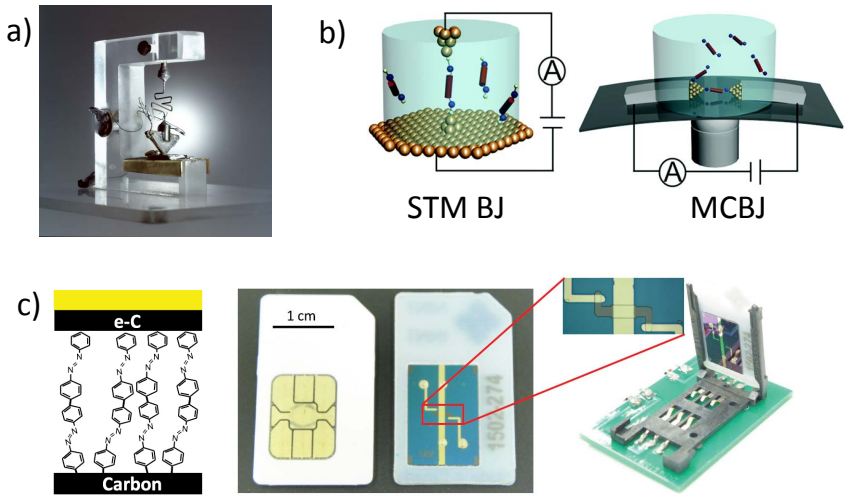

Figure 1.1 a) The first transistor ever assembled, invented in Bell Labs in 1947. **b)** Two common ways of making a single-molecule junction: STM break-junction and mechanically controllable break-junction. [5] - Reproduced by permission of the PCCP Owner Societies. **c)** A "musical molecules" large-area molecular junction and the eventual amplification device by McReery *et al.*. Reprinted with permission from reference [4]. Copyright 2016 IOP Publishing Ltd.

1.2. LARGE-AREA MOLECULAR JUNCTIONS AND SAMS

Wiring molecules to the macro world is an inherently difficult task. The first possible approach that one might think of is to develop electrodes with dimensions small enough so that single molecules can be attached to them. However, state-of-the-art technology does not allow the reproducible formation of atomically sized junctions with high precision and structural definition. One way to get around these drawbacks is to utilize the break-junction technique.[6–8] If an atomically sharp metal electrode comes in contact with another metal electrode, a single atom bridge is formed. When the electrodes are pulled apart and the metal constriction is broken the resulting gap can be populated with molecules either from a solution or directly from the surface of one of the electrodes. To determine whether the molecule is spanning the gap between two electrodes a current vs electrode displacement curve is recorded. Constant value of current (a plateau) before the circuit is broken defines the formation of a single-molecule junction. The bias is then swept with a molecule trapped between the two electrodes resulting in a current-voltage (I/V) characteristic. Because of the transient nature of this method, every other junction is different from the previous one both in the atomic details and the molecular binding geometry. In order to draw meaningful conclusions big sets of data have to be statistically analyzed and the binding geometry of the molecule has to be approximated. This design can be achieved by an ordinary scanning tunneling microscope or a specifically designed MCBJ setup. The break-junction technique provides fundamental information about charge transport properties through single molecules. Yet, in this form it is clearly inapplicable toward any device architecture. Thus, in this theses we will refer to these

methods as single-molecule spectroscopies.

In order to measure molecular charge transport a molecule does not necessarily need to be isolated. All that is required is to separate the two conducting electrodes with a layer that is one-molecule thick. In the first paper of Molecular Electronics Mahn and Kuhn used Langmuir-Blodgett films as molecular layers. Here, self-assembly does the work of defining the smallest dimension of the resulting junction. This approach was developed further to suit the requirement of the field—SAMs can be grown directly on metal surfaces. This fact was discovered in the early 1980-s by Nuzzo and Allara[9] and later popularized by Whitesides[10] and Chidsey[11]. When a metal surface is exposed to a solution of alkanethiols a monomolecular, ordered film is spontaneously formed in minutes. The resulting structure represents a one-molecule thick SAM, which can cover macroscopic areas of the metal substrate. SAMs are pseudo two-dimensional structures with huge aspect ratio (mm^2 area and nm thickness). Since the monolayer is formed directly on top of the conducting metal substrate, one requires simply to put the second electrode on top to form a molecular junction where the distance between electrodes is defined by the thickness of the monolayer (length of the molecule). These junctions are usually referred to as large-area junctions and they rely on self-assembly to direct the formation of the molecular junction.

The driving force for self-assembly of alkanethiols is the formation of a strong S–Au bond, but Au can be substituted with other coinage metals, like Ag. Similarly, a different anchoring group can be used to bind to the substrate and SAMs can tolerate a wide variety of head groups. These flexibilities in the molecular design allow chemists to change the molecular structure while retaining the ability to form SAMs. Thus, a great variety of molecules can be modified to form a SAM—from simple aliphatic chains to substituted heteroaromatic compounds. Even very bulky groups (*e.g.*, a C_{60} buckyball) can pack into a SAM with the help of the mixed monolayer approach.[12] SAMs are invaluable for Molecular Electronics also because their structure and properties can be studied in great detail by a variety of surface-analytical techniques. A simple contact angle measurement provides information about the wettability of the surface and can be used to asses the quality of the SAM. Ellipsometry is widely used to determine the thickness of the SAM. These simple and quick techniques provide good initial characterization. More detailed information on the structure and packing of the molecules in the SAM is obtained through a number of surface spectroscopic techniques. The energy of the electrons in the valence band of the analyte can be measured by exciting them into vacuum with ultraviolet light and subsequently measuring their excess energy (ultraviolet photoelectron spectroscopy, UPS). Thus, UPS provides information about the position of energy levels of the SAM. If X-rays are used instead of UV-light, deep inner-shell electrons of atoms are exited and their binding energy is measured (X-ray photoelectron spectroscopy, XPS). XPS is a powerful tool for characterization of SAMs, as it provides information about the electronic state of each element. With enough resolution different oxidation states can be distinguished, which can reveal the intricacies of the structural arrangement of the molecules in the SAM. Lastly, low-temperature STM measurements are used to derive the order of packing of molecules in the monolayer. Thus, self-assembly provides a simple way to form well-defined ordered molecular monolayers.

Self-assembled monolayers are dynamic systems that are able to self-repair due to

the reversible nature of the bonding to metals. However, there can be many sources of defects in a monolayer, *e.g.*, defects at grain boundaries and step edges, vacancy islands, surface impurities, etc.[13] Some of them come directly from the properties of the metal surface and can be reduced by increasing its quality. Usually, the metal electrodes are fabricated by means of metal deposition techniques, which result in a rough surface (as-deposited films). Consequent annealing procedures can be employed to reduce the roughness. However, an ultra-smooth surface can be prepared according to the template stripping procedure.[14] An atomically smooth silicon wafer serves as a template for metal deposition and further mechanical template stripping (TS). Films that are formed by these techniques have lower root-mean-square roughness than as-deposited or annealed films. The metal surfaces, before being cleaved, are completely protected from contact with the ambient atmosphere. This protection allows metal surfaces intended to support SAMs to be prepared in large batch lots, stored, and then used as needed. Low surface roughness, high reproducibility and simplicity make TS procedure a perfect fabrication technique for the SAM-based molecular junctions.

1.3. EUTECTIC GA-IN ALLOY AS THE TOP ELECTRODE

Self-assembly provides a simple and reliable way to define the molecular dimension of the large-area junctions. The last step toward a complete metal/SAM/metal junction is attachment of a top electrode. Ideally, the top contact has to be conductive, conformal, non-damaging and have a well-defined interface. Traditional Si-based technology utilizes three main steps (imaging, deposition and etching) to fabricate integrated circuits in a layer by layer fashion. So, naturally, one way to attach a metal top electrode is to use metal vapor deposition. However, evaporating metals on top of a nm-thick organic monolayers is challenging. Hot atoms can easily penetrate and damage the film.[15] This problem can be partially solved by installing specific head groups that can interact with vapor deposited metal atoms and prevent penetration.[16] This complexity, however, limits the structural flexibility of molecular design. In addition, the larger the area of deposition, the bigger the probability of metal atoms penetrating through defects in the SAM. An elegant way to overcome the latter problem was developed in our group.[17] By utilizing a microtome one large-area junction can be sliced into a number of smaller ones, cutting around the short-circuited regions. Another promising approach was recently developed in the IBM laboratory in Switzerland. Lörtsher *et al.* used a protective layer of Au nanoparticles to prevent metal penetration while retaining a conductive contact to the SAMs.[18] This method, however, brings unwanted complexity and low reproducibility remains an issue. In general, the use of the metal evaporation techniques is desirable because of the already existing Si-based technology, scalability and potential for mass-production. Yet, many challenges are still to be overcome.

SAMs have proven to be the perfect candidates for defining molecular junctions of the resulting device. Thus, studying the charge transport properties of SAMs is of high relevance not only as a fundamental scientific inquiry, but also as a step toward a future technology. For this purpose a specific measurement technique is required. Close examination of the requirements for the ideal top contact concludes that liquid metal as the top electrode can suffice. Majda and Slowinski utilized Hg to establish electrical contact with SAMs.[19] Several junction geometries were developed, but essentially all of them

utilized a hanging Hg drop as a top electrode (Figure 1.2 f). Because of the high affinity of Hg towards amalgamation with other metals the drop has to be covered with a protective SAM. The resulting junction is Hg/SAM1//SAM2/M, where "/" stands for covalent interface and "//" stands for van der Waals interface. Although utilization of a protective SAM improves the yield of working junctions it does not solve all issues—it is still a slow and laborious technique. In addition, the presence of two SAMs inside of the molecular junction reduces the sensitivity of the measurement. Despite these drawbacks the hanging Hg drop was the main tool for addressing molecular junctions for almost a decade and provided important insight into the nature of molecular charge transport.[20–22]

In 2008 Chiechi *et al.* developed a technique that successfully eliminated most of the drawbacks of Hg junctions.[25] The key innovation was the utilization of eutectic alloy of Ga and In (EGaIn) instead of Hg. EGaIn (75% In and 25% Ga by weight, m.p.= 15.5 °C) is liquid at room temperature and in ambient conditions it is covered with a thin self-limiting skin of Ga_2O_3. This layer grants EGaIn the properties of a shear-thinning non-Newtonian fluid, *i.e.*, its viscosity decreases under shear stress, such that it can be molded into non-spherical shapes greatly reducing the electrical contact area down to the micro-meter scale (Figure 1.2 a-d). Smaller measurement areas are desired as they reduce the number of probed defects, which are invariably present in any SAM. EGaIn is commercially available, nontoxic, has low vapor pressure and can be applied with a pipette or syringe without high temperatures or vacuum. These properties grant EGaIn its main advantage over other methods—high throughput. Acquisition of big sets of data is crucial for subsequent statistical analysis, which enables more precise determination of the electrical properties of the SAM. The distinction of whether the SAM or the defects dominate electrical transport is not trivial to make, but extremely important, considering that the field of Molecular Electronics has already been under scrutiny over a series of high-profile discoveries that turned out to be completely fraudulent (Schön's scandal).[26]

EGaIn is easy to implement, cheap, reliable and it allows for rapid collection of big sets of data. This is a perfect combination for performing systematic studies in the spirit of physical organic chemistry—isolating variables and looking for trends. However, before EGaIn became well established it was treated with skepticism. The main issue of concern was an ill-defined interface between EGaIn and the SAM (Figure 1.2 e). The obtained data could be dominated by the layer of Ga_2O_3, which would make the data analysis wrong and all the conclusions false. However, carefully conducted experiments repeatedly pointed at the opposite. In the first paper on EGaIn Chiechi *et al.* performed electrical characterization of the SAMs of alkanethiols with varying chain length and determined a β-value (β is a tunneling decay coefficient according to Simmons' approximation $J = J_0 e^{-\beta d}$, see Section 1.4 for details).[25] The reported β-value was lower than the consensus value for alkanethiolates, but it was later remeasured and found to be in a good agreement with other techniques.[23] Moreover, utilizing EGaIn as the top electrode allowed Whitesides *et al.*[27] to distinguish the difference between transport properties of SAMs of alkanethiols with odd and even number of methylenes. This effect, known as the "odd-even effect", is related to the differences in the orientation of terminal methyl groups at the top interface. Nijhuis *et al.* were first to observe a high magnitude of the rectification of current in large-area junctions comprising SAMs

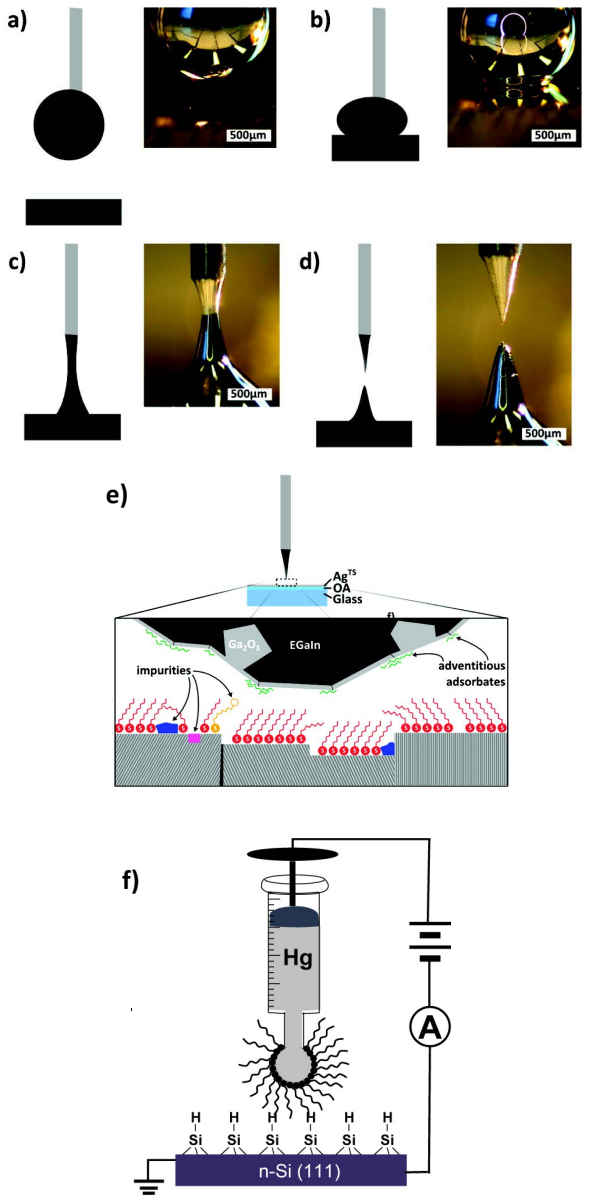

Figure 1.2 a-d) Fabrication of an EGaIn tip. **e)** Schematic of a Ag/SAM//EGaIn junction. Reprinted with permission from reference [23]. Copyright 2012 American Chemical Society. **f)** Hanging Hg drop junction in contact with Si substrate. Reprinted with permission from reference [24]. Copyright 2014 American Chemical Society.

of ferrocene-terminated alkanethiols utilizing EGaIn.[28] These SAMs were later studied in great detail and the rectification mechanism was established.[29–31] All these findings point to the fact that the SAM, not the oxide, dominate charge transport in EGaIn junctions.[32] Since then EGaIn has been successfully utilized to measure the highest rectification ratio in SAMs,[33] address monolayers of proteins[34], measure quantum interference effects in SAMs of conjugated organic wires[35] and study the effects of dipole moments in SAMs (Chapters 2 and 3).

1.4. MECHANISM OF CHARGE TRANSPORT

Molecular Electronics is fundamentally interested in the way molecules conduct charge. In order to experimentally test the properties of the molecular junctions, a variety of techniques was developed. All of them, in principle, achieve a configuration where two metal electrodes are bridged by a molecule/molecular layer, resulting in a metal-molecule-metal structure. Since the separation between the two electrodes is defined by the length of the molecule/thickness of the monolayer, the operating length scale is a few nanometers. At this quantum scale the dominant mechanism of charge transport becomes tunneling. Quantum tunneling is defined as a phenomenon where a particle is able to go through a barrier that it classically could not surmount. In terms of band theory organic matter can be generally considered a wide band gap semiconductor or an insulator. That is why the most widely used theoretical model in Molecular Electronics was outlined by Simmons in 1963, who described electron tunneling through thin insulating film.[36] The most useful for ME, however, turned out to be an approximation of Simmons' model that describes how the tunneling current scales with the tunneling distance:

$$J = J_0 e^{-\beta d}, \tag{1.1}$$

where J is the tunneling current density, d is the barrier width, J_0 equals to the tunneling current density at $d = 0$ and β is the tunneling decay coefficient. The tunneling decay coefficient β, which represents the tunneling barrier, is a very well reproduced parameter and its value for alkanethiols ($\approx$0.75 Å^{-1}) is used as a benchmark for determining whether the molecules dominate the transport in a given experimental setup.[37] For a simple system of alkanethiols the transport can be described as coherent non-resonant tunneling.

Theoretical calculations of the charge transport in molecular junctions are often used to support experimental findings. The most common approach to predicting transport properties of molecular junctions was developed by Rolf Landauer in 1957.[38] Landauer showed that conductance through atomic-scale metallic junctions can be calculated as the sum of all transmission probabilities for each current-carrying eigenmode:

$$G = \frac{2e^2}{h} \sum_{n=1}^{N} T_n, \tag{1.2}$$

The summation is performed over all available conduction eigenmodes and T_n are their individual transmissions. Transmission here plays the key role and it can be understood by examining a classical quantum mechanical problem—a wave impinging on a potential barrier. The solution to this problem provides a dependance of the transmission

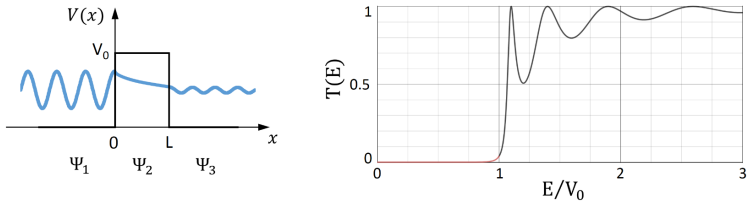

Figure 1.3 Classical quantum mechanical problem—a wave approaching a potential barrier. The wave functions in each region 1-3 can be described with corresponding Ψ_{1-3}. Further matching of Ψ_{1-3} and their first spatial derivatives at the boundaries ($x = 0$ and $x = L$) allows to obtain the formula for calculating the transmission probability as a function of energy ($T(E)$). The resulting function is plotted for the barrier with $L = 1$ nm and $V_0 = 4$ eV. Red and black parts of the function correspond to the regions where $E < V_0$ and $E > V_0$, respectively. In the region where $E < V_0$ transmission probability decays exponentially.

probability on the energy of the wave (Figure 1.3). This model provides a natural explanation for the exponential decay of the low-bias conductance as a function of the tunneling distance. However, this problem becomes incredibly complex when a molecule is introduced instead of a symmetrical rectangular barrier and no accurate analytical solution can be obtained. The most successful theoretical models are usually based on the non-equilibrium Green's function formalism.[39] Combining the self-consistent matrix Green's function approach with the density functional theory of electronic structure opens up the possibility of using the existing well-established technique of molecular electronic structure theory in transport calculations with little change and allows to use the language of qualitative molecular orbital theory to interpret and rationalize the results of the computation.[40]

1.5. THESIS OUTLINE

In **Chapter 2** we study the influence of embedded dipole moments in SAMs. We designed three molecules based on a p-terphenyl structure in which the central aromatic ring is either phenyl or a dipole-inducing pyrimidyl in one of two different orientations. All three form well-defined SAMs with similar thickness, packing density and tilt angle, with dipole moments embedded in the SAM, isolated from either interface. Transition voltages (V_T) show a clear linear correlation with the shift in the work function of Au bottom electrode induced by the collective action of the embedded dipoles. This observation demonstrates that V_T can be manipulated synthetically, without altering either the interfaces or electrodes and that trends in V_T can be related to experimental observables on the SAMs before installing the top contact. Calculated projected density of states of the SAMs on Au surfaces that relate HOMO-derived states to V_T further show that energy level alignment within an assembled junction can be predicted and adjusted by embedding dipoles in a SAM without altering any other properties of the junction.

In **Chapter 3** we further study the dipole containing series of compounds and observe asymmetric conductance in the form of differing ratios of current density as a function of voltage. Monolayers comprising compounds with nearly identical physical and electronic properties show opposite directions of this asymmetry. We tested the statistical significance of the effect and ascribed it to the collective action of embedded dipoles

arising from pyrimidyl groups that are arranged parallel or antiparallel to the transport direction. We ascribe the effect to the bias-induced (de)localization of the frontier orbitals that mitigate transport.

In **Chapter 4** we describe tunneling junctions comprising SAMs that can be converted between resistor and diode functionality in-place. The rectification ratio is afected by the protonation state of densely-packed carboxylic acid groups at the interface between the top-contact and the monolayer. We studied this process by treatment with water and a water scavenger using three different top-contacts, EGaIn, conducting-probe atomic force microscopy and reduced graphene-oxide. We propose a mechanism in which the tunneling junctions convert to diode behavior through the creation of surface-states that result from the polarization of the monolayer when the carboxylic acid groups are protonated, which we support with X-ray photoelectron spectroscopy. We also describe a light-driven modulation using spiropyran as a photo-acid.

In **Chapter 5** we perform a systematic study of the influence of the substitution pattern on the charge transport properties of oligo(*p*-phenylene ethynylene)s (OPEs). We take OPE3 as a backbone and attach electron withdrawing/donating groups in different patterns and address their SAMs with EGaIn. This allows us to vary the position of the frontier energy levels, dipole moments and strength of coupling to the bottom electrode while keeping the length of the molecules constant. Surprisingly, we found the latter to have the most significant effect on the properties of resulting junctions.

BIBLIOGRAPHY

[1] A. von Hippel. Molecular engineering. *Science*, 123(3191):315–317, 1956.

[2] Bernhard Mann and Hans Kuhn. Tunneling through fatty acid salt monolayers. *J. Appl. Phys.*, 42(11):4398–4405, 1971.

[3] Arieh Aviram and Mark A. Ratner. Molecular rectifiers. *Chem. Phys. Lett.*, 29(2):277 – 283, 1974.

[4] Adam Johan Bergren, Lucas Zeer-Wanklyn, Mitchell Semple, Nikola Pekas, Bryan Szeto, and Richard L McCreery. Musical molecules: the molecular junction as an active component in audio distortion circuits. *J. Phys.: Condens. Matter*, 28(9): 094011, 2016.

[5] Veerabhadrarao Kaliginedi, Alexander V. Rudnev, Pavel Moreno-Garcia, Masoud Baghernejad, Cancan Huang, Wenjing Hong, and Thomas Wandlowski. Promising anchoring groups for single-molecule conductance measurements. *Phys. Chem. Chem. Phys.*, 16:23529–23539, 2014.

[6] Bingqian Xu and Nongjian J. Tao. Measurement of single-molecule resistance by repeated formation of molecular junctions. *Science*, 301(5637):1221–1223, 2003.

[7] John Moreland and J. W. Ekin. Electron tunneling experiments using Nb-Sn “break” junctions. *J. Appl. Phys.*, 58(10):3888–3895, 1985.

[8] C.J. Muller, J.M. van Ruitenbeek, and L.J. de Jongh. Experimental observation of the transition from weak link to tunnel junction. *Physica C: Superconductivity*, 191(3): 485 – 504, 1992.

[9] Ralph G. Nuzzo and David L. Allara. Adsorption of bifunctional organic disulfides on gold surfaces. *J. Am. Chem. Soc.*, 105(13):4481–4483, 1983.

[10] Colin D. Bain, E. Barry Troughton, Yu Tai Tao, Joseph Evall, George M. Whitesides, and Ralph G. Nuzzo. Formation of monolayer films by the spontaneous assembly of organic thiols from solution onto gold. *J. Am. Chem. Soc.*, 111(1):321–335, 1989.

[11] Marc D. Porter, Thomas B. Bright, David L. Allara, and Christopher E. D. Chidsey. Spontaneously organized molecular assemblies. 4. structural characterization of n-alkyl thiol monolayers on gold by optical ellipsometry, infrared spectroscopy, and electrochemistry. *J. Am. Chem. Soc.*, 109(12):3559–3568, 1987.

[12] Li Qiu, Yanxi Zhang, Theodorus L. Krijger, Xinkai Qiu, Patrick van't Hof, Jan C. Hummelen, and Ryan C. Chiechi. Rectification of current responds to incorporation of fullerenes into mixed-monolayers of alkanethiolates in tunneling junctions. *Chem. Sci.*, 8:2365–2372, 2017.

[13] J. Christopher Love, Lara A. Estroff, Jennah K. Kriebel, Ralph G. Nuzzo, and George M. Whitesides. Self-assembled monolayers of thiolates on metals as a form of nanotechnology. *Chem. Rev.*, 105(4):1103–1170, 2005.

[14] Emily A. Weiss, George K. Kaufman, Jennah K. Kriebel, Zhefeng Li, Richard Schalek, and George M. Whitesides. Si/SiO_2-Templated formation of ultraflat metal surfaces on glass, polymer, and solder supports: Their use as substrates for self-assembled monolayers. *Langmuir*, 23(19):9686–9694, 2007.

[15] Gregory L. Fisher, Amy V. Walker, Andrew E. Hooper, Timothy B. Tighe, Kevin B. Bahnck, Hope T. Skriba, Michael D. Reinard, Brendan C. Haynie, Robert L. Opila, Nicholas Winograd, and David L. Allara. Bond insertion, complexation, and penetration pathways of vapor-deposited aluminum atoms with HO- and CH_3O-terminated organic monolayers. *J. Am. Chem. Soc.*, 124(19):5528–5541, 2002.

[16] Bert de Boer, Martin M. Frank, Yves J. Chabal, Weirong Jiang, Eric Garfunkel, and Zhenan Bao. Metallic contact formation for Molecular Electronics: interactions between vapor-deposited metals and Self-Assembled monolayers of conjugated mono- and dithiols. *Langmuir*, 20(5):1539–1542, 2004.

[17] Parisa Aghbolagh Pourhossein. *The fabrication of nanogap electrodes using nanoskiving*. PhD thesis, University of Groningen, 2014.

[18] Gabriel Puebla-Hellmann. Nanoparticle-molecule-metal junctions: a scalable, ambient stable strategy for wafer-scale molecular integration. In *9th International Conference on Materials for Advanced Technologies*, 2017.

[19] Krzysztof Slowinski, Richard V. Chamberlain, Renata Bilewicz, and Marcin Majda. Evidence for inefficient chain-to-chain coupling in electron tunneling through liquid alkanethiol monolayer films on mercury. *J. Am. Chem. Soc.*, 118(19):4709–4710, 1996.

[20] Maria A. Rampi and George M. Whitesides. A versatile experimental approach for understanding electron transport through organic materials. *Chem. Phys.*, 281(2): 373 – 391, 2002.

[21] Krzysztof Slowinski, Harold K. Y. Fong, and Marcin Majda. Mercury-mercury tunneling junctions. 1. Electron tunneling across symmetric and asymmetric alkanethiolate bilayers. *J. Am. Chem. Soc.*, 121(31):7257–7261, 1999.

[22] Elizabeth Tran, Christian Grave, George M. Whitesides, and Maria A. Rampi. Controlling the electron transfer mechanism in metal–molecules–metal junctions. *Electrochim. Acta*, 50(25):4850 – 4856, 2005.

[23] Ludovico Cademartiri, Martin M. Thuo, Christian A. Nijhuis, William F. Reus, Simon Tricard, Jabulani R. Barber, Rana N. S. Sodhi, Peter Brodersen, Choongik Kim, Ryan C. Chiechi, and George M. Whitesides. Electrical resistance of Ag^{TS}-$S(CH)_{n-1}CH_3$//Ga_2O_3/EGaIn tunneling junctions. *J. Phys. Chem. Cd*, 116(20): 10848–10860, 2012.

[24] Lixia Zhu, Richard T. W. Popoff, and Hua-Zhong Yu. Metastable molecular metal–semiconductor junctions. *J. Phys. Chem. C*, 119(4):1826–1831, 2015.

[25] Ryan C. Chiechi, Emily A. Weiss, Michael D. Dickey, and George M. Whitesides. Eutectic Gallium-Indium (EGaIn): A moldable liquid metal for electrical characterization of self-assembled monolayers. *Angew. Chem. Int. Ed.*, 47(1):142–144, 2008.

[26] Report of the investigation comittee on the possibility of scientific misconduct in the work of Hendrik Schön and coauthors. Distributed by the American Physical Society with permission of Lucent Technologies, 2002.

[27] Martin M. Thuo, William F. Reus, Christian A. Nijhuis, Jabulani R. Barber, Choongik Kim, Michael D. Schulz, and George M. Whitesides. Odd-even effects in charge transport across self-assembled monolayers. *J. Am. Chem. Soc.*, 133(9):2962–2975, 2011.

[28] Christian A. Nijhuis, William F. Reus, and George M. Whitesides. Molecular recrification in metal-SAM-metal oxide-metal junctions. *J. Am. Chem. Soc.*, 131(49):17814–17827, 2009.

[29] Christian A. Nijhuis, William F. Reus, and George M. Whitesides. Mechanism of rectification in tunneling junctions based on molecules with asymmetric potential drops. *J. Am. Chem. Soc.*, 132(51):18386–18401, 2010.

[30] Li Yuan, Nisachol Nerngchamnong, Liang Cao, Hicham Hamoudi, Enrique del Barco, Max Roemer, Ravi K. Sriramula, Damien Thompson, and Christian A.

Nijhuis. Controlling the direction of rectification in a molecular diode. *Nat. Commun.*, 6:6324–6334, 2015.

[31] Nisachol Nerngchamnong, Li Yuan, Dong-Chen Qi, Jiang Li, Damien Thompson, and Christian A. Nijhuis. The role of van der Waals forces in the performance of molecular diodes. *Nat. Nanotechnol.*, 8:113–118, 2013.

[32] William F. Reus, Martin M. Thuo, Nathan D. Shapiro, Christian A. Nijhuis, and George M. Whitesides. The SAM, not the electrodes, dominates charge transport in metal-monolayer//Ga_2O_3/Gallium–Indium eutectic junctions. *ACS Nano*, 6(6): 4806–4822, 2012.

[33] Xioping Chen, Max Roemer, Li Yuan, Wei Du, Damien Thompson, Enrique del Barco, and Christian A. Nijhuis. Molecular diodes with rectification ratios exceeding 10^5 driven by electrostatic interactions. *Nat. Nanotechnol.*, 12(110):897–803, 2017.

[34] Pavlo Gordiichuk, Diego Pesce, Olga E. Castañeda Ocampo, Alessio Marcozzi, Gert-Jan A. H. Wetzelaer, Avishek Paul, Mark Loznik, Ekaterina Gloukhikh, Shachar Richter, Ryan C. Chiechi, and Andreas Herrmann. Orientation and incorporation of photosystem I in bioelectronics devices enabled by phage display. *Adv. Sci.*, 4(5): 1600393, 2017.

[35] Davide Fracasso, Hennie Valkenier, Jan C. Hummelen, Gemma C. Solomon, and Ryan C. Chiechi. Evidence for quantum interference in SAMs of arylethynylene thiolates in tunneling junctions with eutectic Ga–In (EGaIn) top-contacts. *J. Am. Chem. Soc.*, 133(24):9556–9563, 2011.

[36] John G. Simmons. Generalized formula for the electronic tunnel effect between similar electrodes separated by a thin insulating film. *J. Appl. Phys.*, 34(6):1793–1803, 1963.

[37] Felice C. Simeone, Hyo Jae Yoon, Martin M. Thuo, Jabulani R. Barber, Barbara Smith, and George M. Whitesides. Defining the value of injection current and effective electrical contact area for EGaIn-based molecular tunneling junctions. *J. Am. Chem. Soc.*, 135(48):18131–18144, 2013.

[38] R. Landauer. Spatial Variation of Currents and Fields Due to Localized Scatterers in Metallic Conduction. *IBM J. Res. Dev.*, 1(3):223–231, 1957.

[39] A. R. Williams, Peter J. Feibelman, and N. D. Lang. Green's-function methods for electronic-structure calculations. *Phys. Rev. B*, 26:5433–5444, 1982.

[40] Yongqiang Xue, Supriyo Datta, and Mark A. Ratner. First-principles based matrix Green's function approach to molecular electronic devices: general formalism. *Chem. Phys.*, 281(2):151 – 170, 2002.

2

SYNTHETIC CONTROL OVER TRANSITION VOLTAGES

Abstract: *The question whether the molecules or the electrodes dominate tunneling charge transport is important and ubiquitous in Molecular Electronics. A way to manipulate the transition voltage and, subsequently, answer the aforementioned question via synthetic manipulation of molecular dipoles is shown in the following chapter.*

The contents of this chapter were published in Chemical Science, Royal Society of Chemistry (10.1039/c5sc03097h). I would like to thank Tarek Abu-Husein and Andreas Terfort for synthesis and purification of the molecules studied herein, Michael Zharnikov for characterization of self-assembled monolayers and David Egger and Egbert Zojer for performing DFT calculations on the monolayers.

2.1. INTRODUCTION

Two main approaches are currently used to contact molecules, which is a key step in the examination of charge transport: single-molecule and large-area (*i.e.*, ensembles) measurements. In both cases the molecules under investigation are placed in between two metal electrodes that are on the order of 2 nm apart (the exact distance is defined by the dimensions of the molecules under investigation). In these systems interfaces play an important role in defining the characteristics of a junction and both approaches suffer from an uncertainty—is transport dominated by molecules or by interfaces?[1, 2] Electron transport in large-area junctions is affected by defects in SAMs that can dominate transport in certain cases,[3] while single-molecule junctions exhibit background currents in which tunneling charges flow directly from one electrode to the other, bypassing the molecule in between.[4] Thus, the magnitude of J or I (current-density or current) by itself varies considerably and therefore carries little useful information on the intrinsic electronic properties of the molecules in the junction.

One of the most reliable metrics that seeks to resolve these issues is β, which is an empirical parameter derived from a form of the Simmons equation $J = J_0 e^{-\beta d}$, where J is the current density, d is the tunneling distance defined by the length of the molecular backbone and J_0 is the theoretical value of J at $d = 0$. Values of β are derived from measurements of series of molecules that differ only by length, while both top and bottom interfaces are kept constant, thus isolating the molecular component in charge transport.[5, 6] This approach to data analysis is particularly robust when comparing saturated molecules (*i.e.*, where the backbone comprises mostly sp^3-hybridized C atoms), for which the consensus value of β is ~ 0.75 Å^{-1}.[6] Saturated molecules have frontier orbitals that are typically not accessible in the typical bias windows used in Molecular Electronics and they are not very polarizable. With the exception of end groups that introduce accessible gap states[7] these properties tend to make saturated molecules less sensitive to the details of the contacts, in general; *e.g.*, tail-groups,[8–10] anchoring groups,[11, 12] and minor alterations to the backbone[13] have little impact on the tunneling transport in terms of the magnitudes of I or J. Unsaturation, by contrast, adds significant complexity and even subtle changes in conjugation patterns can have pronounced and non-distance dependent effects on transport.[14–18] Tuning the length of fully conjugated molecules is also synthetically challenging and not always possible, since a minimal step size is a π bond (*i.e.*, two carbons) or an aromatic ring (usually phenylene) and, unlike alkanes, conjugated molecules become markedly less soluble with increasing length.[19] Thus, a parameter other than β, but that is comparably independent from non-molecular variables (*e.g.*, interfaces), could greatly assist in the description of tunneling transport phenomena in conjugated molecules and, importantly, in the deconvolution of molecular properties from those of the experimental platform.

Beebe *et al.*[20] introduced the transition voltage (V_T) as an approximate measure of the tunneling barrier height, which was later related to level alignment—*i.e.*, the difference between the energy of the accessible frontier orbital of a molecule (highest occupied molecular orbital E_{HOMO} and lowest unoccupied molecular orbital E_{LUMO}) and the Fermi level (E_F) of the electrode (*e.g.*, $E_{LUMO} - E_F$ or $E_F - E_{HOMO}$) in an assembled junction. The parameter V_T can be extracted from the minimum of a Fowler-Nordheim plot, $ln(I/V^2)$ versus $1/V$. The possibility of determining the level alignment of a junc-

tion by simply re-plotting conductance data has led to a number of experimental[21–28] and theoretical studies[29–33].

While β provides information about the effective tunneling distance (and barrier height), V_T provides information about energy level alignment. Multiple experiments showed a correlation between V_T and apparent energetic separation between the Fermi energy level and the dominant frontier molecular orbital.[34, 35] However, the precise physical meaning of V_T is still under debate; *e.g.*, current becomes "superquadratic" with bias and might not always correlate to energy spectral transition.[30, 36]. Sotthewes *et al.*,[37] studied vacuum gaps in ultra-high vacuum STM junctions and found that transition voltage is inversely proportional to $1/d$; *i.e.*, that work showed that V_T can even be measured in the absence of molecules.

Summarizing the above considerations, we assert that the interpretation of V_T is not straightforward and that V_T is highly dependent on interfaces and is a conflation of two effects—interfacial and molecular—underscoring the importance of separating one from the other. Here we describe the control over V_T by manipulating a single parameter—embedded dipoles—while keeping the interfaces and electrodes constant, allowing the unambiguous assignment of *trends* in V_T and energy level alignment to an intrinsic molecular property.

2.2. RESULTS AND DISCUSSION

2.2.1. J/V MEASUREMENTS

We investigated the influence of embedded dipoles on electron transport of SAMs placing them in EGaIn junctions of the form Au^{TS}/SAM//Ga_nO_m/ EGaIn (where "/" denotes an interface defined by chemisorption and "//" by physisorption).[38] Here EGaIn stands for eutectic alloy of Ga and In (75.5% Ga and 24.5% In by weight, mp = 15.7 °C) which is covered by a superficial layer of ~ 0.7 nm of conductive Ga_nO_m. Multiple studies have shown that the oxide layer has a negligible effect on transport properties in EGaIn junctions and is orders of magnitude more conductive than the contacts.[6, 38–40] We designed three structures (depicted and assigned in Figure 2.1) for this study that possess identical length, surface chemistry, and nearly identical gas-phase frontier orbital energies; for TP1-down and up they are identical (as is their empirical formula). All three compounds form well-defined SAMs on template-stripped Au (Au^{TS})[41] and were extensively characterized by a number of complementary surface-analytical techniques,[42] exhibiting comparable film thickness and packing densities (see Table 2.1). The discernible difference is the dipole moment associated with the central aromatic ring (either a pyrimidine or benzene).

An immediate consequence of the collective effect of SAMs of polar pyrimidyl groups is the modification of the electrostatic potential profile, which shifts the vacuum level and the energy separation between E_F and frontier molecular orbitals. Transition voltages offer insight into the effects of electrostatic fields induced by SAMs because they carry information about the level alignment between the frontier molecular orbitals and the Fermi energies of the electrodes. This information is inaccessible experimentally and is challenging to model theoretically, as the details of alignment between molecular and electrode levels are difficult to predict.[43, 44] Our experimental approach is to vary an

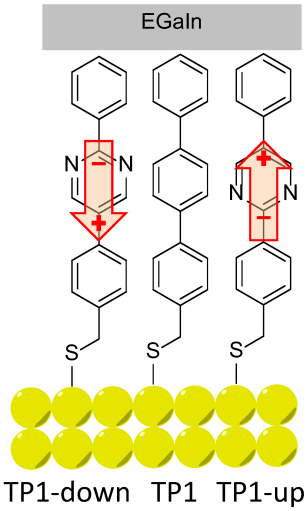

Figure 2.1 Schematic of a junction with two pyrimidyl-containing compounds (TP1-down and TP1-up) and the reference compound (TP1). Arrows indicate directions of dipole moments associated with the embedded pyrimidine rings (from negative to positive charge).

internal, molecular property—in this case dipole moments—and measure the effect in a SAM supported by a bottom electrode (*i.e.*, *ex situ*) before the top contact is installed. We chose shifts in the work function of the bottom electrode (Φ) because work function shift ($\Delta\Phi$) is defined by the collective effect of embedded dipoles in the SAM.[45] This collective effect is preserved when the top contact is installed (*i.e.*, *in situ*), because the dipoles are embedded in the SAM and are isolated from both interfaces. After assembling the junction and performing electrical measurements, we extracted V_T and plotted it against $\Delta\Phi$ to give us two experimental parameters, one intrinsic to the SAM/bottom-contact ($\Delta\Phi$) and one to the bottom-contact/SAM//top-contact (V_T). This approach is similar to that of the β analysis, where tunneling distance d (which is an *ex situ* parameter and can be calculated and measured in multiple ways) is correlated to current density J (an *in situ* characteristic of an assembled junction). It is important to compare trends because the absolute magnitude of V_T is still affected by the details of the contacts.[26, 36]

Figure 2.2 summarizes measurements of tunneling current through SAMs of TP1, TP1-down, and TP1-up. These data were acquired by sweeping the potential in EGaIn junctions through a range of ±1V. As expected, the conductances of all SAMs are nearly identical. The magnitude of current is dominated by the tunneling distance, which is identical along the series, and is influenced only slightly, if at all, by the embedded dipoles ($\beta \approx 0.4$ Å^{-1} for these backbones[46]). All of the curves are slightly asymmetric,[47] with TP1-up showing opposite asymmetry—it conducts slightly more at negative bias as opposed to TP1 and TP1-down, which are slightly less conductive at negative bias (but values of $J(+)$ and $J(-)$ are within error for most values of V for all three SAMs). There is evidence that terminal pyrimidine rings can induce asymmetry in J/V traces[48–50] (which can theoretically be caused by internal dipole moments as well[51],). A more de-

SAM	Effective thickness (nm)	Packing density (molecules/cm^2)	Tilt angle	WF shift[a] (eV)
TP1	1.78 ± 0.04	4.6×10^{14}	18 ± 3°	0.98
TP1-up	1.74 ± 0.05	4.2×10^{14}	18 ± 3°	1.41 (+0.43[b])
TP1-down	1.75 ± 0.05	4.3×10^{14}	17 ± 3°	0.43 (−0.55[b])

Experimental values are from Reference 42.

[a] Measured with a Kelvin probe; we use opposite sign conventions for Φ.

[b] Difference from TP1.

Table 2.1 X-ray photoemission spectroscopy derived effective thickness and packing density of TP1, TP1-up and TP1-down SAMs; X-ray absorption spectroscopy derived tilt angles; WF shifts with respect to pristine gold.

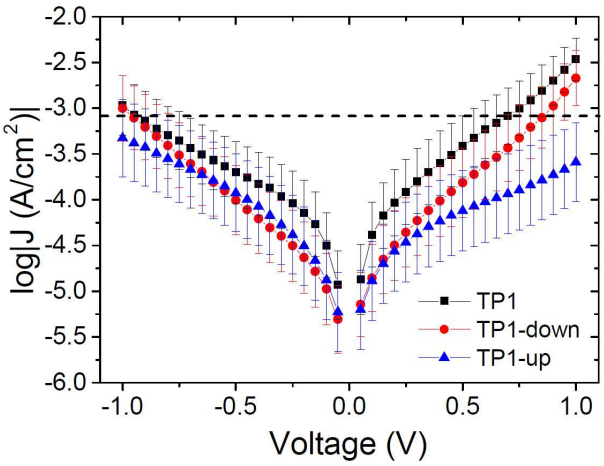

Figure 2.2 Plots of log current-density versus applied potential for SAMs of TP1 (black squares), TP1-down (red circles) and TP1-up (blue triangles). Values of $log|J|$ at $V = 0$ are omitted for clarity. Error bars represent 95% confidence intervals. The three traces are hardly distinguishable at negative bias, while, at positive bias, TP1-up deviates from the rest showing opposite asymmetry (J(+1V) is slightly higher than J(-1V) for TP1 and TP1-down and opposite for TP1-up).

tailed analysis is presented in the next Chapter and the difference in the symmetry of the J/V curves of TP1-up is related to the effect of the direction of the dipole moments on the hybridization of the HOMO with states in the gold electrode.

2.2.2. TRANSITION VOLTAGE MEASUREMENTS

we calculated V_T by re-plotting raw I/V data as $ln(I/V^2)$ versus $1/V$ for both positive and negative biases for each J/V curve and extrapolating the minimum. The peak values of Gaussian fits (μ) to the resulting distributions are taken as V_T and the error is derived from the widths (σ). These data are summarized in Table 2.2 along with gas-phase HOMO energies and dipole moments calculated using structural information from the characterization of the SAMs (as described in reference 46). The HOMO energies serve only to highlight the electronic similarities between the three compounds, not the SAMs.

The values of V_T at negative bias (denoted V_T^-) are systematically higher than the corresponding values of V_T^+, which is common for EGaIn junctions,[26, 46] but they follow the same trend; increasing from TP1-down to TP1 to TP1-up. The value of V_T^+ for TP1 is in good agreement with the previously reported value of 0.55 ± 0.10 V.[46] The general trend is also in agreement; "down" dipole moments lower both V_T^- and V_T^+ with respect to "up" dipole moments.

SAM	V_T^+ (V)	V_T^- (V)	HOMO[a] (eV)	μ_{net}[a] (D)
TP1	0.52 ± 0.05	−0.65 ± 0.05	−5.65	+0.01
TP1-up	0.80 ± 0.06	−0.85 ± 0.03	−6.08	−2.75
TP1-down	0.40 ± 0.02	−0.43 ± 0.04	−6.08	+2.34

[a] Gas-phase HSE06/6-311+g(2d,2p) DFT calculations.

Table 2.2 Values of V_T for all SAMs for positive (V_T^+) and negative bias (V_T^-) and gas-phase calculated HOMO energies. Errors are 95% confidence intervals (CI).

2.2.3. LEVEL ALIGNMENT

As a result of a collective effect of individual dipoles, SAMs of TP1-down and TP1-up shift the electrostatic energy within the junction, which alters the relative positions of the frontier orbitals and the Fermi levels of the electrodes leading to a change in V_T. The magnitude of the shift can be approximated by measuring the work function of the bare Au^{TS} substrate and the substrate supporting a SAM using Kelvin probe measurements or UPS.[46] Kim *et al.*[24] demonstrated correlation of V_T versus $\Delta\Phi$ using conducting AFM tips to contact SAMs; however, they adjusted Φ by varying materials of either bottom or top electrodes, not the electronics of the molecules. Another study found a correlation between V_T and interfacial dipoles, but could not unambiguously assign it to a molecular property[46]. The effects of embedded dipolar groups have also been investigated in aliphatic SAMs (*i.e.*, comprising CH_2 backbones), including a study of the physical and electronic structure effects of embedded esters[52] as well as a study of the J/V properties of embedded amides,[9] however, no correlation to V_T has been established. Taking TP1 as a reference point, the shifts in TP1-down and up are $\Delta\Phi = -0.55$ and $+0.43$ eV (see Table 2.1), respectively; they are shifted by approximately the same amount, but opposite in sign, from TP1. Figure 2.3 shows plots of V_T^+ and V_T^- versus $\Delta\Phi$. The plots are approximately linear, fitting with $R^2 = 0.77$ and 0.99 respectively, demonstrating that V_T correlates to the shift in vacuum level of Au^{TS} induced by the embedded dipoles of the SAMs. A symmetric offset is apparent for V_T^-, which differs from TP1 by ~ ±0.2 V, but less so for V_T^+; however, the correlation of the latter to $\Delta\Phi$ is also less robust. Thus, it appears that the simple picture in Figure 2.1 is a reasonable, qualitative description of the synthetic manipulation of V_T.

2.2.4. DFT CALCULATIONS

Valuable insight can be gained from the level alignment of the molecular states relative to the Fermi energy of the Au substrate in the absence of the EGaIn (top) electrode. Thus, we plot the DFT calculated projected densities of states (PDOS) associated with the three studied monolayers in Figure 2.4. We used the hybrid functional HSE[53, 54]

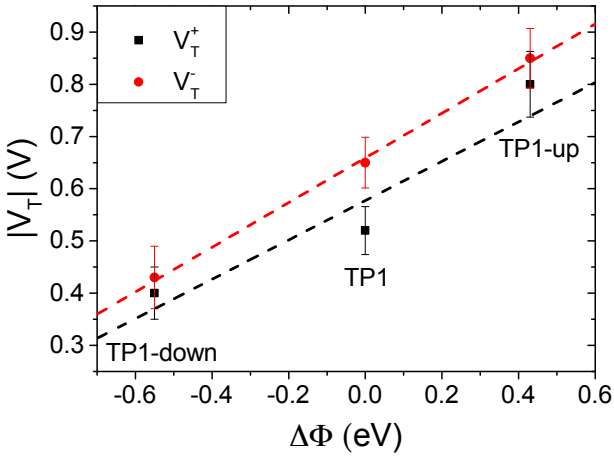

Figure 2.3 Plot of V_T^+ (black squares, fitting with the slope of 0.38 and $R^2 = 0.77$) and V_T^- (red circles, slope of 0.43 and $R^2 = 0.99$) versus work function shift. Values of $\Delta\Phi$ are taken from Table 1.

for the periodic band-structure calculations (performed with the VASP code[55]) for the metal-SAM systems as, due to the mixing of short-range Hartree Fock and semi-local exchange, orbital self-interactions errors that would distort the electronic structure of pyrimidyl-containing systems can be reduced[56, 57]. However, the absolute values of the calculated level alignment, especially for the case of upright-standing molecules,[58] cannot quantitatively reproduce the experiment even with the hybrid-functionals used here[43, 59, 60]. Nevertheless, for chemically similar systems such as the ones studied here, advanced hybrid DFT-calculations allow for predicting trends in the level alignment.

In Figure 2.4, one clearly sees that in TP1-down the highest occupied states are shifted towards E_F compared to the reference TP1 system, while they are shifted away in the TP1-up case. These shifts can be understood from the peculiar distribution of the electrostatic energy within the SAM where, due to collective electrostatic effects[61, 62] (i.e., the superposition of the fields of the pyrimidyl dipoles arranged in a 2D pattern), the electrostatic energy in the topmost rings is shifted relative to E_F (as schematically shown in Figure 2.5, a plot of the calculated plane-averaged potentials can be found in ref. 42). This shift has been confirmed by high-resolution XPS experiments[42]. And because the occupied frontier states are largely delocalized over the SAM, a shift in the electrostatic energy induces a shift in the SAM eigenstates relative to E_F (see Figure 2.5).

The frontier orbitals are largely delocalized over the molecular backbone, likely leading to highly transmissive channels in the transport experiments. Nevertheless, one can see that in the TP1-down (TP1-up) case the HOMO-derived PDOS has a larger weight on the ring far from (close to) the Au substrate, which is the behavior expected for such a situation[63], as can be understood, for example, from the analogy of SAM-states and electron- and hole-states in quantum-well states in the presence of a potential gradient. [56] This difference in the spatial distribution of PDOS densities might also be responsible for the qualitative differences in the shapes of the J/V curves for SAMs of TP1-up

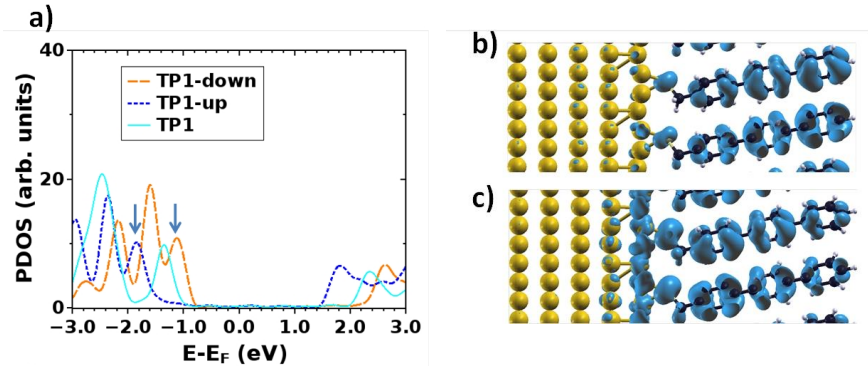

Figure 2.4 Density of states of TP1, TP1-up and TP1-down projected (PDOS) onto the molecular region as calculated with HSE (a). The energy scale is given relative to the Fermi-energy, E_F. Charge density associated with the highest occupied peaks in the PDOS (derived from the molecular HOMO) of TP1-down (b) and TP1-up (c). The latter are calculated per system in a ± 0.1 eV interval centered at the energy indicated by an arrow (isodensity value: 0.01 $-e\text{Å}^{-3}$).

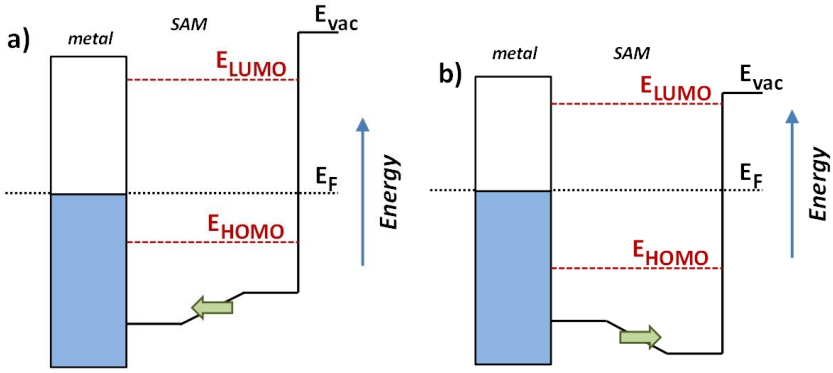

Figure 2.5 Schematics of the electrostatic energy distribution and the resulting energy-level alignment in TP1-down (a) and TP1-up (b) SAMs on Au electrode. The right (upper) parts of the potential well are shifted up, respectively down in energy as a consequence of the pyrimidyl dipoles arranged in a 2D plane. The SAM eigenstates (partially) follow that shift.

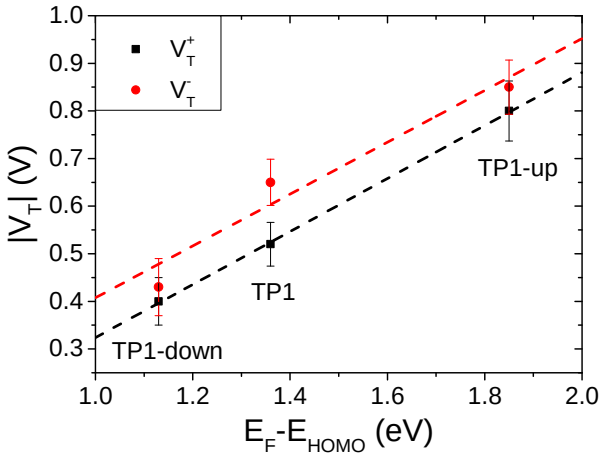

Figure 2.6 Plot of V_T^+ (black squares, fitting with the slope of 0.56 and $R^2 = 1$) and V_T^- (red circles, slope of 0.55 and $R^2 = 0.87$) vs $E_F - E_{HOMO}$ from the calculated density of states. Error bars are 95% CI.

and TP1-down (Figure 2.2).

The question remains as to what exactly happens at V_T, *e.g.*, if the tail of density of states comes into resonance with E_F. A calculation of the PDOS for SAMs bound to a metal surface made by plotting the peaks in Figure 2.4 produces good correlation of V_T versus peak values of HOMO levels (Figure 2.6). The slopes of linear fits for both V_T^+ and V_T^- are almost equal (0.56 and 0.55 respectively) and in good agreement with the experimentally determined slope of 0.55 reported by Beebe *et al.* [21] Regardless of the exact physical meaning of the magnitude of V_T, from the trend it is clearly possible to "feel" energy level alignment in these SAMs. Moreover, the agreement in the slopes suggests that shifting the vacuum level by embedding dipoles in a SAM is physically similar to changing the identity of the electrodes, while the effects of dipoles placed at the physisorbed interface are more convoluted.[46]

2.2.5. TRENDS IN TRANSITION VOLTAGES

Just as the absolute value of J for an isolated member of a series of molecules (from which one cannot make a J vs d plot to extract β) is significantly less useful than β, the absolute value of V_T carries complex, inseparable information and is less useful than a trend that relates a shift in V_T to a controllable variable. The trend presented in Figure 2.3 shows that a shift in V_T is correlated to a change in Φ (hence dipole moment) revealing a molecular fingerprint in the transport properties. For any series of molecules of equal length β is obviously not applicable, thus trends in V_T might serve as empirical evidence that transport is dominated by tunneling through molecules (Figure 2.7). The ability to make this distinction is both important and non-trivial. For example, one can observe quantum interference effects as a length-independent decrease in J with varying conjugation patterns,[14] a lack of measurable current in *meta* substituted stilbene thiols[64] or negative curvature in $log|\frac{dI}{dV}|$,[16] but these interpretations all rely on

the underlying assumption that I and J are dominated by transport through molecules. Likewise, applying theoretical models to explain the interference effects relies on the same assumptions. This problem is particularly evident when experimental observations that disagree with theory are based on a somewhat ambiguous interpretations of data (*e.g.*, bi-modal distributions of conductance).[65] The series of molecules in this work is not expected to exhibit any unusual transport properties, but despite the lack of a distance-dependence the J/V data presented in Figure 2.2 are unambiguously dominated by transport through molecules. And we have shown that embedded dipoles have a measurable influence on the energetics within molecular tunneling junctions comprising TP1, TP1-down, and TP1-up, but do not have a significant influence on the magnitude of tunneling charge-transport.

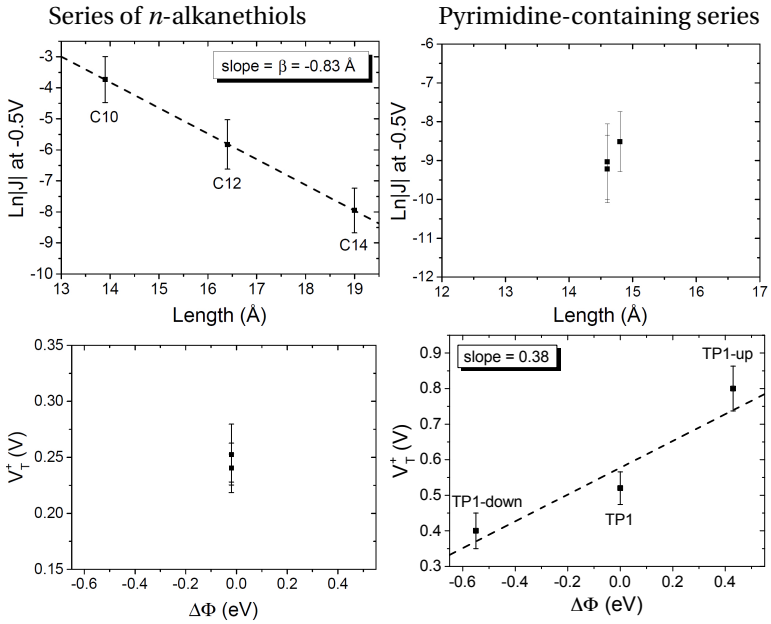

Figure 2.7 β-plots from Au^{TS}/SAM//EGaIn junctions for series of n-alkanethiols (decanethiol, dodecanethiol, and tetradecanethiol) and pyrimidine-containing series (TP1, TP1-down, and TP1-up)—top row. Plots of V_T vs WF shift for both series—bottom row, which show how a trend in V_T can be used as a molecular fingerprint (as an example data only of V_T^+ is presented for both series) similar to β for situations where d is invariant.

2.3. CONCLUSIONS

We examined tunneling junctions comprising SAMs of three molecules of nearly identical length, packing density, tilt angle, torsional angle and gas-phase HOMO energies.[42] The only difference is the inclusion of a central pyrimidine ring, which introduces a dipole moment, the direction of which is synthetically controllable by adjusting the orientation of the ring. The resulting dipole moments are embedded in the SAM as opposed to being introduced as a head (tail) group in contact with the top (bottom) electrode. Thus, we can eliminate both electrode interfaces, tunneling distance, packing, tilt, tor-

sional angles, and gas-phase HOMO energies as variables and compare the tunneling transport properties.

We find that, apart from a slight difference in J at $+1V$, the J/V curves are indistinguishable. The transition voltages, however, differ systemically and follow the same trend as the experimentally-determined vacuum level shift induced by the direction and magnitude of the embedded dipoles. The trends in Figure 2.3 and 2.6 capture the critical aspect of investigating systematic behavior in V_T. The former relates an external experimental observable, Φ, to an internal experimental observable, V_T. The latter relates this internal observable to the details of the level alignment that takes place when molecules are chemisorbed to a metal, which can in turn be related to experimentally observable energy positions of frontier electronic states.[24] Thus, the ability to manipulate V_T systematically through synthetic modifications away from the electrode interfaces simultaneously provides evidence that the charge transport is dominated by molecules and provides quantitative information about their electronic states. This physical interpretation of V_T is not new, but the isolation of the internal electrostatic profile of a molecule as a variable that affects V_T is an important step forward in the fundamental understanding of tunneling transport through molecular junctions and, ultimately, control over functionality.

This result demonstrates that (i) V_T can be manipulated synthetically in a predictable manner, (ii) changes to V_T can be ascribed to an intrinsic property of the molecules inside the tunneling junction, (iii) the energy level alignment can be adjusted using embedded dipoles without altering any other characteristic of a SAM. And, while the length dependence of conductance can be described by β, V_T carries information about energy levels; trends in V_T can separate some of these influences. The inclusion of embedded dipoles (or specifically pyrimidine rings) instills a "molecular fingerprint" to tunneling transport that is separate from the magnitude of I or J. This observation is in agreement with studies showing that polar groups (and embedded dipoles in saturated molecules) have no influence on β.[9] While the lone pairs of a pyrimidyl moiety can interfere with edge-to-π interactions, in this particular case all three SAMs pack nearly identically.[42] Thus, this effect is sufficiently weak that it is overcome by the flanking phenyl rings, suggesting that the use of pyrimidine rings specifically to create a dipole moment is generalizable. We suggest that, irrespective of the precise physical interpretation of transition voltages, trends in V_T—specifically V_T versus $\Delta\Phi$—are particularly useful for unsaturated molecules in which molecular length is synthetically or experimentally inaccessible or in cases where β is not sensitive to synthetic alterations.

2.4. EXPERIMENTAL DETAILS

Sample preparation. The Au substrates used in this work are made by mechanical template stripping (TS) as described elsewhere.[41] In our case, we deposited 100 nm of Au (99.99%) by thermal vacuum deposition onto a 3" Silicon wafer (with no adhesion layer). Using UV-curable optical adhesive (OA) Norland 61, 1 cm^2 glass chips were glued on the metal surfaces. The TS procedure provides ultra flat smooth surfaces, which allows self-assembly process to achieve high yields of working junctions. All samples were made by incubation of freshly cleaved gold slides in 1 mM solutions in ethanol at room temperature for ~ 24h. Prior to making a solution ethanol was degassed by bubbling nitrogen gas

through for at least 20 minutes and all solutions were kept under nitrogen atmosphere to prevent undesirable oxidation of thiol anchoring group.

Data acquisition and analysis. Data were acquired in a home-built setup that is described in detail elsewhere.[14] Samples were taken out from solution, carefully rinsed with pure ethanol and gently blown to dryness with nitrogen. Each SAM was then measured by placing a sharp tip of EGaIn in visual contact with the surface and acquiring at least 1000 scans across 10 substrates for an average of ~15 scans per junction. The traces in which the instrument reached compliance were considered short circuits and were discarded (they reflect only the compliance limit of the instrument and have no physical meaning). TP1-up showed lower solubility than both TP1 and TP1-down and showed signs of partial precipitation onto the gold surface leading to the appearance of traces where values of J were systematically *ca.* two of orders of magnitude lower than the geometric mean. These traces, which were present only in TP1-up data and made up a small fraction of the total traces, most likely reflect junctions comprising multilayers and were discarded. Histograms of the values of J at each value of V were then fit to Gaussian distributions. The standard deviation of a fit (σ) was then recalculated into 95% confidence interval using following equation CI $= t\frac{\sigma}{\sqrt{N}}$, where t is the coefficient in t-distribution and N is the number of degrees of freedom for our system ($N_{junctions} - 1$).

Transition voltages. We calculate transition voltage by re-plotting each I/V trace in Fowler-Nordheim coordinates, $ln(I/V^2)$ versus $1/V$, Figure 2.8, and found the minimum from the numerical derivative. All values were then plotted in a histogram to which a Gaussian distribution was fit to get a peak value and a standard deviation (which is then recalculated into 95% CI as described above). We used Scientific Python to automate the entire process, providing only raw J/V data as an input.

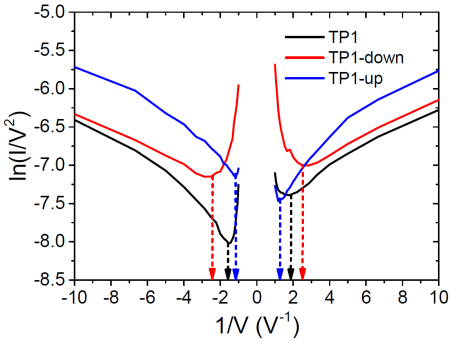

Figure 2.8 Fowler-Nordheim plot for selected $I(V)$ traces of SAMs of TP1, TP1-up and TP1-down. Arrows indicate values, acquired after statistical analysis of all $I(V)$ data combined.

Calculations. The substrate-SAM interfaces were modeled using a $(\sqrt{3} \times 3)$ surface unit cell containing two molecules in herringbone arrangement[42]. The geometries of the SAMs were optimized using the VASP code[55] applying the PBE functional[66] and using the repeated-slab approach. The corresponding procedure is explained in detail in 42. For calculating the electronic states in the SAMs considered here, we had to apply a hybrid functional (in the present case HSE06), to ensure a correct ordering of the

electronic states bearing in mind the strongly differing self-interaction errors associated with *s*- and *p*-states and the high-lying occupied *s*-states in pyrimidines[56]. For the LUMO-derived states the opposite localization trend is observed in TP1-down and TP1-up SAMs. We note that the reason for the decreased localization of the states observed here compared to the specially designed SAMs discussed in ref. 63 is a consequence of (i) the smaller dipoles and corresponding energy shifts of the pyrimidines used here compared to the methylated bipyrimidines in ref. 63 and (ii) the smaller conjugation length of the molecular segments above and below the polar units making a localization of the states energetically more costly.

BIBLIOGRAPHY

[1] Lloyd A. Bumm. Measuring molecular junctions: What is the standard? *ACS Nano*, 2(3):403–407, 2008.

[2] Steven L Bernasek. Can we understand the molecule in molecular electronics? *Angew. Chem. Int. Ed.*, 51(39):9737–9738, 2012.

[3] Li Jiang, C. S. Suchand Sangeeth, Albert Wan, Ayelet Vilan, and Christian A. Nijhuis. Defect scaling with contact area in EGaIn-based junctions: Impact on quality, Joule heating, and apparent injection current. *J. Phys. Chem. C*, 119(2):960–969, 2015.

[4] B. Gotsmann, H. Riel, and E. Lörtscher. Direct electrode-electrode tunneling in break-junction measurements of molecular conductance. *Phys. Rev. B*, 84:205408, 2011.

[5] Emily A. Weiss, Ryan C. Chiechi, George K. Kaufman, Jennah K. Kriebel, Zhefeng Li, Marco Duati, Maria Anita Rampi, and George M. Whitesides. Influence of defects on the electrical characteristics of mercury-drop junctions: self-assembled monolayers of n-alkanethiolates on rough and smooth silver. *J. Am. Chem. Soc.*, 129(14): 4336–4349, 2007.

[6] Felice C. Simeone, Hyo Jae Yoon, Martin M. Thuo, Jabulani R. Barber, Barbara Smith, and George M. Whitesides. Defining the value of injection current and effective electrical contact area for egain-based molecular tunneling junctions. *J. Am. Chem. Soc.*, 135(48):18131–18144, 2013.

[7] Christian A. Nijhuis, William F. Reus, Jabulani R. Barber, Michael D. Dickey, and George M. Whitesides. Charge transport and rectification in arrays of SAM-based tunneling junctions. *Nano Lett.*, 10(9):3611–3619, 2010.

[8] Hyo Jae Yoon, Nathan D. Shapiro, Kyeng Min Park, Martin M. Thuo, Siowling S Soh, and George M. Whitesides. The rate of charge tunneling through self-assembled monolayers is insensitive to many functional group substitutions. *Angew. Chem. Int. Ed.*, 51(19):4658–4661, 2012.

[9] Hyo Jae Yoon, Carleen Morris Bowers, Mostafa Baghbanzadeh, and George M. Whitesides. The rate of charge tunneling is insensitive to polar terminal groups in

self-assembled monolayers in $Ag^{TS}S(CH_2)_nM(CH_2)_mT//Ga_2O_3$/EGaIn junctions. *J. Am. Chem. Soc.*, 136(1):16–19, 2014.

[10] Fatemeh Mirjani, Joseph M. Thijssen, George M. Whitesides, and Mark A. Ratner. Charge transport across insulating self-assembled monolayers: Non-equilibrium approaches and modeling to relate current and molecular structure. *ACS Nano*, 8 (12):12428–12436, 2014.

[11] Kung Ching Liao, Hyo Jae Yoon, Carleen Morris Bowers, Felice C Simeone, and George M Whitesides. Replacing $Ag^{TS}SCH_2$-R with $Ag^{TS}O_2C$-R in EGaIn-based tunneling junctions does not significantly change rates of charge transport. *Angew. Chem. Int. Ed.*, 53(15):3889–3893, 2014.

[12] Davide Fracasso, Sumit Kumar, Petra Rudolf, and Ryan C. Chiechi. Self-assembled monolayers of terminal acetylenes as replacements for thiols in bottom-up tunneling junctions. *RSC Adv.*, 4:56026–56030, 2014.

[13] Martin M. Thuo, William F. Reus, Felice C. Simeone, Choongik Kim, Michael D. Schulz, Hyo Jae Yoon, and George M. Whitesides. Replacing -CH_2CH_2- with -CONH- does not significantly change rates of charge transport through Ag(TS)-SAM//Ga_2O_3/EGaIn junctions. *J. Am. Chem. Soc.*, 134(26):10876–10884, 2012.

[14] Davide Fracasso, Hennie Valkenier, Jan C. Hummelen, Gemma C. Solomon, and Ryan C. Chiechi. Evidence for quantum interference in SAMs of arylethynylene thiolates in tunneling junctions with eutectic Ga-In (EGaIn) top-contacts. *J. Am. Chem. Soc.*, 133(24):9556–9563, 2011.

[15] Natalie Gorczak, Nicolas Renaud, Simge Tarkuç, Arjan J. Houtepen, Rienk Eelkema, Laurens D. A. Siebbeles, and Ferdinand C. Grozema. Charge transfer versus molecular conductance: molecular orbital symmetry turns quantum interference rules upside down. *Chem. Sci.*, 6(7):4196–4206, 2015.

[16] Constant M. Guédon, Hennie Valkenier, Troels Markussen, Kristian S. Thygesen, Jan C. Hummelen, and Sense Jan van der Molen. Observation of quantum interference in molecular charge transport. *Nature Nanotech.*, 7(5):305–309, 2012.

[17] Carlos R. Arroyo, Simge Tarkuc, Riccardo Frisenda, Johannes S. Seldenthuis, Charlotte H. M. Woerde, Rienk Eelkema, Ferdinand C. Grozema, and Herre S. J. van der Zant. Signatures of quantum interference effects on charge transport through a single benzene ring. *Angew. Chem. Int. Ed.*, 52(11):3152–3155, 2013.

[18] Hennie Valkenier, Constant M Guédon, Troels Markussen, Kristian S Thygesen, Sense J van der Molen, and Jan C Hummelen. Cross-conjugation and quantum interference: a general correlation? *Phys. Chem. Chem. Phys.*, 16(2):653–662, 2014.

[19] Qi Lu, Ke Liu, Hongming Zhang, Zhibo Du, Xianhong Wang, and Fosong Wang. From tunneling to hopping: A comprehensive investigation of charge transport mechanism in molecular junctions based on oligo(*p*-phenylene ethynylene)s. *ACS Nano*, 3(12):3861–3868, 2009.

[20] Jeremy M. Beebe, BongSoo Kim, J. W. Gadzuk, C. Daniel Frisbie, and James G. Kushmerick. Transition from direct tunneling to field emission in metal-molecule-metal junctions. *Phys. Rev. Lett.*, 97:026801, 2006.

[21] Jeremy M. Beebe, BongSoo Kim, C. Daniel Frisbie, and James G. Kushmerick. Measuring relative barrier heights in molecular electronic junctions with transition voltage spectroscopy. *ACS Nano*, 2(5):827–832, 2008.

[22] Neil Bennett, Gengzhao Xu, Louisa J. Esdaile, Harry L. Anderson, J. Emyr Macdonald, and Martin Elliott. Transition voltage spectroscopy of porphyrin molecular wires. *Small*, 6(22):2604–2611, 2010.

[23] Shaoyin Guo, Joshua Hihath, Ismael Díez-Pérez, and Nongjian Tao. Measurement and statistical analysis of single-molecule current-voltage characteristics, transition voltage spectroscopy, and tunneling barrier height. *J. Am. Chem. Soc.*, 133 (47):19189–19197, 2011.

[24] BongSoo Kim, Seong Ho Choi, X.-Y. Zhu, and C. Daniel Frisbie. Molecular tunnel junctions based on π-conjugated oligoacene thiols and dithiols between Ag, Au, and Pt contacts: Effect of surface linking group and metal work function. *J. Am. Chem. Soc.*, 133(49):19864–19877, 2011.

[25] M. Christina Lennartz, Nicolae Atodiresei, Vasile Caciuc, and Silvia Karthäuser. Identifying molecular orbital energies by distance-dependent transition voltage spectroscopy. *J. Phys. Chem. C*, 115(30):15025–15030, 2011.

[26] Guillaume Ricœur, Stéphane Lenfant, David Guérin, and Dominique Vuillaume. Molecule/electrode interface energetics in molecular junction: A transition voltage spectroscopy study. *J. Phys. Chem. C*, 116(39):20722–20730, 2012.

[27] Xavier Lefèvre, Fabrice Moggia, Olivier Segut, Yu-Pu Lin, Younal Ksari, Grégory Delafosse, Kacem Smaali, David Guérin, Vincent Derycke, Dominique Vuillaume, Stéphane Lenfant, Lionel Patrone, and Bruno Jousselme. Influence of molecular organization on the electrical characteristics of π-conjugated self-assembled monolayers. *J. Phys. Chem. C*, 119(10):5703–5713, 2015.

[28] Shaoyin Guo, Gang Zhou, and Nongjian Tao. Single molecule conductance, thermopower, and transition voltage. *Nano Lett.*, 13(9):4326–4332, 2013.

[29] Ioan Bâldea. Interpretation of stochastic events in single-molecule measurements of conductance and transition voltage spectroscopy. *J. Am. Chem. Soc.*, 134(18): 7958–7962, 2012.

[30] Masaaki Araidai and Masaru Tsukada. Theoretical calculations of electron transport in molecular junctions: Inflection behavior in Fowler-Nordheim plot and its origin. *Phys. Rev. B*, 81:235114, 2010.

[31] Everardus H. Huisman, Constant M. Guédon, Bart J. van Wees, and Sense Jan van der Molen. Interpretation of transition voltage spectroscopy. *Nano Lett.*, 9(11): 3909–3913, 2009.

[32] Jingzhe Chen, Troels Markussen, and Kristian S. Thygesen. Quantifying transition voltage spectroscopy of molecular junctions: *Ab initio* calculations. *Phys. Rev. B*, 82: 121412, 2010.

[33] Ioan Bâldea. Ambipolar transition voltage spectroscopy: Analytical results and experimental agreement. *Phys. Rev. B*, 85:035442, 2012.

[34] Aaron Tan, Janakiraman Balachandran, Barry D. Dunietz, Sung-Yeon Jang, Vikram Gavini, and Pramod Reddy. Length dependence of frontier orbital alignment in aromatic molecular junctions. *Appl. Phys. Lett.*, 101(24):243107, 2012.

[35] Gunuk Wang, Yonghun Kim, Seok-In Na, Yung Ho Kahng, Jamin Ku, Sungjun Park, Yun Hee Jang, Dong-Yu Kim, and Takhee Lee. Investigation of the transition voltage spectra of molecular junctions considering frontier molecular orbitals and the asymmetric coupling effect. *J. Phys. Chem. C*, 115(36):17979–17985, 2011.

[36] Ayelet Vilan, David Cahen, and Eli Kraisler. Rethinking transition voltage spectroscopy within a generic taylor expansion view. *ACS Nano*, 7(1):695–706, 2013.

[37] K. Sotthewes, C. Hellenthal, A. Kumar, and H. J. W. Zandvliet. Transition voltage spectroscopy of scanning tunneling microscopy vacuum junctions. *RSC Adv.*, 4: 32438–32442, 2014.

[38] Ryan C. Chiechi, Emily A. Weiss, Michael D. Dickey, and George M. Whitesides. Eutectic Gallium–Indium (EGaIn): A moldable liquid metal for electrical characterization of self-assembled monolayers. *Angew. Chem. Int. Ed.*, 120(1):148–150, 2008.

[39] William F. Reus, Martin M. Thuo, Nathan D. Shapiro, Christian A. Nijhuis, and George M. Whitesides. The SAM, not the electrodes, dominates charge transport in metal-monolayer//Ga_2O_3/Gallium–Indium eutectic junctions. *ACS Nano*, 6(6): 4806–4822, 2012.

[40] Christian A. Nijhuis, William F. Reus, Jabulani R. Barber, and George M. Whitesides. Comparison of SAM-based junctions with Ga_2O_3/EGaIn top electrodes to other large-area tunneling junctions. *J. Phys. Chem. C*, 116(26):14139–14150, 2012.

[41] Emily A. Weiss, George K. Kaufman, Jennah K. Kriebel, Zhefeng Li, Richard Schalek, and George M. Whitesides. Si/SiO_2-templated formation of ultraflat metal surfaces on glass, polymer, and solder supports: Their use as substrates for self-assembled monolayers. *Langmuir*, 23(19):9686–9694, 2007.

[42] Tarek Abu-Husein, Swen Schuster, David A. Egger, Martin Kind, Tobias Santowski, Adrian Wiesner, Ryan Chiechi, Egbert Zojer, Andreas Terfort, and Michael Zharnikov. The effects of embedded dipoles in aromatic self-assembled monolayers. *Adv. Func. Mater.*, 25:3943–3957, 2015.

[43] J. B. Neaton, Mark S. Hybertsen, and Steven G. Louie. Renormalization of molecular electronic levels at metal-molecule interfaces. *Phys. Rev. Lett.*, 97:216405, 2006.

[44] Su Ying Quek, Latha Venkataraman, Hyoung Joon Choi, Steven G. Louie, Mark S. Hybertsen, and J. B. Neaton. Amine-gold linked single-molecule circuits: Experiment and theory. *Nano Lett.*, 7(11):3477–3482, 2007.

[45] Dana M. Alloway, Michael Hofmann, Darrin L. Smith, Nadine E. Gruhn, Amy L. Graham, Ramon Colorado, Vicki H. Wysocki, T. Randall Lee, Paul A. Lee, and Neal R. Armstrong. Interface dipoles arising from self–assembled monolayers on gold: UV–photoemission studies of alkanethiols and partially fluorinated a lkanethiols. *J. Phys. Chem. B*, 107(42):11690–11699, 2003.

[46] Davide Fracasso, Mutlu Iskender Muglali, Michael Rohwerder, Andreas Terfort, and Ryan C. Chiechi. Influence of an atom in EGaIn/Ga_2O_3 tunneling junctions comprising self-assembled monolayers. *J. Phys. Chem. C*, 117(21):11367–11376, 2013.

[47] Hyo Jae Yoon, Kung Ching Liao, Matthew R. Lockett, Sen Wai Kwok, Mostafa Baghbanzadeh, and George M. Whitesides. Rectification in tunneling junctions: 2,2'-bipyridyl-terminated n-alkanethiolates. *J. Am. Chem. Soc.*, 136(49):17155–17162, 2014.

[48] Gustavo M. Morales, Ping Jiang, Shenwen Yuan, Youngu Lee, Arturo Sanchez, Wei You, and Luping Yu. Inversion of the rectifying effect in diblock molecular diodes by protonation. *J. Am. Chem. Soc.*, 127(30):10456–10457, 2005.

[49] Youngu Lee, Brian Carsten, and Luping Yu. Understanding the anchoring group effect of molecular diodes on rectification. *Langmuir*, 25(3):1495–1499, 2009.

[50] Ismael Díez-Pérez, Joshua Hihath, Youngu Lee, Luping Yu, Lyudmyla Adamska, Mortko A. Kozhushner, Ivan I. Oleynik, and Nongjian Tao. Rectification and stability of a single molecular diode with controlled orientation. *Nature Chem.*, 1(8): 635–641, 2009.

[51] Gaibo Zhang, Mark A. Ratner, and Matthew G. Reuter. Is molecular rectification caused by asymmetric electrode couplings or by a molecular bias drop? *J. Phys. Chem. C*, 119(11):6254–6260, 2015.

[52] Orlando M. Cabarcos, Andrey Shaporenko, Tobias Weidner, Sundararajan Uppili, Linda S. Dake, Michael Zharnikov, and David L. Allara. Physical and electronic structure effects of embedded dipoles in self-assembled monolayers: Characterization of mid-chain ester functionalized alkanethiols on Au(111). *J. Phys. Chem. C*, 112(29):10842–10854, 2008.

[53] Jochen Heyd, Gustavo E. Scuseria, and Matthias Ernzerhof. Hybrid functionals based on a screened coulomb potential. *J. Chem. Phys.*, 118(18):8207–8215, 2003.

[54] Jochen Heyd, Gustavo E. Scuseria, and Matthias Ernzerhof. Erratum: "hybrid functionals based on a screened coulomb potential" [j. chem. phys.118, 8207 (2003)]. *J. Chem. Phys.*, 124(21):219906, 2006.

[55] G. Kresse and J. Furthmüller. Efficient iterative schemes for *ab initio* total-energy calculations using a plane-wave basis set. *Phys. Rev. B*, 54:11169–11186, 1996.

[56] Ferdinand Rissner, David A. Egger, Amir Natan, Thomas Körzdörfer, Stephan Kümmel, Leeor Kronik, and Egbert Zojer. Collectively induced quantum-confined stark effect in monolayers of molecules consisting of polar repeating units. *J. Am. Chem. Soc.*, 133(46):18634–18645, 2011.

[57] Navit Dori, Mahesh Menon, Lennart Kilian, Moritz Sokolowski, Leeor Kronik, and Eberhard Umbach. Valence electronic structure of gas-phase 3,4,9,10-perylene tetracarboxylic acid dianhydride: Experiment and theory. *Phys. Rev. B*, 73:195208, 2006.

[58] Anna M. Track, Ferdinand Rissner, Georg Heimel, Lorenz Romaner, Daniel Käfer, Asif Bashir, Gerold M. Rangger, Oliver T. Hofmann, Tomáš Bučko, Gregor Witte, and Egbert Zojer. Simultaneously understanding the geometric and electronic structure of anthraceneselenolate on Au(111): A combined theoretical and experimental study. *J. Phys. Chem. C*, 114(6):2677–2684, 2010.

[59] Ariel Biller, Isaac Tamblyn, Jeffrey B. Neaton, and Leeor Kronik. Electronic level alignment at a metal-molecule interface from a short-range hybrid functional. *J. Chem. Phys.*, 135(16):164706, 2011.

[60] David A. Egger, Zhen-Fei Liu, Jeffrey B. Neaton, and Leeor Kronik. Reliable energy level alignment at physisorbed molecule-metal interfaces from density functional theory. *Nano Lett.*, 15(4):2448–2455, 2015.

[61] A. Natan, L. Kronik, H. Haick, and R.T. Tung. Electrostatic properties of ideal and non-ideal polar organic monolayers: Implications for electronic devices. *Adv. Mater.*, 19(23):4103–4117, 2007.

[62] Georg Heimel, Ferdinand Rissner, and Egbert Zojer. Modeling the electronic properties of π-conjugated self-assembled monolayers. *Adv. Mater.*, 22(23):2494–2513, 2010.

[63] Bernhard Kretz, David A. Egger, and Egbert Zojer. A toolbox for controlling the energetics and localization of electronic states in self-assembled organic monolayers. *Adv. Sci.*, 2(3):1400016, 2015.

[64] Sriharsha V. Aradhya, Jeffrey S. Meisner, Markrete Krikorian, Seokhoon Ahn, Radha Parameswaran, Michael L. Steigerwald, Colin Nuckolls, and Latha Venkataraman. Dissecting contact mechanics from quantum interference in single-molecule junctions of stilbene derivatives. *Nano Lett.*, 12(3):1643–1647, 2012.

[65] Jianlong Xia, Brian Capozzi, Sujun Wei, Mikkel Strange, Arunabh Batra, Jose R. Moreno, Roey J. Amir, Elizabeth Amir, Gemma C. Solomon, Latha Venkataraman, and Luis M. Campos. Breakdown of interference rules in azulene, a nonalternant hydrocarbon. *Nano Lett.*, 14(5):2941–2945, 2014.

[66] John P. Perdew, Kieron Burke, and Matthias Ernzerhof. Generalized gradient approximation made simple. *Phys. Rev. Lett.*, 77:3865–3868, 1996.

3

DIPOLE-INDUCED ASYMMETRIC CONDUCTION

Abstract: *In this chapter we, for the first time, relate the intrinsic molecular dipole moment of a SAM to asymmetry in the current/voltage characteristic. We tested the statistical significance of the effect and ascribed it to the collective action of embedded dipoles arising from pyrimidyl groups that are arranged parallel or antiparallel to the transport direction. Additional calculations reveal, that the bias-induced (de)localization of the frontier states that mitigate transport is the cause of the observed asymmetry.*

The contents of this chapter were published in RSC Advances, Royal Society of Chemistry (10.1039/c6ra10471a). I would like to thank Tarek Abu-Husein and Andreas Terfort for synthesis and purification of the molecules studied herein and David Egger and Egbert Zojer for performing in-depth DFT calculations on the monolayers.

3.1. INTRODUCTION

Research efforts in Molecular Electronics fall into two broad and complementary experimental approaches to constructing tunneling junctions: single-molecule and large-area. The principal goal of the former is to develop a fundamental understanding of electron transport through junctions comprising single molecules, a construct that is relatively straightforward to treat computationally. The principal goal of the latter is functionality on the device-level, utilizing ensembles of molecules, usually in the form of SAMs, to define the properties and the smallest dimension of the junction.[1] There are many phenomena that are unique to single-molecule junctions and that cannot be replicated in SAM-junctions; for example, contacting a molecule in different positions along its long axis,[2] modulating conductance by changing rupture mechanics[3, 4] and utilizing anchoring groups that bind to electrodes through weak, non-covalent interactions.[5] Likewise, SAMs exhibit collective effects that cannot be observed at the single-molecule level; for example, odd-even effects driven by the conformation of close-packed alkyl chains[6–8] and the collective action of molecular dipoles affecting transition voltages (V_{trans}) by shifting vacuum levels.[9, 10] Although single-molecule junctions are generally studied in greater detail, the technological relevance of SAM-junctions is more apparent and mature.[11] In this chapter, we report the asymmetric conduction in tunneling junctions using eutectic Ga-In (EGaIn) top-contacts [12] that is driven by the collective action of dipole moments embedded in a SAM comprising molecules of identical empirical formula, frontier orbital energies (for isolated molecules) and interfaces with the electrodes (Figure 3.1 on the left).

Zhang *et al.* have shown theoretically that asymmetry in J/V characteristics can be caused by internal dipoles, if they induce an asymmetric voltage drop across the junction.[13] We observed asymmetric J/V curves in junctions comprising SAMs of photosystem I (PSI) using both EGaIn and conducting-probe AFM.[14] The direction of this asymmetry could not be ascribed to the electron-transport chain within the PSI complexes, rather it correlated to the net dipole induced by the peptide chains on the periphery. Although the mechanism seems obvious, it has received little experimental attention. And, while the results with PSI seem intuitive (and do induce a shift in vacuum level),[15] the complexity of large protein complexes makes it difficult to isolate the underlying cause of the asymmetry. Thus, we turned to small molecules.

3.2. RESULTS AND DISCUSSION

The SAMs we chose for this study (TP1-down, TP1-up; Figure 3.1) have been extensively characterized by a number of techniques: High-resolution X-ray photoelectron spectroscopy (XPS), ellipsometry, infrared reflection absorption spectroscopy, near-edge X-ray absorption fine structure spectroscopy (NEXAFS), and scanning tunneling microscopy (STM).[16] They exhibit nearly identical packing densities, thicknesses and tilt angles (see Table 3.1). The key difference is the orientation of a central pyrimidyl moiety that reverses the direction of its contribution to the net dipole moment along the direction of transport. These dipole moments act collectively in SAMs to affect the electrostatic profile across the junction[17, 18] (*i.e.*, spanning the electrodes.) We previously observed this effect experimentally in SAMs of three series of compounds as a shift in the work

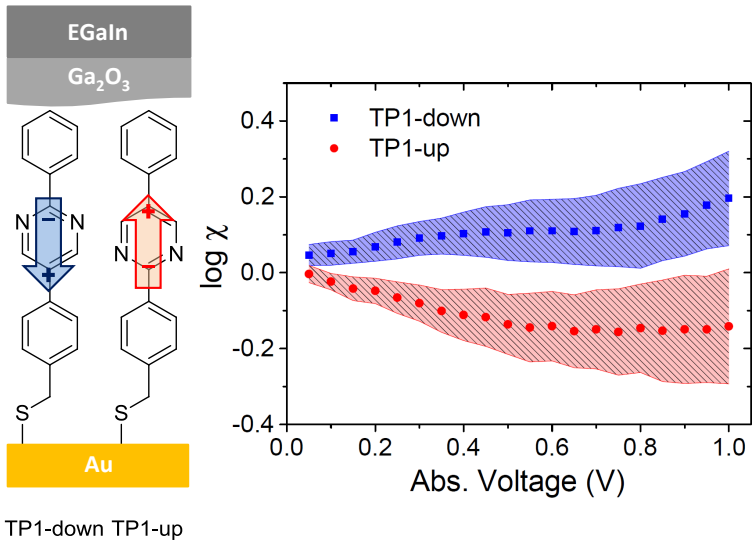

Figure 3.1 Left: Schematic of a junction with two pyrimidyl-containing compounds (TP1-down and TP1-up) in junctions with Au and EGaIn electrodes. Arrows indicate directions of dipole moments associated with the embedded pyrimidine rings (from negative to positive). Right: Plots of asymmetry (log χ, log of the ratio of $|J|$ at each value of $|V|$) versus absolute voltage for SAMs of TP1-down (blue squares) and TP1-up (red circles) with 95 % confidence intervals depicted as shaded areas.

function (WF) of the bottom electrode (described in Chapter 2) and characterized its impact on tunneling charge-transport.[9, 10] Thus, the compounds used to form the SAMs in this study are regioisomers with nearly identical frontier orbitals (Figure 3.4) that form tunneling junctions of nearly identical geometries (Table 2.1.)

SAM	Effective thickness (nm)	Packing density (molecules/cm^2)	Tilt angle
TP1-up	1.74 ± 0.05	4.2×10^{14}	18 ± 3°
TP1-down	1.75 ± 0.05	4.3×10^{14}	17 ± 3°

Table 3.1 Effective thicknesses, packing densities and tilt angles of SAMs of TP1-up and TP1-down determined by ellipsometry, XPS and NEXAFS, respectively. Experimental values are from Ref. 16.

We measured the J/V characteristics of SAMs of TP1-up and TP1-down on template-stripped gold (Au^{TS}) by contacting them with sharp tips of EGaIn as described elsewhere. [10] The absolute value of current density J is dominated by tunneling distance d (which is identical for both SAMs) and we observe statistically indistinguishable conductance at negative bias and ordinary, bowl-shaped conductance associated with non-resonant tunneling. However, the magnitude of J differs at positive bias, creating asymmetry; *i.e.*, TP1-down is more conductive at positive bias than negative bias and *vice versa*. To quantify this behavior we use an asymmetry parameter χ, defined as $\chi = |J^+(V)/J^-(V)|$, and plot log χ versus $|V|$ (Figure 3.1). We show confidence intervals as error bars to high-

light that values of log χ are statistically different across the full bias window; however, we cannot resolve whether Δlog χ saturates or continues to increase with bias. Furthermore, to analyze statistical significance of an effect in J/V and χ data we carried out a Welch's t-test to compute the p-value comparing histograms of $log\,|J|$ and $log\,\chi$ for TP1-up and TP1-down at each voltage step (see Figure 3.2). A p-value, in this instance, is a measure of the probability of the difference in the mean values of the two histograms being due to random chance *i.e.*, with what statistical certainty we can claim that the dipole moment is affecting J or χ. Low p-values mean that the null hypothesis is likely to be false, *i.e.*, an effect is unlikely to be due to random chance. The χ plot has 95% CI as error bars simply by convention, such that our plots are easily comparable to the literature. However, all values of χ past 0.2 V also pass the much more rigorous 99.9% confidence test. Thus, we can state with 99.9% statistical certainty that J differs at positive bias and that χ differs almost everywhere and that the difference is not due to random fluctuations.

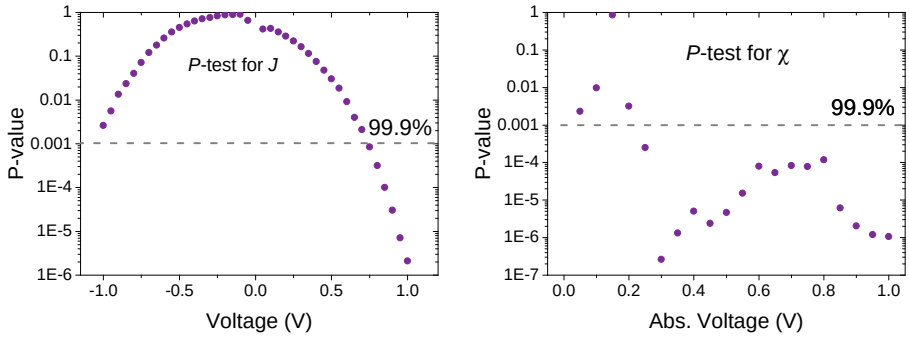

Figure 3.2 Determination of statistical significance of an effect between SAMs of TP1-up and TP1-down using a p-test in current density (J, on the left) and asymmetry (χ, on the right) parameters. Dashed line corresponds to the chosen confidence level of 99.9%. The p-test for J shows that the null hypothesis can be rejected with a high degree of certainty for high positive bias, *i.e.*, the statistical certainty of the difference in distributions of J being due to an experimental effect and not random chance is > 99.9%. For χ all values past 0.2 V show statistical significance of the effect.

The absolute value of log χ is small compared to previous reports of SAM-based rectifiers based on localized π systems combined with n-alkyl chains.[19, 20] However, the mechanism of rectification in those SAMs requires an intrinsic molecular property—isolated, accessible states in the gap—and is therefore unrelated to our observation that the direction of asymmetry is correlated to the direction of embedded dipole moment.

To explain asymmetric J/V behavior we first compared it to the asymmetry in SAMs of PSI.[14] According to that model, co-direction of the internal, perpendicular dipole moment of the SAM with the flow of electrons (which is incorrectly labeled as J in Ref. 14) should result in higher current than anti-direction. Thus, TP1-up should be more conductive under positive bias and TP1-down at negative bias. However, we observe the opposite. To obtain further insight into the mechanism responsible for rectification, we calculated the transmission probability for TP1-up and TP1-down employing the model of single-molecule junctions consisting of an isolated TP1-up, respectively, TP1-down molecule and two Au clusters as electrodes. These simulations are not meant as mod-

els for Au^{TS}/SAM//EGaIn junctions, rather they are meant to isolate the effects of the intrinsic electronic properties of TP1-up and TP1-down on transmission by examining a single molecule between ideal Au electrodes. If these transmission spectra differ, we cannot ascribe asymmetric conduction *only* to collective effects arising from packing into a SAM. The resulting transmission spectra (Figure 3.3) are essentially identical for the two molecules. Consistent with the discussions in Refs.10, 21 and 22, this result implies that the peculiar transport properties of TP1-up and TP1-down layers must arise solely from collective electrostatic effects induced by the parallel alignment of the pyrimidine dipoles within the SAMs.[21, 22] One can imagine that these effects induce asymmetric conduction either by affecting the level alignment in a peculiar way or by changing the nature of the molecular states such that, *e.g.*, their spatial localization and the resulting transmission depend on the bias direction.

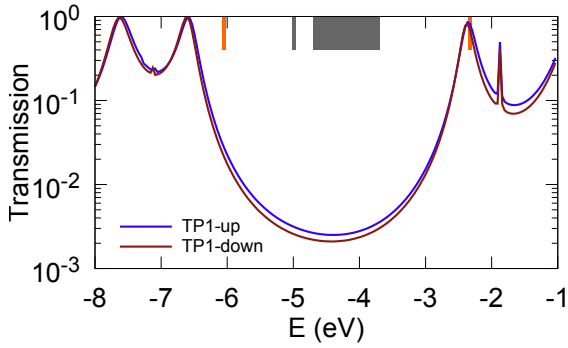

Figure 3.3 Calculated zero-bias transmission probabilities for TP1-up (blue) and TP1-down (red) single-molecule junctions plotted against energy (eV). The molecules are bound to face-centred cubic (FCC) hollow sites on Au(111) electrodes in their minimized geometries using identical Au-S lengths and angles. The top Au(111) contacts are physisorbed at equal lengths and angles. The gas-phase HOMO and LUMO are marked with orange bars along the top at −6.03 and −2.35 eV respectively. The thin grey bar shows the uncorrected Fermi energy $E_f = -4.96$ eV and the thick grey bar estimates the range of E_f for EGaIn.

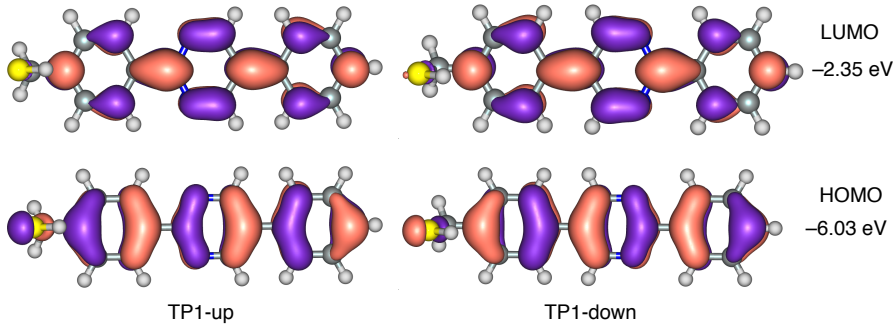

Figure 3.4 Visualizations of the frontier orbitals of TP1-up and TP1-down showing subtle differences in the symmetries, particularly near the pyrimidyl rings.

In order to clarify the effects of packing in a SAM on transport, we first consider the details of the level-alignment at the interface(s). Explicitly modelling the behavior of the entire Au/SAM//Ga_2O_3/EGaIn is beyond the scope of this work, as the atomistic structure of the interface between Ga_2O_3 and the SAM is far from fully understood, particularly with respect to the strength of the coupling between the EGaIn electrode and the SAM. One can, however, draw insightful conclusions from considering two limiting cases; (i) a much weaker coupling between the SAM and EGaIn than between the SAM and Au and (ii) comparable coupling between the SAM and both electrodes. The former case is reminiscent of I/V measurements by STM, where the top electrode is decoupled from the SAM by vacuum and the bias direction determines whether transport occurs through occupied or unoccupied states. Non-zero values of $\log \chi$ are observed when the Fermi level E_f of the Au electrode (which is strongly coupled to the SAM) does not lie in the exact center of the gap between these states. Since the values of $\log \chi$ are positive for TP1-down and negative for TP1-up, this mechanism would require that the highest occupied π-state (HOPS) of SAMs of TP1-down lie closer to E_f than the lowest unoccupied π-state (LUPS) and *vice versa* for TP1-up. However, this situation is at odds with simulations of the projected density of states (PDOS) of these SAMs bonded to Au, where the occupied states are closer to E_f for both SAMs (Chapter 2, Figure 2.4). The same study shows that the experimental values of $|V_{trans}|$ are comparable under positive and negative bias for both SAMs as well, which is only possible if transport takes place only through the HOPS. The other limiting case—assuming similar couplings between the SAM and the electrodes on both sides of the junction—is not unreasonable considering that the layer of Ga_2O_3 is on the order of 7 Å[23] and that there is a methylene spacer between the Au-thiolate anchor and the π-backbone. The aforementioned similarity in $|V_{trans}|$ also supports this hypothesis. In this scenario transport takes place through only one set of frontier states and, therefore, differences between the offsets of the HOPS and LUPS with the electrodes do not affect transport as they do in the case of weak coupling. Asymmetry is not expected in this case since the HOPS spans the junction as is assumed to couple similarly to both electrodes. Thus, transport through the LUPS is almost certainly not responsible for the observed trend in χ. In either case, there is no apparent reason why the level alignment should lead to non-zero values of $\log \chi$.

Having reasonably excluded level-alignment as the cause of asymmetry, we propose an alternative explanation based on bias-dependent de/localization of the frontier π states in SAMs of TP1-up and TP1-down. This electrostatic effect is related to the collective action of the dipoles of the pyrimidine rings spatially shifting the HOPS in TP1-down (TP1-up) towards (away from) the Au electrode. It is particularly evident when comparing the plane-averaged charge-density associated with the first peak in the PDOS of the SAM averaged over planes parallel to the surface, which is shown in Figure 3.5 and were calculated with density functional theory using the VASP code,[24] employing the HSE06 hybrid functional.[25, 26] That this de/localization is a consequence of collective electrostatics can be seen by comparing the plane-averaged charge-densities associated with the HOPS of isolated TP1-up and TP1-down molecules and the respective free-standing SAMs; the densities associated with the HOPS of isolated TP1-up and TP1-down molecules (orange lines, Figure 3.5 b and c) are virtually identical. The free-standing SAMs (grey shaded curves), however, differ from the isolated molecules and instead display es-

sentially the same localization as the SAMs bound to Au (Figure 3.5 a). Thus, the spatial distribution of the orbitals through which transport occurs—the HOPS—is defined by the electrostatic environment of the SAM that results from the alignment of dipoles.

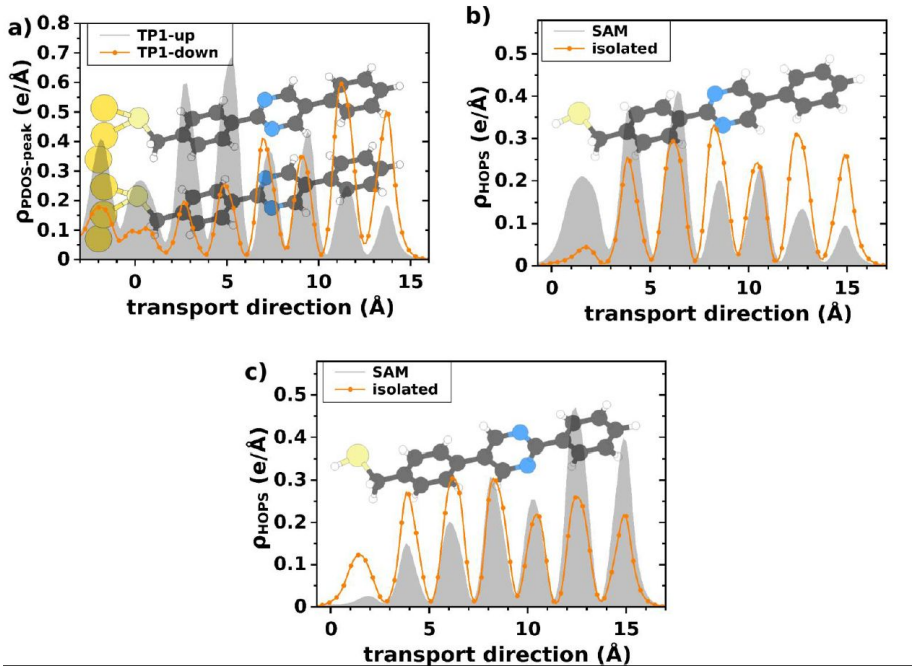

Figure 3.5 Plane-averaged charge density associated with the highest occupied peaks in the PDOS (derived from the molecular HOMO) of SAMs of TP1-up and TP1-down bonded to a Au electrode (panel a); the highest occupied π-state in the SAMs (without the electrode) and isolated molecules of TP1-up (panel b) and TP1-down (panel c). Note that for the SAMs without the Au electrode we plotted the charge density associated with the Γ-point of the corresponding band. The z-position of the first atom of the molecules/SAMs is chosen as the zero of the horizontal axis. Schematic representations of the structures[27] are shown as a guide to the eye. All calculations on free-standing and Au-bonded SAMs rely on a periodic arrangement of the molecules.

The distribution of the HOPS at zero bias alone does not explain the asymmetric conductance. There are two important considerations. First, the difference in couplings between the Au/SAM and SAM/EGaIn interfaces cannot be discounted entirely. Second, considering that the localization of the HOPS is a consequence of the dipole-induced potential steps within the SAMs, one should expect a further de/localization of the states depending on the direction of the applied bias; *i.e.*, when the external field points in the same direction as the molecular dipole moment, localization should be reduced and *vice versa*. Assuming a direct correlation between delocalization and transmission, J should be higher in magnitude for TP1-down and lower for TP1-up at positive bias, which is exactly what we observe (Figure 3.1).

To test the influence of bias on the direction-dependent localization of the states, we simulated the electronic structure of the two SAMs in an applied external field. This calculation can be done for the (hypothetical) free-standing SAMs in a relatively straight-

forward manner and we know from the data shown in Figure 3.5 that the presence of the Au-electrode does not qualitatively alter the localization. The choice of the free-standing SAM as a model system has the additional advantage that it allows SAM-related effects and interface-related effects to be separated and does not require guessing at the atomistic details of the SAM/Ga_2O_3 interface. The results of these simulations are shown in Figure 3.6, confirming the hypothesis that the localization of states depends both on the direction of the dipole and the applied field (note that the definitions of the direction of the electric field, from + to −, and the dipole moment, from − to +, differ.) Provided that the coupling at the side of the SAM where the charge-density is lower limits the current through the junction, positive bias (further localizing the HOPS) will lead to $\log \chi < 0$ in SAMs of TP1-up. Conversely, by *de*localizing the HOPS in SAMs of TP1-down, it will lead to $\log \chi > 0$, in agreement with our experimental observations.

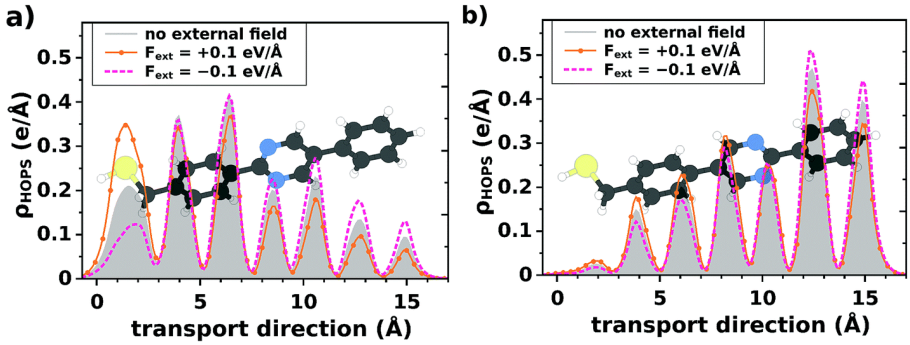

Figure 3.6 Plane-averaged charge density associated with the highest occupied π-state in the SAM (at the Γ-point; without Au electrode) for TP1-up (panel a) and TP1-down (panel b), as a function of an externally applied electric field. The coordinate of the first atom of the SAM is chosen as the zero for the horizontal axis. Schematic representations of the structures are shown as a guide to the eye. As screening effects are self-consistently considered in our simulations, we can estimate the average electric field within the SAM from the magnitude of the electrostatic energy in the vacuum regions above and below the free-standing monolayer. We find that screening is significant and that for an external field of 0.1 eVÅ^{-1} the average internal field in the case of TP1-up amounts to 0.018 eVÅ^{-1}. Assuming an oxide thickness of 0.7 nm and a dielectric constant of 10 for β-Ga_2O_3,[28] this field corresponds to a bias of 0.4 V—well within the experimental range.

3.3. CONCLUSIONS

We observed a statistically significant asymmetry in tunneling charge-transport through SAMs of TP1-up and TP1-down. The direction of bias at which the conductance is higher correlates with the direction of the dipole moments arising from the central pyrimidine rings. The cause of this asymmetry is likely the result of the electrostatic profile of the SAMs arising from the collective effects of aligned dipoles affecting the de/localization

of the frontier states. This mechanism is distinct from mechanisms that rely on isolated π systems or transport that occurs through both occupied and unoccupied states in that it is solely attributable to the supramolecular structure of the SAM.

3.4. EXPERIMENTAL DETAILS

Sample preparation. The Au substrates were prepared by mechanical template stripping (TS) as described elsewhere.[29] We deposited 100 nm of Au (99.99%) by thermal vacuum deposition onto a 3" Silicon wafer (with no adhesion layer). Using UV-curable optical adhesive (OA) Norland 61, 1 cm^2 glass chips are glued on the metal surface. All samples were prepared following the procedure from Ref. 16. In brief: freshly cleaved gold slides were incubated in 1 mM solutions in ethanol at room temperature for ~ 24h. Prior to making a solution ethanol was degassed by bubbling nitrogen gas through for at least 20 minutes and all solutions were kept under nitrogen atmosphere to prevent undesirable oxidation of thiol anchoring group. All compounds were synthesized and purified according to Ref. 16.

Data acquisition and analysis. Data were acquired in a home-built setup that is described in detail elsewhere.[30] Samples were taken out from solution, carefully rinsed with pure ethanol and gently dried with nitrogen. Each SAM was then measured by placing a sharp tip of EGaIn in visual contact with the surface and acquiring at least 1000 scans across 10 substrates. In all measurements the EGaIn tip was biased, while the substrate was grounded. The traces in which the instrument reached compliance were considered short circuits and were discarded (they reflect only the compliance limit of the instrument and have no physical meaning). TP1-up showed lower solubility than and TP1-down and showed signs of partial precipitation onto the gold surface leading to the appearance of traces where values of J were systematically *ca.* two of orders of magnitude lower than the geometric mean. These traces, which were present only in TP1-up data and made up a small fraction of the total traces, most likely reflect junctions comprising multilayers and were discarded. Histograms of the values of J at each value of V were then fit to Gaussian distributions. The standard deviation of a fit (σ) was then recalculated into 95% confidence interval using following equation CI = $t\frac{\sigma}{\sqrt{N}}$, where t is the coefficient in t-distribution and N is the number of degrees of freedom for our system ($N_{junctions}-1$). The same procedure was applied to calculate asymmetry parameter ($log\ \chi$).

Single-molecule transport simulations. We calculated the zero-bias transmission probability for TP1-up and TP1-down in single-molecule junctions using DFT[31] to probe the electronic effects of the molecule/electrode complex on transport. We simulated single-molecule junctions using 11- and 12-atom clusters of Au(111) as electrodes. The "bottom" electrode is coupled through a S-Au bond at a FCC hollow site and the "top" electrode is physisorbed; all angles and distances are conserved. The DOS and transmission curves were calculated with Gaussian 09 using B3LYP/LANL2DZ in accordance with literature procedures.[32] We computed gas-phase orbital energies with Gaussian 09 using HSE06/6-311g*. The frontier orbitals from these calculations are shown in Figure 3.4. The resulting transmission spectra, shown in Figure 3.3, overlap almost completely with only a slight—and insignificant—offset in magnitude. Thus, single-

molecule transmission calculations do not predict any difference in the conductance of TP1-up and TP1-down nor any difference in the frontier orbitals. Thus, the mechanism of asymmetry is likely due to a collective effect that is present in SAM-junctions, but absent in single-molecule junctions.

Simulations employing periodic boundary conditions. The substrate-SAM interfaces and free-standing SAMs were modelled using a $(\sqrt{3} \times 3)$ surface unit-cell containing two molecules in herringbone arrangement as in our previous work.[16] For the isolated molecule calculations the unit cells vectors were doubled 3 times in x- and 2 times in y-direction. In all calculations without a metal surface, the molecules were capped with hydrogen atoms. Our DFT calculations were performed with the plane-wave VASP code[24] applying the HSE screened hybrid functional[25, 26] and an $8 \times 5 \times 1$ k-grid for the laterally periodic systems. In all our calculations, a dipole correction was used. The external electric fields were applied fully self-consistently in our VASP calculations, using the EFIELD tag. In these calculations, we used the wavefunctions of the field-free calculations as a starting guess for the self-consistent field procedures. The use of a hybrid functional for calculating the electronic states in the here considered SAMs and molecules is important to ensure a reliable ordering of the electronic states bearing in mind the different self-interaction errors associated with σ- and π-states among the high-lying occupied orbitals in pyrimidines[33]. Nevertheless, when calculating the molecular orbital densities of the isolated molecules and free-standing SAMs, in some cases a localized state was found to be the HOMO even with the HSE functional, and the delocalized π-orbital was deeper in energy. As only reasonably delocalized orbitals represent relevant transport channels, we analyzed the charge density associated with the highest-lying delocalized orbital, *i.e.*, the highest occupied π-state (HOPS), in all cases. The average field within the TP1-up SAM, for an external field of $-0.1\,\mathrm{eV\AA^{-1}}$, was determined in the following way: the potential step in vacuum to generate the electric field for the free-standing SAM was +2.3 eV. Note that this includes not only the external field present in the calculation, but also the −1.0 eV drop in energy due to the polar monolayer, which we determined self-consistently in a calculation of the free-standing SAM under field-free conditions. Our unit cell in the calculations was 48 Å long, and the thickness of the TP1-up SAM is 18.2 Å. It follows that the total potential drop over the SAM amounts to 0.32 eV, yielding an internal field of $0.018\,\mathrm{eV\AA^{-1}}$. Using the ratio of the external and internal fields, we find that the effective dielectric constant of the SAM is 5.6. We can then determine the total potential drop over a junction in which an average field of $0.018\,\mathrm{eV\AA^{-1}}$ is present in the SAM: as the perpendicular component of the electric displacement field remains constant at the SAM/Ga_2O_3 interface, we obtain for the field within the oxide a value of $E_{Ga_2O_3} = E_{SAM} \times \epsilon_{SAM}/\epsilon_{Ga_2O_3} = 0.01\,\mathrm{eV\AA^{-1}}$. Consequently, the total potential drop including a 7 Å thick dielectric amounts to 0.39 V.

BIBLIOGRAPHY

[1] Yanxi Zhang, Zhiyuan Zhao, Davide Fracasso, and Ryan C. Chiechi. Bottom-up molecular tunneling junctions formed by self-assembly. *Isr. J. Chem.*, 54(5-6):513–533, 2014.

[2] Delia Miguel, Luis Álvarez de Cienfuegos, Ana Martín-Lasanta, Sara P. Mor-

cillo, Linda A. Zotti, Edmund Leary, Marius Bürkle, Yoshihiro Asai, Rocío Jurado, Diego J. Cárdenas, Gabino Rubio-Bollinger, Nicolás Agraït, Juan M. Cuerva, and M. Teresa González. Toward multiple conductance pathways with heterocycle-based oligo(phenyleneethynylene) derivatives. *J. Am. Chem. Soc.*, 137:13818–13826, 2015.

[3] Timothy A. Su, Haixing Li, Michael L. Steigerwald, Latha Venkataraman, and Colin Nuckolls. Stereoelectronic switching in single-molecule junctions. *Nature Chem.*, 7:215–220, 2015.

[4] Mickael L. Perrin, Riccardo Frisenda, Max Koole, Johannes S. Seldenthuis, Jose A. Celis Gil, Hennie Valkenier, Jan C. Hummelen, Nicolas Renaud, Ferdinand C. Grozema, Joseph M. Thijssen, Diana Dulić, and Herre S. J. van der Zant. Large negative differential conductance in single-molecule break junctions. *Nature Nanotech.*, 9:830–834, 2014.

[5] Veerabhadrarao Kaliginedi, Alexander V. Rudnev, Pavel Moreno-Garcia, Masoud Baghernejad, Cancan Huang, Wenjing Hong, and Thomas Wandlowski. Promising anchoring groups for single-molecule conductance measurements. *Phys. Chem. Chem. Phys.*, 16:23529–23539, 2014.

[6] Mostafa Baghbanzadeh, Felice C. Simeone, Carleen M. Bowers, Kung-Ching Liao, Martin Thuo, Mahdi Baghbanzadeh, Michael S. Miller, Tricia Breen Carmichael, and George M. Whitesides. Odd-even effects in charge transport across *n*-alkanethiolate-based SAMs. *J. Am. Chem. Soc.*, 136(48):16919–16925, 2014.

[7] Li Jiang, C. S. Suchand Sangeeth, and Christian A. Nijhuis. The origin of the odd-even effect in the tunneling rates across EGaIn junctions with Self-Assembled Monolayers (SAMs) of *n*-alkanethiolates. *J. Am. Chem. Soc.*, 137(33):10659–10667, 2015.

[8] Aaron Tan, Janakiraman Balachandran, Barry D. Dunietz, Sung-Yeon Jang, Vikram Gavini, and Pramod Reddy. Length dependence of frontier orbital alignment in aromatic molecular junctions. *Appl. Phys. Lett.*, 101(24):243107, 2012.

[9] Davide Fracasso, Mutlu Iskender Muglali, Michael Rohwerder, Andreas Terfort, and Ryan C. Chiechi. Influence of an atom in EGaIn/Ga_2O_3 tunneling junctions comprising Self-Assembled Monolayers. *J. Phys. Chem. C*, 117(21):11367–11376, 2013.

[10] Andrii Kovalchuk, Tarek Abu-Husein, Davide Fracasso, David A. Egger, Egbert Zojer, Michael Zharnikov, Andreas Terfort, and Ryan C. Chiechi. Transition voltages respond to synthetic reorientation of embedded dipoles in self-assembled monolayers. *Chem. Sci.*, 7:781–787, 2016.

[11] Paul A. Van Hal, Edsger C. P. Smits, Tom C. T. Geuns, Hylke B. Akkerman, Bianca C. De Brito, Stefano Perissinotto, Guglielmo Lanzani, Auke J. Kronemeijer, Victor Geskin, Jérôme Cornil, Paul W. M. Blom, Bert De Boer, and Dago M. De Leeuw. Upscaling, integration and electrical characterization of molecular junctions. *Nature Nanotech.*, 3:749–754, 2008.

[12] Ryan C Chiechi, Emily A Weiss, Michael D Dickey, and George M Whitesides. Eutectic Gallium–Indium (EGaIn): A moldable liquid metal for electrical characterization of self-assembled monolayers. *Angew. Chem. Int. Ed.*, 120(1):148–150, 2008.

[13] Gaibo Zhang, Mark A. Ratner, and Matthew G. Reuter. Is molecular rectification caused by asymmetric electrode couplings or by a molecular bias drop? *J. Phys. Chem. C*, 119(11):6254–6260, 2015.

[14] Olga E. Castañeda Ocampo, Pavlo Gordiichuk, Stefano Catarci, Daniel A. Gautier, Andreas Herrmann, and Ryan C. Chiechi. Mechanism of orientation-dependent asymmetric charge transport in tunneling junctions comprising Photosystem I. *J. Am. Chem. Soc.*, 137(26):8419–8427, 2015.

[15] Pavlo I. Gordiichuk, Gert-Jan A. H. Wetzelaer, Dolev Rimmerman, Agnieszka Gruszka, Jan Willem de Vries, Manfred Saller, Daniel A. Gautier, Stefano Catarci, Diego Pesce, Shachar Richter, Paul W. M. Blom, and Andreas Herrmann. Solid-state biophotovoltaic cells containing Photosystem I. *Adv. Mater.*, 26(28):4863–4869, 2014.

[16] Tarek Abu-Husein, Swen Schuster, David A. Egger, Martin Kind, Tobias Santowski, Adrian Wiesner, Ryan Chiechi, Egbert Zojer, Andreas Terfort, and Michael Zharnikov. The effects of embedded dipoles in aromatic self-assembled monolayers. *Adv. Func. Mater.*, 25:3943–3957, 2015.

[17] Amir Natan, Leeor Kronik, Hossam Haick, and Raymond T. Tung. Electrostatic properties of ideal and non-ideal polar organic monolayers: Implications for electronic devices. *Adv. Mater.*, 19(23):4103–4117, 2007.

[18] Georg Heimel, Ferdinand Rissner, and Egbert Zojer. Modeling the electronic properties of π-conjugated self-assembled monolayers. *Adv. Mater.*, 22(23):2494–2513, 2010.

[19] Li Yuan, Rochus Breuer, Li Jiang, Michael Schmittel, and Christian A. Nijhuis. A molecular diode with a statistically robust rectification ratio of three orders of magnitude. *Nano Lett.*, 15(8):5506–5512, 2015.

[20] Hyo Jae Yoon, Kung Ching Liao, Matthew R Lockett, Sen Wai Kwok, Mostafa Baghbanzadeh, and George M Whitesides. Rectification in tunneling junctions: 2,2'-bipyridyl-terminated n-alkanethiolates. *J. Am. Chem. Soc.*, 136(49):17155–17162, 2014.

[21] David A. Egger, Ferdinand Rissner, Egbert Zojer, and Georg Heimel. Polarity switching of charge transport and thermoelectricity in self-assembled monolayer devices. *Adv. Mater.*, 24(32):4403–4407, 2012.

[22] Veronika Obersteiner, David A. Egger, Georg Heimel, and Egbert Zojer. Impact of collective electrostatic effects on charge transport through molecular monolayers. *J. Phys. Chem. C*, 118(38):22395–22401, 2014.

[23] Ludovico Cademartiri, Martin M. Thuo, Christian Albertus Nijhuis, William F. Reus, Simon Tricard, Jabulani R. Barber, Rana N. S. Sodhi, Peter Brodersen, Choongik Kim, Ryan C. Chiechi, and George M. Whitesides. Electrical resistance of Ag^{TS}-$S(CH_2)_{n-1}CH_3$//Ga_2O_3/EGaIn tunneling junctions. *J. Phys. Chem. C*, 116(20): 10848–10860, 2012.

[24] G. Kresse and J. Furthmüller. Efficient iterative schemes for *ab initio* total-energy calculations using a plane-wave basis set. *Phys. Rev. B*, 54:11169–11186, 1996.

[25] Jochen Heyd, Gustavo E. Scuseria, and Matthias Ernzerhof. Hybrid functionals based on a screened coulomb potential. *J. Chem. Phys.*, 118(18):8207–8215, 2003.

[26] Jochen Heyd, Gustavo E. Scuseria, and Matthias Ernzerhof. Erratum: "hybrid functionals based on a screened coulomb potential" [j. chem. phys.118, 8207 (2003)]. *J. Chem. Phys.*, 124(21):219906, 2006.

[27] Anton Kokalj. Xcrysden—a new program for displaying crystalline structures and electron densities. *J. Mol. Graphics Mod.*, 17(3,Äì4):176–179, 1999.

[28] B. Hoeneisen, C.A. Mead, and M-A. Nicolet. Permittivity of β-Ga_2O_3 at low frequencies. *Solid-State Electron.*, 14(10):1057–1059, 1971.

[29] Emily A. Weiss, George K. Kaufman, Jennah K. Kriebel, Zhefeng Li, Richard Schalek, and George M. Whitesides. Si/SiO_2-templated formation of ultraflat metal surfaces on glass, polymer, and solder supports: Their use as substrates for self-assembled monolayers. *Langmuir*, 23(19):9686–9694, 2007.

[30] Davide Fracasso, Hennie Valkenier, Jan C. Hummelen, Gemma C. Solomon, and Ryan C. Chiechi. Evidence for quantum interference in sams of arylethynylene thiolates in tunneling junctions with eutectic ga-in (egain) top-contacts. *J. Am. Chem. Soc.*, 133(24):9556–9563, 2011.

[31] Veronika Obersteiner, David A. Egger, and Egbert Zojer. Impact of anchoring groups on ballistic transport: Single molecule vs monolayer junctions. *J. Phys. Chem. C*, 119 (36):21198–21208, 2015.

[32] Carmen Herrmann, Gemma C. Solomon, Joseph E. Subotnik, Vladimiro Mujica, and Mark A. Ratner. Ghost transmission: How large basis sets can make electron transport calculations worse. *J. Chem. Phys.*, 132(2):024103, 2010.

[33] Ferdinand Rissner, David A. Egger, Amir Natan, Thomas KÖrzdÖrfer, Stephan Kümmel, Leeor Kronik, and Egbert Zojer. Collectively induced quantum-confined stark effect in monolayers of molecules consisting of polar repeating units. *J. Am. Chem. Soc.*, 133(46):18634–18645, 2011.

4

IN-PLACE SWITCHING OF RECTIFICATION

Abstract: *This chapter describes reversible in-place switching of molecular tunneling junctions comprising SAMs between rectifying (diode) and non-rectifying (resistor) states. The switching process is affected by the protonation state of densely-packed carboxylic acid groups at the interface between the top-contact and the monolayer. We studied the switching process by treatment with water and a water scavenger using three different top-contacts. We propose a mechanism in which the tunneling junctions switch to diode behavior through the creation of surface-states that result from the polarization of the monolayer when the carboxylic acid groups are protonated.*

I would like to thank Yong Ai and Yanxi Zhang for performing EGaIn measurements of the SAMs of carboxylic acid, Xinkai Qiu for perfoming AFM measurements and Kasper Nørgaard for performing measurements utilizing reduced graphene oxide as the top electrode.

4.1. INTRODUCTION

Modern information technology relies on computational platforms across a broad range of length-scales from embedded, Internet of Things devices to personal, mobile devices to supercomputing clusters to datacenters. These platforms increasingly demand specialized electronics suited to a particular application, e.g., low-power and neuromorphic chips.[1] Molecular electronics (the transport of charge through molecules spanning two or more electrodes) has tremendous potential for specialized computation because changes at the Ångstrom-scale can translate into exponential effects at the device level.[2] And because the functional units are molecules, these effects can arise from chemical phenomenon like photoisomerization.[3, 4] Molecular diodes, the basis of logic circuits,[5] are now well established both in single-molecule junctions[6] and devices[7] comprising SAMs with EGaIn as a top-contact.[8] However, the realization of new concepts in computation requires new functionality that exploits the chemical nature of Molecular Electronics.

In this chapter we describe the reversible switching of molecular tunneling junctions comprising SAMs between diodes and resistors. The molecules in the SAM are terminated by carboxylic groups ($-CO_2H$), which, when densely packed, can tightly bind protons, affecting surface-states in the SAM, hence the current-density vs. voltage (J/V) characteristics. The rectification ratio, $R = |J(V^+)/J(V^-)|$, of tunneling junctions comprising SAMs is highly sensitive both to the structure of the SAM and of the molecules in the SAM and can be tuned synthetically, *i.e.*, by comparing R between junctions formed from structurally similar SAMs.[9, 10] Rectification can also be induced by breaking the symmetry of electrodes in an electrochemical (ionic) environment.[11] However, these approaches cannot produce a device that can be switched between states because they rely either on comparing different SAMs or different environments around a transient single-molecule junction. Because we alter the properties of the SAM in-place, the same junction can be switched between functioning as a diode and a resistor by switching it between rectifying and non-rectifying states. Moreover, through the use of a photo-acid, we demonstrate that this process can be coupled to light and, therefore, any extrinsic phenomenon that generates free protons.

4.2. RESULTS AND DISCUSSION

We followed literature procedures for forming high-quality SAMs of long-chain ω-thiol carboxylic acids, which require care to avoid the formation of bilayers and internally hydrogen-bonded structures[12]. We grew the SAMs on either template-stripped[13] Au (Au^{TS}) or vapor deposited Au (Au^{VD}) and formed Au^{TS}/SAM//EGaIn, Au^{TS}/SAM//Au^{AFM} and Au^{VD}/SAM//rGO junctions where '/' and '//' denote covalent and van der Waals contacts, respectively, Au^{AFM} is a gold-coated atomic force microscopy (AFM) tip and rGO is reduced graphene oxide.[14] Using EGaIn and Au^{AFM} top-contacts, we switched the J/V characteristics from the as-prepared, non-rectifying (resistor) to the rectifying (diode) state by exposure to water or a photo-acid and back to the non-rectifying state using 2,2-dimethoxypropane (DMP) as a water scavenger.[15]

Figure 4.1a shows the value of $\log|R|$ over two complete switching cycles of alternating exposure to H_2O and DMP. The exposures were performed with liquid and vapour

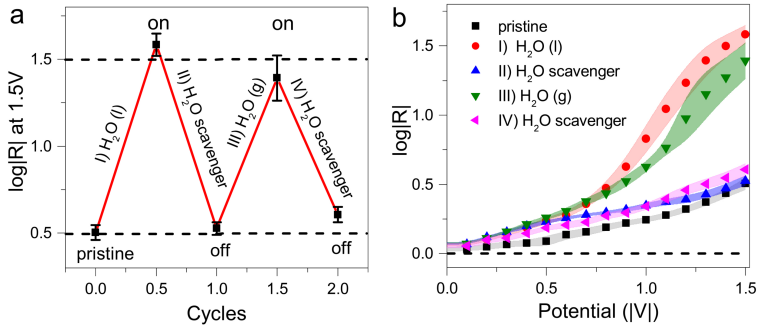

Figure 4.1 In-place switching of the rectification of junctions comprising SAMs of $S(CH_2)_{11}CO_2H$ in $Au^{TS}/S(CH_2)_{11}CO_2H//EGaIn$ junctions. **a,** $\log|R|$ at 1.5 V versus H_2O/DMP switching cycles. **b,** Semilog plots of the rectification ratio ($\log|R|$) versus absolute potential ($|V|$) before and after the SAMs are treated with H_2O or H_2O and then DMP. black, pristine, as-prepared; red, after exposure to H_2O (l); blue, after exposure to H_2O (l) and then DMP; green, after exposure to H_2O (g); magenta, after exposure to H_2O (g) and then DMP.

4

H_2O to highlight that the "on" state can be achieved with both ways. Further cycling past two proved to be difficult as the samples would show fatigue and predominantly short circuit. Figure 4.1b shows semi-log plots of $\log|R|$ vs. full potential window (R/V) curves of $Au^{TS}/S(CH_2)_{11}CO_2H//EGaIn$ junctions. Each value of $\log|R|$ is the peak of a Gaussian fit to a histogram of $\log|R|$ for that value of $|V|$ and the shaded areas are the 99 % confidence intervals. These measurements were performed inside a flowbox with 1 % to 3 % O_2 in N_2 and relative humidity (RH) < 10 %.[16] (The presence of O_2 is necessary to form tips of EGaIn.) It is possible that the non-zero RH induces the small degree of rectification in the as-prepared SAMs (the dashed line in Figure 4.1b shows a perfect resistor, $\log|R| = 0$) or that the asymmetric nature of $Au^{TS}/S(CH_2)_{11}CO_2H//EGaIn$ junctions introduces a slight asymmetry in the J/V characteristics.[7] However, after exposure to H_2O (vapor or liquid), $\log|R|$ increases exponentially with $|V|$. An obvious explanation for this observation is that H_2O in the junction undergoes redox chemistry and the R/V dependence is simply a reflection of the different oxidation reduction potentials; however, that behavior is both time-dependent and hysteretic,[17] neither of which are true for the junctions we measured. Moreover, subsequent exposure to a 1:1 by volume solution of DMP in ethanol returns the R/V curve to the pristine, non-rectifying state, which is a clear indication that no irreversible processes occur during J/V cycling in the rectifying state (*i.e.*, after exposure to H_2O). Although the switching process dampens, the fact that the junctions survive multiple switching cycles proves that the switching mechanism is inherently reversible and can therefore likely be improved with better molecular design and junction/device optimizations.

The junctions are stable in both rectifying and non-rectifying states. To test the robustness of the rectifying state of the SAMs they were heated in a vacuum oven. Figure 4.2 shows that $S(CH_2)_{11}COOH$ is non-rectifying in its pristine state (black). However, upon exposure to liquid water (red) the rectification ratio increases tenfold. There is no significant change in rectification when heating the SAMs up to 80 °C in vacuum (purple). This test shows that water bound to the surface $-CO_2H$ groups through hydrogen bonding is stable under heating and vacuum and, therefore, is not simply phys-

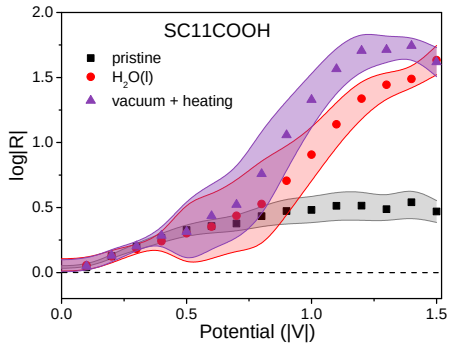

Figure 4.2 Semilog plots of the rectification ratio ($\log|R|$) vs absolute potential ($|V|$) of $Au^{TS}/S(CH_2)_{11}COOH//EGaIn$ junctions under various conditions: pristine, non-rectifying (black); after exposure to H_2O (l), rectifying (red); after exposure to H_2O (l) and then placed in a vacuum oven for 12 h at 80 °C, rectifying (purple). The shaded areas represent the variance of Gaussian fits to distributions of $\log|R|$.

4

isorbed.

The rate of tunneling charge-transport through $S(CH_2)_{15}CH_3$ (C16) junctions is sensitive both to ambient humidity and exposure to H_2O (g), which affects the height of the tunneling barrier.[18] To exclude the possibility that H_2O alone can induce rectification we treated samples comprising SAMs of alkanethiols ($S(CH_2)_{11}CH_3$ and $S(CH_2)_{15}CH_3$) with H_2O in similar fashion (Figure 4.3). In their pristine state these SAMs exhibit small asymmetry ($logR < 0.5$ at 1.5 V), which is likely the result of the inherent asymmetry of the electrodes/couplings in EGaIn junctions. In the case of the SAM of C12 treatment with H_2O induced a change in $\log|R|$, but the magnitude decreased when treated with H_2O vapor and increased when treated with liquid H_2O. On the other hand, the magnitude of $\log|R|$ for SAMs of C16 is completely unaffected by exposure to H_2O. Overall, we can safely conclude, that H_2O presence in an EGaIn junction is not sufficient to cause rectification of SAMs of alkanethiols.

The simplest, most robust and widely-accepted measure of the barrier-height of a tunneling junction is the tunneling decay coefficient, β, which is extracted from a Simmons' approximation $J = J_0 e^{-\beta d}$, where d is the barrier-width and J_0 is the theoretical value of J when $d = 0$. We determined β for the series {$S(CH_2)_7CO_2H$, $S(CH_2)_{11}CO_2H$, $S(CH_2)_{15}CO_2H$} in the non-rectifying and rectifying states (rectification was induced by exposure to H_2O vapor). The low-bias value of $\beta = 0.55\,Å^{-1}$ is slightly lower than the consensus value of $0.70\,Å^{-1}$ for SAMs of alkanethiolates,[19–21] but it does not differ between the non-rectifying and rectifying states. The β, however, does exhibit a strong voltage dependence in the bias region above 0.4 V. It is hard to conclude what happens at that voltage since there are no reports of voltage dependance of β even for SAMs of alkanethiols. Regardless of the details of β vs V plots, it is not straightforward that the voltage dependance of β and subsequent alteration of the tunneling barrier should cause any rectification at all. Thus, the mechanism of rectification does not involve changing the average barrier height imposed by the aliphatic molecular backbone. The rectification inducing effects of exposure to H_2O are likely confined to the SAM//top-contact interface via strong interactions between the terminal $-CO_2H$ groups and H_2O, which

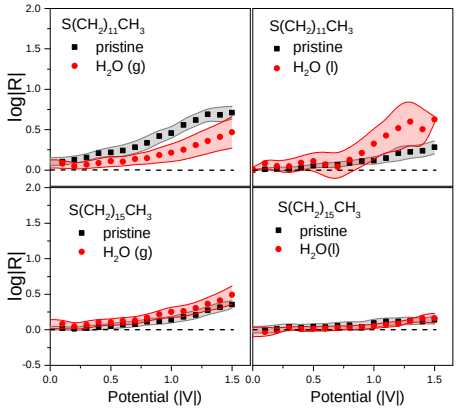

Figure 4.3 Plots of $\log|R|$ versus absolute potential ($|V|$) of Au^{TS}/SAM//EGaIn junctions comprising SAMs of $S(CH_2)_{11}CH_3$ (at the top) and $S(CH_2)_{15}CH_3$ (at the bottom) in the pristine states (black) and after exposure to H_2O (g) (red, on the left) and H_2O (l) (red, on the right). Neither SAM exhibited a significant change upon exposure to H_2O.

is supported spectroscopically (see below) and by the observation that H_2O does not desorb in vacuum with heating.

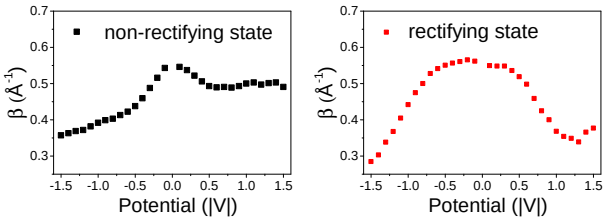

Figure 4.4 The tunneling decay coefficient, β, extracted from fits of $\ln|J|$ versus molecular length in Ångstroms. At low bias ($V < 0.4$ V) the curves show weak voltage dependence in the non-rectifying state and almost no voltage dependence in the rectifying state.

It is possible to induce rectification (with symmetric molecules) in molecular tunneling junctions by altering the electric double layer of the electrodes such that they experience different electrostatic environments.[11] This mechanism is plausible, as EGaIn forms a 7 Å-thick layer of Ga_2O_3 that should interact strongly with both carboxylic acids and H_2O molecules.[22] However, Figure 4.5a shows R/V curves for $Au^{TS}/S(CH_2)_{11}CO_2H//Au^{AFM}$ junctions, which exhibit the same behavior as $Au^{TS}/S(CH_2)_{11}CO_2H//$EGaIn junctions; as-prepared SAMs do not rectify until exposed to H_2O (l) and they return to their initial state upon exposure to DMP. A mechanism that depends on the electrodes should show markedly different behavior between dissimilar Au^{TS}/EGaIn and nearly-identical Au^{TS}/Au^{AFM} pairs of electrodes. To exclude electrode effects completely, we measured $Au^{TS}/S(CH_2)_{15}CO_2H//$rGO junctions, however, without in situ access to the SAM, we compared the rectifying state (because the devices are prepared in a water bath) to $Au^{TS}/S(CH_2)_{15}CH_3//$rGO junctions. Figure 4.5b shows an abrupt increase in $\log|R|$ around

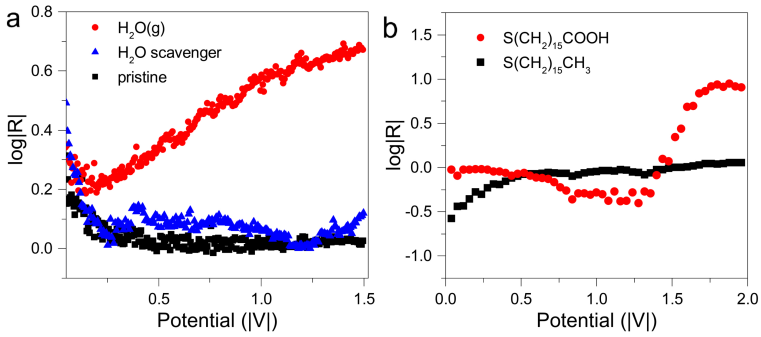

Figure 4.5 In-place switching of the rectification of junctions comprising SAMs of $S(CH_2)_{11}CO_2H$ in Au^{AFM} and rGO junctions. **a,** Plots of $\log|R|$ versus $|V|$ for $Au^{TS}/S(CH_2)_{11}CO_2H//Au^{AFM}$ junctions after the SAMs are treated with H_2O or H_2O and then DMP. black, pristine; red, after exposure to H_2O (g); blue, after exposure to H_2O (g) and then DMP. **b,** Plots of $\log|R|$ versus $|V|$ for $Au^{VD}/S(CH_2)_{15}CH_3//rGO$ (black) and $Au^{VD}/S(CH_2)_{15}CO_2H//rGO$ (red) junctions.

1.5 V for the $-CO_2H$-terminated SAMs that is absent for the SAMs of alkanthiolates. Thus, the effect is entirely molecular and independent of the identity and composition of the electrodes. This is an important observation, as it means that the underlying mechanism of rectification-switching is generalizable and can be utilized in any present or future device platform.

In order to get further insight into the mechanism of switching, we characterized SAMs of $S(CH_2)_{11}CO_2H$ by X-ray photoelectron spectroscopy (XPS) in the pristine state, after exposure to water and after subsequent treatment with DMP. These data are summarized in Figure 4.6. The three main peaks in the C1s core-level region correspond to aliphatic CH_2-CH_2, CH_2-S, and $-CO_2H$ carbons.[23] The binding energies associated with these carbons in both the pristine and DMP-treated SAMs (*i.e.*, the non-rectifying sates) are 285.1 eV, 286.6 eV and 288.8 eV, respectively. In the C1s spectra of the SAMs in the rectifying state (*i.e.*, after exposure to H_2O, but before DMP treatment) the $-CO_2H$ peak shifts to a higher binding energy by 0.3 eV, suggesting that $-CO_2H$ is protonated and, therefore, becomes more electropositive.[23, 24] Simultaneously, the aliphatic Carbon CH_2-CH_2 and CH_2-S peaks shift to lower binding energies by 0.3 eV and 0.2 eV, which suggests a commensurate increase in the electronegativity of the backbone that polarizes the SAM. Although the effects of polarization decay rapidly it is not possible to precisely determine which carbon atoms are effected. Importantly, all three C1s peaks return to the binding energies of the pristine state after exposure to H_2O and subsequent treatment with DMP, indicating that the effects of binding H_2O are chemically reversible. Thus, the dampening effect in Figure 4.1 is not due to irreversible chemical processes and is most likely physical stress that introduces disorder, pinholes, etc. This type of fatigue can be mitigated through optimization and/or the use of different device platforms much more readily than chemical fatigue.

From the experimental data described above and the observation that SAMs bearing terminal $-CO_2H$ groups are readily protonated by relatively weak acids[24] we propose the mechanism shown in Figure 4.7. In the non-rectifying state, the width of the tunnel-

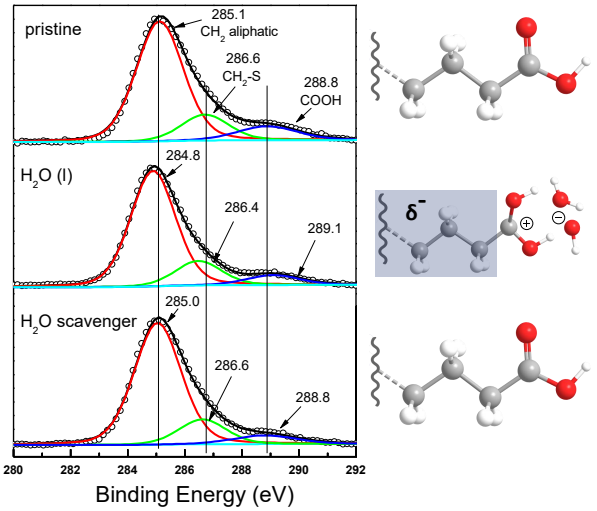

Figure 4.6 C 1s core X-ray photoemission spectra of SAMs of $S(CH_2)_{11}CO_2H$ before and after exposure to H_2O and H_2O subsequent treatment with DMP. Top: C1s core-level region of a pristine SAM showing three main peaks located at 285.1 eV, 286.6 eV and 288.8 eV, corresponding to CH_2 aliphatic, CH_2-S and $-CO_2H$ respectively. Center: After exposure to H_2O (l) the $-CO_2H$ peak shifts 0.3 eV to higher binding energy while the CH_2 aliphatic and CH_2-S peaks shift 0.3 eV to lower binding energy. Bottom: After exposure to H_2O and then DMP, the three main C1s peaks shift back to their initial position with respect to the pristine state.

ing barrier is defined by the physical length of the molecules in the SAM at both positive and negative bias (Figure 4.7a). Exposure to H_2O creates an interfacial state comprising $-CO_2H_2^+$ groups formed by the dissociation of H_2O and, potentially, fewer than six monolayers[25] of H_2O. While it is possible that the resulting dipoles directly lead to rectification,[26] the magnitude of $\log|R|$ suggests a tunneling-hopping mechanism[27] in which the interfacial state created by the $-CO_2H_2^+$ groups is sufficiently close to the Fermi level that it is brought into resonance with the bottom electrode at bias, decreasing the width of the tunneling barrier by the approximate thickness of the interfacial state as shown in Figure 4.7b. This mechanism is consistent with the observation that rectification is conserved across electrode pairs of Au^{TS}/EGaIn, Au^{TS}/Au^{AFM} and Au^{TS}/rGO. It is further supported by the observation that the conductance drops slightly at negative bias in the rectifying state due to the increased width of the barrier, but not positive bias since the widths of the barriers at positive bias are defined by the aliphatic backbone and, therefore, are comparable in the rectifying and non-rectifying states (Figure 4.9).

If the mechanism depends largely or entirely on the protonation of the $-CO_2H$ groups, SAMs of $SC(CH_2)_{11}CO_2H$ should respond to photo-generated acid enabling a junction to be converted between a resistor and a diode using light. We chose a protonated merocyanine (MCH^+) as a photo-acid because it is well-characterized[28] and has been shown to protonate $-CO_2H$-terminated SAMs upon photo-induced ring-closure to spiropyran (SP).[24] The switching process and a schematic of the resulting protonation is shown in Figure 4.8a and the resulting R/V data are shown in Figure 4.8 b. Exposure to 1 mM ethanolic solutions of MCH^+ for 30 min has no effect on $\log|R|$ for Au^{TS}/

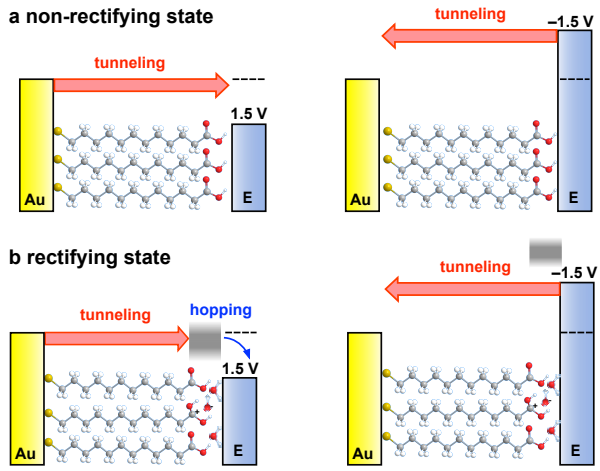

Figure 4.7 Proposed mechanism of rectification. **a,** Au/$S(CH_2)_{11}CO_2H$//E (where E is either EGaIn, Au or rGO) junctions are resistors in the pristine state because charges traverse the entire width of the junction by non-resonant tunneling irrespective of the bias applied at E. The width of the tunneling barrier is defined by the lengths of the $S(CH_2)_{11}CO_2H$ molecules. **b,** When $CO_2H_2^+$ forms at the $S(CH_2)_{11}CO_2H$//E interface from protonation by H_2O or a Brønsted-Lowry acid, unoccupied states are created close to the Fermi level of the Au electrode. These states, which may include some tightly-bound H_2O or conjugate base, come close to resonance when E is biased positively, shortening the width of the tunneling barrier by the thickness of the states. At negative bias the states are pushed away from the Fermi level of Au, restoring the width of the tunneling barrier to the entire lengths of the $S(CH_2)_{11}CO_2H$ molecules.

$S(CH_2)_{11}COOH$// EGaIn junctions, indicating that the pKa of MCH^+ in ethanol is too high to protonate $-CO_2H$-terminated SAMs directly. Similarly, the exposure of the solution to the blue (350 nm to 450 nm) light without the MCH^+ does not turn the rectification on. With the two present together, however, the junctions switch to the rectifying state, producing R/V curves that are almost indistinguishable from those that result from exposure to H_2O (Figure 4.1 b). This observation is remarkable as it allows us to narrow down the necessary cause of inducing rectifying behavior—a proton source. It seems, that H_2O treatment is just an easy and effective way to achieve the rectifying protonated state of the SAM and is not limited to it. The ability to couple switching of functionality between diode and resistor to external stimulus is a key step toward further implementation in a device.

4.3. CONCLUSIONS

The ability to switch the function of a tunneling junction reversibly between resistor and diode creates the possibility of fabricating molecular-electronic devices that exhibit unique functions that are difficult or impossible to achieve with conventional semiconductor technology. And, because rectification is self-referencing (*i.e.*, it is independent of the absolute magnitude of J), rectification-switching can potentially be used as a sensor or dosimeter. Although we used exposure to H_2O to characterize the effect and prove that it is molecular in nature, the XPS spectra and the MCH^+-induced switching

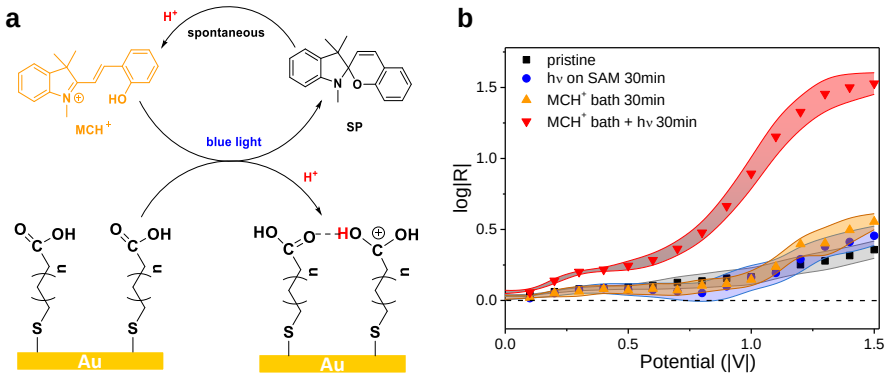

Figure 4.8 Switching between a resistor and a diode using a photo-acid. a, When MCH^+ is exposed to blue (350 nm to 450 nm) light it loses a proton and undergoes a reversible ring-closure to form SP. That proton is then transferred to the surface of the CO_2H-terminated SAM, forming $CO_2H_2{}^+$. **b,** Semilog plots of $\log|R|$ versus $|V|$ for $Au^{TS}/S(CH_2)_{11}CO_2H//EGaIn$ junctions before and after the SAMs are exposed to MCH^+, light ($h\nu$) or MCH^+ with light. black, pristine; orange exposure to $h\nu$ for 30 min; blue, exposure to 1 mM MCH^+ in ethanol for 30 min; red, exposure to 1 mM MCH^+ in ethanol and $h\nu$ for 30 min.

demonstrate that the switching process is driven by the protonation of $-CO_2H$ groups at the surface and that it can, therefore, be controlled with light or other inputs to produce devices with unique properties. For example, the function of a diode-logic circuit would depend on the outcomes of previous, proton-coupled events through the reversible switching of individual circuit elements. There are myriad ways of delivering and transporting protons and because the switching effect does not depend on the electrodes, proton-mediated rectification switching can potentially be both fast and robust with sufficient optimization in an appropriate device platform.

4.4. METHODS

Chemicals. 8-Mercaptooctanoic acid, 12-Mercaptododecanoic acid, 16-Mercaptohexadecanoic acid and 2,2-dimethoxypropane were purchased from Sigma-Aldrich and used as-received. Extra-dry ethanol (Acros) was used as the solvent.

Au substrates. Template-striped Au was prepared according to established literature procedures;[13] Au (100 nm) was vapor-deposited onto technical grade Si wafers in a thermal evaporator. Typical evaporation rates were 0.5 nms^{-1}. Glass substrates (1 cm × 1 cm) were cleaned by Piranha solution (3:1 H_2SO_4:H_2O_2 by volume) and then glued onto the Au film with Norland optical adhesive. The glass/Au/Si sandwich substrates were cured under UV lamp for 300 s. The Au/glass was mechanically peeled off separate from the silicon wafer, exposing the ultra-smooth, buried Au interface.

Self-assembled monolayers. SAMs used in EGaIn and CP-AFM junctions were prepared inside a nitrogen-filled glovebox with both humidity and O_2 in the sub-ppm level. Au^{TS} substrates were immersed in 1 mM ethanolic solutions overnight. SAMs were sonicated for 1 minute, then rinsed with extra dry ethanol, followed by drying in a stream of

dry N_2.

EGaIn/Ga_2O_3//SAM/Au Junction measurement. The EGaIn tip was formed by extruding a droplet from a 15 µl syringe, placing it in contact with a sacrificial substrate and withdrawing it slowly. A conical EGaIn tip is created when the EGaIn tip breaks down into two parts. Using a micromanipulator, the syringe was moved towards the SAMs until the tip contacted the Au surfaces supporting a SAM. A Keithley 6430 electrometer was employed for the electronic and transport current measurement. The Au substrate was grounded while the EGaIn tip was biased. All current density measurements were carried out inside a flowbox with 1 % to 3 % O_2 in N_2 and relative humidity (RH) < 10 %. Tunneling junctions comprising SAMs were formed by contacting the SAMs with a sharp tip of EGaIn.[8]

The software used for the gathering and analysis of the data comprise homemade LabView scripts for acquiring raw data. The raw data, consist of five traces per junction, were filtered through a pruning algorithm (written in Python using the SciPy package) to remove short circuit traces, no-contact traces, and other anomalous traces. A repeated cycling bias of 0→ 1.5V→ 0→ -1.5V was applied to the SAMs. The measured potential was limited at 1.5V to avoid the short circuit. The traces are filtered by defining shorts as I/V curves where I >10 mA ($J \approx 103$ A/cm^2) at 0.2 V and no-contact traces where I is in the noise level (0.1 pA) at 0 V, or in which dI/dV changes sign five or more times during a forward or reverse trace. A trace that shorts or converts to no-contact at any point is entirely discarded.

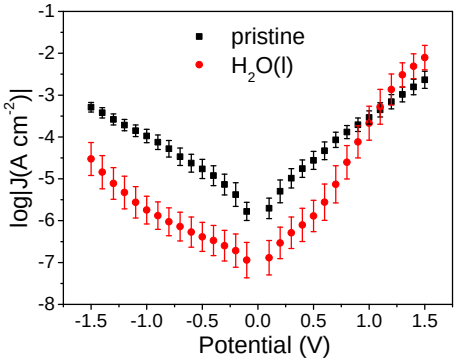

Figure 4.9 Plots of $log|J|$ vs applied bias (V) of $Au^{TS}/S(CH_2)_{11}COOH//EGaIn$ junctions in the non-rectifying (black) and rectifying (red) states. Each datapoint is the mean value from a Gaussian fit to a histogram of $\log|J|$ for a value of V. The error bars are the 95 % confidence intervals of the fit. The J/V data are approximately symmetric in the non-rectifying state. After exposure to H_2O (l), $\log|J|$ decreases by approximately 1.5 at −1.5 V, giving rise to rectification.

Conducting probe atomic force microscopy. CP-AFM I/V measurements were performed on a Bruker AFM Multimode MMAFM-2 equipped with a PeakForce TUNA Application Module (Bruker). The SAMs were contacted with a Au-coated silicon nitride tip with a nominal radius of 130 nm (NPG-10, Bruker; tip A, resonant frequency = 65 kHz, spring constant = 0.35 N/m; tip B, resonant frequency = 23 kHz, spring constant = 0.12 N/m; tip C, resonant frequency = 56 kHz, spring constant 0.24 N/m; tip D, res-

onant frequency = 18 kHz, spring constant 0.06 N/m; tip A was chosen in this work) in TUNA mode. The AFM tip was grounded and all samples were prepared on Au^{TS} and biased from -1.5 V to +1.5 V and from +1.5 V to -1.5 V to record the I/V curves: a max of 10 trace/retrace cycles per junction were performed and the top electrode was removed from SAMs between junctions.

Reduced Graphene oxide device. 5 nm Cr and 100 nm Au was evaporated on the UV-lithography patterned substrate via thermal evaporation under optimized condition for ultra-flatness to produce micro-chips. A 30 nm aluminum oxide layer was then grown via atomic layer deposition (ALD) to serve as an isolating layer. Electron Beam lithography was used to pattern micro-pores with radius ≈1 µM on the chips. The micro-pores were characterized by AFM for pore size and Au flatness, only the ones with root-mean-square roughness less than 0.5 nm was selected for growing SAMs.

The micro-pore device was cleaned by acetone, methanol and iso-propanol, blown dry with nitrogen and immersed in the SAM forming solution (100 µM in 99% ethanol) overnight in nitrogen atmosphere. After SAM formation, the device was rinsed by ethanol to eliminate any physisorbed molecules.

High quality chemically derived graphene oxide solution was prepared by modified Eigler's method followed by centrifugation. The refined solution was spin coated on oxygen plasma treated SiO_2 wafer (285 nm) to make a graphene oxide (GO) film. The thickness of the film was characterized by AFM. The GO film was reduced by treatment in HI at 120 °C for 2 hours, and then thermally treated in a tube-furnace at 650 °C for 1 hour under a continuous nitrogen flow. A few drops of 1 M NaOH solution was dropped onto the corner of the rGO film to release the film from the wafer. The film was floated onto a water surface and transferred to a SAM device. A shadow mask and oxygen plasma was used to etch away the undesired rGO to avoid current leakage.

X-ray photoelectron spectroscopy. XPS measurements were conducted using a Surface Science SSX-100 ESCA instrument X-Probe spectrometer equipped with a monochromatic Al Kα source (KE 1486.6 eV). All measurements were carried out using freshly prepared samples. The pressure in the measurement chamber was maintained below 1×10^{-9} mbar during data acquisition. All XPS data were acquired at a nominal photoelectron take off angle of 37°. Winspec (developed in the LISE laboratory of the Facultes Universitaires Notre-Dame de la Paix, Namur, Belgium) analysis software was used to calculate the elemental compositions from the peak areas.

Tuning rectification. To switch a SAM into the rectifying state, they were either immersed in liquid water or exposed to water vapor produced by heating water in a round-bottom flask equipped with a glass tube. To turn off the rectification, the SAMs were immersed a 1:1 by volume mixture of 2,2-dimethoxypropane and ethanol for 30 min to 60 min.

BIBLIOGRAPHY

[1] Robert F. Service. The brain chip. *Science*, 345(6197):614–616, 2014.

[2] Marco Carlotti, Andrii Kovalchuk, Tobias Wächter, Xinkai Qiu, Michael Zharnikov, and Ryan C Chiechi. Conformation-driven quantum interference effects mediated

by through-space conjugation in self-assembled monolayers. *Nat. Commun.*, 7: 13904, 2016.

[3] Sumit Kumar, Jochem T. van Herpt, Régis Y. N. Gengler, Ben L. Feringa, Petra Rudolf, and Ryan C. Chiechi. Mixed monolayers of spiropyrans maximize tunneling conductance switching by photoisomerization at the molecule–electrode interface in egain junctions. *J. Am. Chem. Soc.*, 138(38):12519–12526, 2016.

[4] Chuancheng Jia, Agostino Migliore, Na Xin, Shaoyun Huang, Jinying Wang, Qi Yang, Shuopei Wang, Hongliang Chen, Duoming Wang, Boyong Feng, Zhirong Liu, Guangyu Zhang, Da-Hui Qu, He Tian, M A Ratner, H Q Xu, Abraham Nitzan, and Xuefeng Guo. Covalently bonded single-molecule junctions with stable and reversible photoswitched conductivity. *Science*, 352(6292):1443–1445, 2016.

[5] Albert Wan, C. S. Suchand Sangeeth, Lejia Wang, Li Yuan, Li Jiang, and Christian A. Nijhuis. Arrays of high quality sam-based junctions and their application in molecular diode based logic. *Nanoscale*, 7(46):19547–19556, 2015.

[6] Robert M Metzger. Unimolecular electrical rectifiers. *Chem. Rev.*, 103(9):3803–3834, 2003.

[7] Xiaoping Chen, Max Roemer, Li Yuan, Wei Du, Damien Thompson, Enrique del Barco, and Christian A. Nijhuis. Molecular diodes with rectification ratios exceeding 105 driven by electrostatic interactions. *Nat. Nanotechnol.*, 12(8):797–803, 2017.

[8] Ryan C Chiechi, Emily A Weiss, Michael D Dickey, and George M Whitesides. Eutectic gallium–indium (egain): A moldable liquid metal for electrical characterization of self-assembled monolayers. *Angew. Chem., Int. Ed.*, 120(1):148–150, 2008.

[9] Peng Song, Li Yuan, Max Roemer, Li Jiang, and Christian A Nijhuis. Supramolecular vs electronic structure: The effect of the tilt angle of the active group in the performance of a molecular diode. *J. Am. Chem. Soc.*, 138(18):5769–5772, 2016.

[10] Manuel Souto, Li Yuan, Dayana C Morales, Li Jiang, Imma Ratera, Christian A Nijhuis, and Jaume Veciana. Tuning the rectification ratio by changing the electronic nature (open-shell and closed-shell) in donor–acceptor self-assembled monolayers. *J. Am. Chem. Soc.*, 139(12):4262–4265, 2017.

[11] Brian Capozzi, Jianlong Xia, Olgun Adak, Emma J Dell, Zhen-Fei Liu, Jeffrey C Taylor, Jeffrey B Neaton, Luis M Campos, and Latha Venkataraman. Single-molecule diodes with high rectification ratios through environmental control. *Nat. Nanotechnol.*, 10(6):522–527, 2015.

[12] Ralf Arnold, Waleed Azzam, Andreas Terfort, and Christof Wöll. Preparation, modification, and crystallinity of aliphatic and aromatic carboxylic acid terminated self-assembled monolayers. *Langmuir*, 18(10):3980–3992, 2002.

[13] Emily A Weiss, George K Kaufman, Jennah K Kriebel, Zhefeng Li, Richard Schalek, and George M Whitesides. Si/SiO_2-templated Formation of Ultraflat Metal Surfaces

on Glass, Polymer, and Solder Supports: Their Use as Substrates for Self-Assembled Monolayers. *Langmuir*, 23(19):9686–9694, 2007.

[14] Dan Li, Marc B Mueller, Scott Gilje, Richard B Kaner, and Gordon G Wallace. Processable aqueous dispersions of graphene nanosheets. *Nat. Nanotechnol.*, 3(2): 101–105, 2008.

[15] LL Muller and TJ Jacks. Rapid chemical dehydration of samples for electron microscopic examinations. *J. Histochem. Cytochem.*, 23(2):107–110, 1975.

[16] Marco Carlotti, Maarten Degen, Yanxi Zhang, and Ryan C Chiechi. Pronounced environmental effects on injection currents in egain tunneling junctions comprising self-assembled monolayers. *J. Phys. Chem. C*, 120(36):20437–20445, 2016.

[17] Kim S. Wimbush, Raluca M. Fratila, Dandan Wang, Dongchen Qi, Cao Liang, Li Yuan, Nikolai Yakovlev, Kian Ping Loh, David N. Reinhoudt, Aldrik H. Velders, et al. Bias induced transition from an ohmic to a non-ohmic interface in supramolecular tunneling junctions with Ga_2O_3/EGaIn top electrodes. *Nanoscale*, 6(19): 11246–11258, 2014.

[18] Xiaohang Zhang, Stephen A McGill, and Peng Xiong. Origin of the humidity sensitivity of Al/AlO_x/MHA/Au molecular tunnel junctions. *J. Am. Chem. Soc.*, 129(46): 14470–14474, 2007.

[19] Vincent B. Engelkes, Jeremy M. Beebe, and C. Daniel Frisbie. Length-Dependent transport in molecular junctions based on SAMs of alkanethiols and alkanedithiols: Effect of metal work function and applied bias on tunneling efficiency and contact resistance. *J. Am. Chem. Soc.*, 126(43):14287–14296, 2004.

[20] Felice C. Simeone, Hyo Jae Yoon, Martin M. Thuo, Jabulani R. Barber, Barbara Smith, and George M. Whitesides. Defining the value of injection current and effective electrical contact area for egain-based molecular tunneling junctions. *J. Am. Chem. Soc.*, 135(48):18131–18144, 2013.

[21] Emily A. Weiss, Ryan C. Chiechi, George K. Kaufman, Jennah K. Kriebel, Zhefeng Li, Marco Duati, Maria A. Rampi, and George M. Whitesides. Influence of defects on the electrical characteristics of Mercury-Drop junctions: Self-Assembled monolayers of N-Alkanethiolates on rough and smooth silver. *J. Am. Chem. Soc.*, 129(14): 4336–4349, 2007.

[22] Ludovico Cademartiri, Martin M. Thuo, Christian Albertus Nijhuis, William F. Reus, Simon Tricard, Jabulani R. Barber, Rana N. S. Sodhi, Peter Brodersen, Choongik Kim, Ryan C. Chiechi, and George M. Whitesides. Electrical resistance of Ag^{TS}-$S(CH_2)_{n-1}CH_3$//Ga_2O_3/EGaIn tunneling junctions. *J. Phys. Chem. C*, 116(20): 10848–10860, 2012.

[23] Yuan-Li Huang, Hsi-Wen Tien, Chen-Chi M. Ma, Shin-Yi Yang, Sheng-Yen Wu, Hong-Yuan Liu, and Yiu-Wing Mai. Effect of extended polymer chains on properties of transparent graphene nanosheets conductive film. *J. Mater. Chem.*, 21(45): 18236–18241, 2011.

[24] Pintu K. Kundu, Dipak Samanta, Ron Leizrowice, Baruch Margulis, Hui Zhao, Martin Börner, T. Udayabhaskararao, Debasish Manna, and Rafal Klajn. Light-controlled self-assembly of non-photoresponsive nanoparticles. *Nat. Chem.*, 7(8): 646–652, 2015.

[25] Aimee Tu, Hye Rin Kwag, Anna L. Barnette, and Seong H. Kim. Water adsorption isotherms on CH_3-, OH-, and COOH-terminated organic surfaces at ambient conditions measured with PM-RAIRS. *Langmuir*, 28(43):15263–15269, 2012.

[26] Andrii Kovalchuk, David A. Egger, Tarek Abu-Husein, Egbert Zojer, Andreas Terfort, and Ryan C. Chiechi. Dipole-induced asymmetric conduction in tunneling junctions comprising self-assembled monolayers. *RSC Adv.*, 6(73):69479–69483, 2016.

[27] Li Qiu, Yanxi Zhang, Theodorus L. Krijger, Xinkai Qiu, Patrick van't Hof, Jan C. Hummelen, and Ryan C. Chiechi. Rectification of current responds to incorporation of fullerenes into mixed-monolayers of alkanethiolates in tunneling junctions. *Chem. Sci.*, 8(3):2365–2372, 2017.

[28] Rafal Klajn. Spiropyran-based dynamic materials. *Chem. Soc. Rev.*, 43(1):148–184, 2014.

5

SURPRISING SUBSTITUTED OLIGO(*p*-PHENYLENE ETHYNYLENE)S

Abstract: *Systematic studies in Molecular Electronics are rare and mostly limited to alkanethiols, yet they can reliably reveal important trends. We perform systematic study of the influence of the electronic structure of oligo(p-phenylene ethynylene)s on charge transport in SAM-based EGaIn junctions. Out of many variables we found that electronic coupling to the bottom electrode has the strongest effect on the charge transport properties.*

I would like to thank Marco Carlotti for help in synthesis and EGaIn measurements.

5.1. INTRODUCTION

The challenge of contacting molecules with macroscopic leads gave rise to a variety of experimental techniques, spanning from single-molecule to large area junctions. As the number of experimental platforms and acquired data increased the question of reproducibility and universality became central. Few effects have met these criteria. Rectification, which is the basis for diode functionality, has been well established both in single-molecule junctions and devices comprising self-assembled monolayers (SAMs). Destructive quantum interference, which is suppressed transmission due to specific conjugation pattern, was observed in single-molecule junctions[1] and in SAM-based junctions.[2] And finally switching of conductance in molecular junctions was achieved in a variety of ways.

However important the aforementioned achievements do not allow to establish general structure-function relationship for tuning the properties of molecular junctions at will. First systematic attempts to solve this issue were taken by Whitesides *et al.* in SAM-based large-area molecular junctions using Eutectic Ga-In (EGaIn) as top electrode. First, they functionalized the aliphatic amide backbone with a range of common aliphatic, aromatic and heteroaromatic groups at the top interface.[3] Then, they introduced a number of dipole bearing groups in the middle and to the top of aliphatic backbone.[4] In both cases no discernible differences were detected between the members of the series, except of the distance dependence (when the length of the molecules varied). Counter-intuitively, functional groups—a variable that defines chemical properties of organic molecules—had no influence on charge transport is SAM-based junctions. However, these were aliphatic molecules with inaccessible frontier orbitals, which might be the cause of insensitivity. If we introduce polar functional groups to conjugated backbones (*e.g.*, oligo(*p*-phenylene ethynylene)s, OPEs), along with creating dipoles, we will affect the energy distribution of frontier orbitals. In this work we present a systematic study of substitution patterns of OPEs in SAM-based molecular junctions using EGaIn top electrode.

5.2. RESULTS AND DISCUSSION

In order to test the effects of different groups on tunneling charge transport on a conjugated backbone we take OPE3 as a parent structure and functionalize it with two types of groups, –F and –OMe (Figure 5.1). The –F substituent is an electron-withdrawing group, which has similar volume to –H, thus should have small to no effect on packing of the molecules in SAMs. The –OMe group is electron-donating and is much bigger than a –H. Hence, in the first sub-series (Figure 5.1 on the right), when introducing –OMe group to the OPE3 backbone we chose to place it on the top phenyl ring in *meta*-position to facilitate comparable packing of all SAMs. However, since these substituents are placed at the top interface in contact with EGaIn it is crucial to protect the –OH group to eliminate any strong interaction with Ga_2O_3 skin of EGaIn. This approach allows us to change the position of the frontier energy levels of the molecules, while retaining structural similarity of the SAMs. Both groups, however, introduce opposing dipole moments, which may influence tunneling charge transport properties. To disentangle these two effects we designed the second sub-series (Figure 5.1 on the left), where we

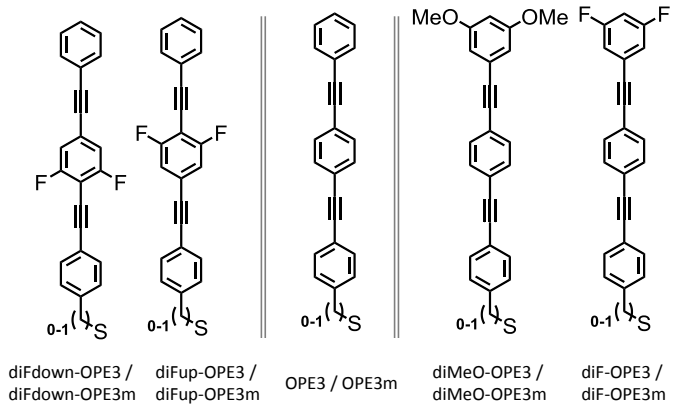

Figure 5.1 Chemical structures of OPE3-based molecular wires presented in the form of sulfides. The middle phenyl ring was substituted with two –F groups in two orientations, pointing up and down (on the left). The top ring was modified in the *meta*-position with electron-withdrawing groups (two –F) and electron-donating groups (two –OMe, on the right). All wires were synthesized with two types of anchoring groups—thioacetate (–SAc) and methylene-bridged thioacetate ($-CH_2SAc$) for in-situ deprotection for SAM formation.

5

put two –F groups on the middle phenyl ring in two orientations, pointing up (diF-up-OPE3) and down (diF-down-OPE3). By choosing to functionalize the middle phenyl ring we make sure that the interfaces stay the same, isolating the effects of dipoles. These molecules have identical molecular formulas, top and bottom interfaces and similar energy level distribution, while having opposite directions of the dipole moment.

Fully conjugated molecular wires can hybridize their electron density with the continuum of states in the bottom metal electrode through a covalent interface of a thiol anchoring group. The electronic coupling (Γ), which describes the degree of hybridization of electron density, can be tuned synthetically by breaking the conjugation using, *e.g.*, aliphatic $-CH_2-$ groups. Thus, every aforementioned molecule was synthesized with two types of anchoring groups, thioacetate (–SAc) and methylene-bridged thioacetate ($-CH_2SAc$). A single methylene unit is enough to change the coupling to the bottom electrode while keeping the molecular end to end distance relatively constant. This strategy provides an access to yet another variable—the electronic coupling constant.

We synthesized these molecules employing a generic Sonogashira coupling approach, which couples a terminal acetylene to an aryl halide using Pd (0) and Cu (I) catalysts. Throughout the synthesis we used two orthogonal acetylene protecting groups—trimethylsilyl (TMS) and triisopropylsilyl (TIPS). TMS can be removed in mild conditions with ethanolic solution of K_2CO_3, while using tetrabutylammonium fluoride (TBAF) will remove both groups. Another common way to control regioselectivity in Sonogashira coupling reactions is to exploit the fact that aryl iodides are more reactive than aryl bromides. Combining these two methodologies we can achieve high flexibility and synthesize all four members of the "up-and-down" sub-series from the common synthon (see Figure 5.2). For the other sub-series it was more optimal to start with a predefined substitution

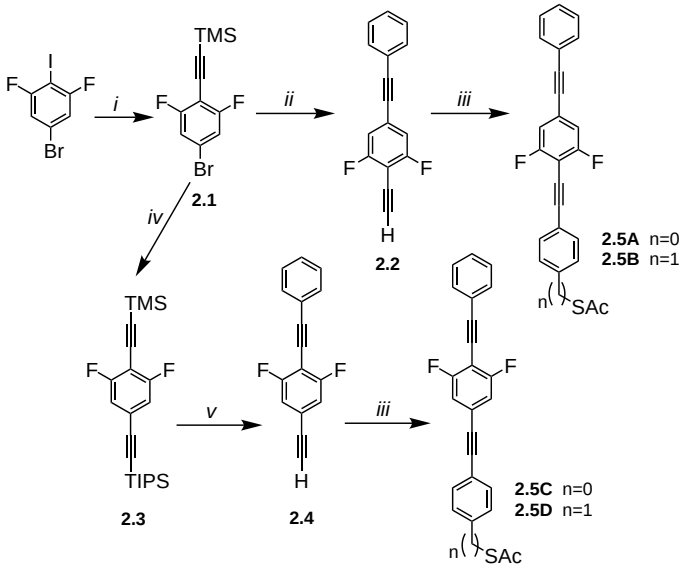

Figure 5.2 Synthesis of the sub-series with two –F substituents on the middle phenyl ring. All four target compounds can be acquired from a common starting 5-bromo-1,3-difluoro-2-iodobenzene. (i) TMS-acetylene, $Pd(PPh_3)_4$, CuI, NEt_3, THF, rt. (ii) 1. Phenylacetylene, $Pd(PPh_3)_4$, CuI, NEt_3, THF, 80 °C; 2. K_2CO_3, EtOH, THF, rt. (iii) 4-Acetylthio-1-iodobenzene (for **A** and **C**) or 1-(S-acetylthiomethyl)-4-iodobenzene (for **B** and **D**), $Pd(PPh_3)_4$, CuI, NEt_3, THF, 80 °C. (iv) TIPS-acetylene, $Pd(PPh_3)_4$, CuI, NEt_3, THF, 80 °C. (v) 1. K_2CO_3, EtOH, THF, rt; 2. Iodobenzene, $Pd(PPh_3)_4$, CuI, NEt_3, THF, 80 °C; 3. TBAF, THF, rt.

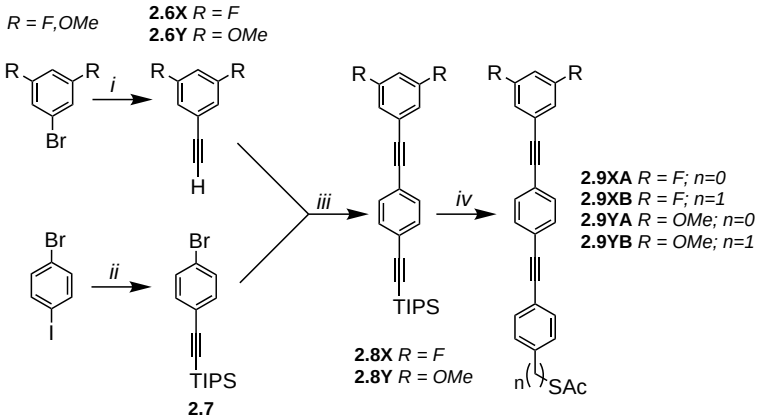

Figure 5.3 Synthesis of the sub-series with substitutions on the top phenyl ring. The substitution pattern is controlled simply by choosing the right starting material (*i.e.*, 1-bromo-3,5-dimethoxybenzene and 1-bromo-3,5-difluorobenzene). (i) 1. TMS-acetylene, $Pd(PPh_3)_4$, CuI, NEt_3, THF, 80 °C; 2. K_2CO_3, EtOH, THF, rt. (ii) TIPS-acetylene, $Pd(PPh_3)_4$, CuI, NEt_3, THF, 80 °C. (iii) $Pd(PPh_3)_4$, CuI, NEt_3, THF, 80 °C. (iv) 1. TBAF, THF, rt; 2. 4-Acetylthio-1-iodobenzene (for **A**) or 1-(S-acetylthiomethyl)-4-iodobenzene (for **B**), $Pd(PPh_3)_4$, CuI, NEt_3, THF, 80 °C.

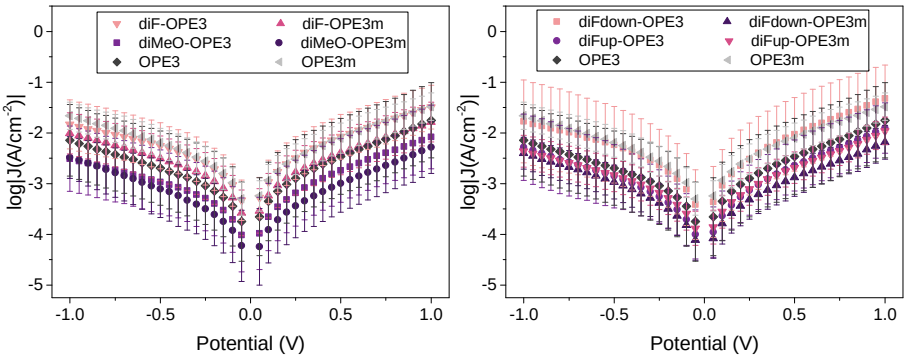

Figure 5.4 Plots of $log|J|$ vs applied potential for the two sub-series. Error bars represent standard deviation of Gaussian fits to histograms of $log|J|$ at each voltage step. All values of conductance are virtually indistinguishable irrespective of the substitution pattern.

pattern and combine the top and middle parts of the target compounds (see Figure 5.3).

We use ultra-flat template stripped Au (Au^{TS}) to grow SAMs of functionalized OPEs performing in situ deprotection of −SAc groups using 1,8-diazabicyclo[5.4.0]undec-7-ene (DBU, a non-nucleophilic base).[5] Current-voltage (I/V) measurements were performed by contacting SAMs with an EGaIn[6] tip, which produces the Au^{TS}/SAM//EGaIn junction (where "/" denotes covalent and "//" van der Waals interface). We sweep the bias from −1 V to +1 V and for each voltage step all values of log current density ($log|J|$, $J = I/S$, where S is contact area) were collected into a histogram and fit with a Gaussian distribution to determine the mean and standard deviation. The results of these measurements are presented in Figure 5.4. Regardless of the types of substituents and their pattern the conductance of all SAMs are virtually indistinguishable from each other (the values of J for all SAMs are within one order of magnitude). We have observed similar insensitivity when looking at pyrimidine-containing terphenyl molecules (Chapter 2). The tunneling distance, which is similar for all SAMs, is dominating the conductance and is hardly influenced by substituents.

Previously, we have shown that transition voltages (V_T) can be used to distinguish between SAMs with similar conductance.[8] The transition voltage is roughly proportional to energy offset between the Fermi level of the electrode and the frontier orbitals. When molecular dipoles in the SAM align they induce an electrostatic field, which may be strong enough to shift the work function (Φ) of the bottom electrode. These effects can propagate into the J/V characteristic of a junction in the form of shifts in V_T. However, there is no apparent trend in V_T for these OPEs.

The Au^{TS}/SAM//EGaIn junction is inherently asymmetrical as the two interfaces are different—the covalent bottom and van der Waals top interface. The result of this asymmetry can be seen in the small asymmetry that is present in all EGaIn J/V data.[7] In our case, we have access to tuning the coupling at the bottom interface via insertion of a $-CH_2-$ group. To see the effects of changing the coupling we plot the log of the rectification ratio ($log|R|$, where $R = J^+(V)/J^-(V)$) vs applied potential for all SAMs (Figure 5.5). Surprisingly, all SAMs are separated into two groups: (i) values of $log|R|$ peak at

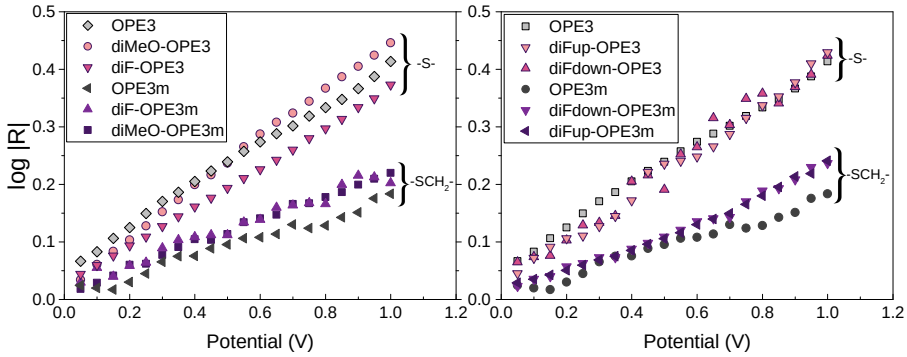

Figure 5.5 Plots of $log|R|$ vs applied potential for the two sub-series. Error bars are omitted for clarity. All the data are clearly separated into two groups: (i) $log|R|$ that peaks at ≈ 0.4 at 1 V and (ii) $log|R|$ that peaks at ≈ 0.2 at 1 V. Subsequently, these two groups follow a division based on the identity of the anchoring group.

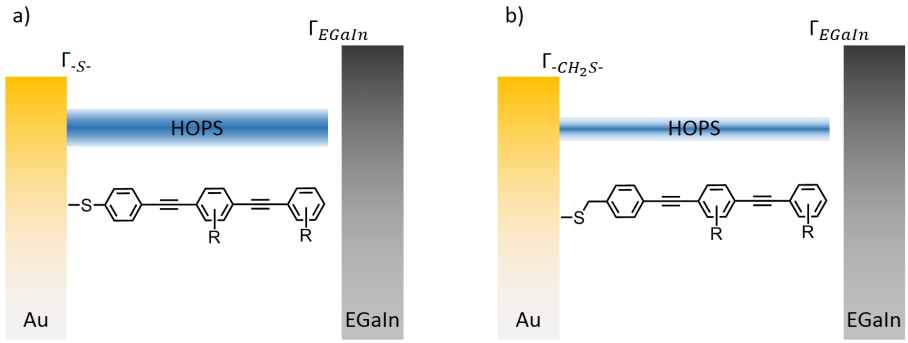

Figure 5.6 Energy level diagram of the Au^{TS}/SAM//EGaIn junction for the SAMs with two anchoring groups −S− (a) and $-CH_2S-$ (b). The presence of a single methylene unit reduces the coupling constant of the highest occupied π-states (HOPS) to the bottom Au electrode such that $\Gamma_{-S-} > \Gamma_{-CH_2S-}$. This effect occurs irrespective of the presence of any substituents or their substitution pattern.

≈ 0.4 at 1 V and these SAMs are bound via −S− anchoring group (ii) values of $log|R|$ that peak at ≈ 0.2 at 1 V and these SAMs are bound via $-CH_2S-$ anchoring group. The presence of a methylene unit lowers the coupling constant so that the junction becomes more symmetrical $\Gamma_{-CH_2S-} \rightarrow \Gamma_{EGaIn}$.

Nijhuis *et al.* used electronic coupling to control the direction of rectification in a ferrocene-based molecular diode.[9] In that work, the ferrocene core, which acts as a hopping site for electron transport, was moved along the aliphatic chain from the top interface to the bottom. The J/V output became completely symmetrical when the core was placed in the middle of the chain and the direction of rectification was reversed when the core was placed near the bottom interface. A lot of work has focused on qualitative analysis of the relation between the strength of the coupling and the nature of the anchoring groups as well as the effect of the coupling on device properties in single-molecule junctions.[10, 11] Our work presents a simple synthetic way to control elec-

tronic coupling in SAMs, which is summarized in Figure 5.6. Stronger coupling through –S– anchoring group (Γ_{-S-}) causes broadening of highest occupied π-states (HOPS) and brings them closer to the Fermi level (E_F) of the electrode. While weaker coupling (Γ_{-CH_2S-}) resembles the top EGaIn interface, which we observe in a more symmetrical J/V characteristic.

5.3. CONCLUSIONS

We attempted to systematically study the effects of functional groups on tunneling charge transport in SAMs of conjugated OPEs in EGaIn junctions. Surprisingly, we found that neither the position of the frontier orbitals, nor the direction of dipole moment has any measurable effect on J/V characteristic. However, the coupling to the bottom electrode clearly influenced the asymmetry of the J/V data. A single methylene unit, which separates the anchoring –S– group from the conjugated core, is enough to measurably reduce the strength of the coupling. These findings provide more tools for engineering molecular junctions with desired properties.

5.4. SYNTHESIS

General comments. 1-Bromo-3,5-difluorobenzene (98%), 1-bromo-3,5-dimethoxybenzene (97%), 1-bromo-4-iodobenzene (98%), $Pd(PPh_3)_4$, CuI, (trimethylsilyl)acetylene, (triisopropylsilyl)acetylene, tetrabutylammonium fluoride (TBAF, 1M in THF, 5% H2O), pipsyl chloride (95%), N,N-dimethylacetamide (99.8%) and dichlorodimethylsilane (> 98.5%) were purchased from Sigma-Aldrich and used as received. 5-bromo-1,3-difluoro-2-iodobenzene (>97.0%), 4-iodobenzyl bromide was purchased from TCI and used as received. Triethylamine (NEt_3) was distilled over CaH_2.

^{1}H-NMR spectra were recorded on a Varian AMX400 (400 MHz) at room temperature. All spectra were referenced to the solvent line of $CDCl_3$ relative to tetramethylsilane (H, 7.26 ppm).

General Sonogashira coupling procedure A. A dry flask was charged with THF, arylhalide coupling reagent (1 eq.), $Pd(PPh_3)_4$ (0.02 eq.), CuI (0.03 eq.) and dry NEt_3 (2-3 eq.) under N_2 atmosphere. The mixture was bubbled with N_2 for ≈ 30 minutes. Then the acetylene coupling reagent (1 eq.) was added, the flask was sealed and the reaction mixture was stirred at 80 °C overnight. A successful coupling is manifested by precipitation of trietylammonium salts, aliquots can be taken to check the completion of the reaction by ^{1}H-NMR. Upon completion the reaction mixture was dried on the rotary evaporator, taken up in dichloromethane (DCM) and purified with column chromatography.

General TMS deprotection procedure B. A flask was charged with TMS-protected acetylene (1 eq.) and ethanolic solution of K_2CO_3 (1.5 eq.). If needed, THF was added until the organic material was dissolved. The reaction mixture was stirred overnight at room temperature. Upon completion 1M HCl was added to the reaction mixture until the pH was acidic and the mixture was extracted with DCM, washed with water and dried over Na_2SO_4. The solvents were evaporated on the rotary evaporator. If needed, the product was purified with column chromatography.

General TIPS deprotection procedure C. A flask was charged with TIPS-protected acetylene (1 eq.), THF and a solution of TBAF (2.5 eq.). After overnight stirring, H_2O and

ether were added to the reaction mixture, the organic phase was separated, washed with H_2O (2 times) and brine (1 time), dried over Na_2SO_4 and organic solvent was removed by rotary evaporation. If needed, the product was purified with column chromatography.

((4-bromo-2,6-difluorophenyl)ethynyl)trimethylsilane (2.1)

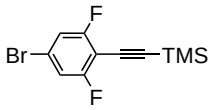

5-bromo-1,3-difluoro-2-iodobenzene (2 g, 6.3 mmol) was reacted with (trimethylsilyl)acetylene (0.9 mL, 6.3 mmol) at 30 °C over 48 hours according to the general coupling procedure A. Chromatography on silica gel (hexanes) yielded **2.1** (1.56 g, 86% yield) as a colorless oil. ^{1}H-NMR (400 MHz, chloroform-*d*) δ 7.06 – 7.00 (m, 2H), 0.25 (s, 9H).

((2,6-difluoro-4-(phenylethynyl)phenyl)ethynyl)trimethylsilane

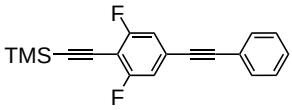

2.1 (600 mg, 2.1 mmol) was reacted with phenylacetylene (240 mg, 2.3 mmol) according to the general coupling procedure A. Chromatography on silica gel (hexanes, R_f = 0.48) yielded the target compound (400 mg, 66% yield) as yellowish solid. ^{1}H-NMR (400 MHz, chloroform-*d*) δ 7.52 (dd, J = 6.5, 3.0 Hz, 2H), 7.40 – 7.34 (m, 3H), 7.07 – 7.01 (m, 2H), 0.28 (s, 9H).

2-ethynyl-1,3-difluoro-5-(phenylethynyl)benzene (2.2)

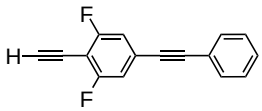

((2,6-difluoro-4-(phenylethynyl)phenyl)ethynyl)trimethylsilane (400 mg, 1.28 mmol) was deprotected according to the general deprotection procedure B. The workup directly yielded **2.2** (290 mg, 94% yield) as yellowish oil that solidified upon standing. ^{1}H-NMR (400 MHz, chloroform-*d*) δ 7.53 (dd, J = 6.6, 2.9 Hz, 2H), 7.40 – 7.35 (m, 3H), 7.10 – 7.04 (m, 2H), 3.58 (s, 1H).

((2,6-difluoro-4-((triisopropylsilyl)ethynyl)phenyl)ethynyl)trimethylsilane (2.3)

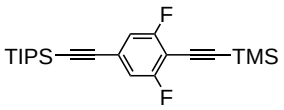

2.1 (902 mg, 3.12 mmol) was reacted with (triisopropylsilyl)acetylene (680 mg, 3.74 mmol) according to the general coupling procedure A. Chromatography on silica gel (hexanes, R_f = 0.8) yielded **2.3** (882 mg, 73% yield) as colorless oil that solidified upon standing. ^{1}H-NMR (400 MHz, chloroform-*d*) δ 7.01 – 6.94 (m, 2H), 1.13 (s, 21H), 0.29 (s, 9H).

((4-ethynyl-3,5-difluorophenyl)ethynyl)triisopropylsilane

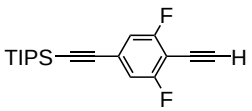

2.3 (780 mg, 2 mmol) was deprotected according to the general deprotection procedure B. The workup directly yielded the target compound (636 mg, 84% yield) as a colourless oil. ^{1}H-NMR (400 MHz, chloroform-*d*) δ 7.03 – 6.98 (m, 2H), 3.57 (s, 1H), 1.13 (s, 21H).

((3,5-difluoro-4-(phenylethynyl)phenyl)ethynyl)triisopropylsilane

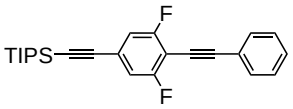

((4-ethynyl-3,5-difluorophenyl)ethynyl)triisopropylsilane (600 mg, 1.88 mmol) was reacted with iodobenzene (0.32 mL, 2.8 mmol) according to the general coupling procedure A. Chromatography on silica gel (hexanes) yielded the target compound (511 mg, 69% yield) as an opalecent oil that crystallized upon standing. ^{1}H-NMR (400 MHz, chloroform-*d*) δ 7.60 (dd, J = 6.4, 2.7 Hz, 2H), 7.41 – 7.35 (m, 3H), 7.08 – 7.01 (m, 2H), 1.16 (s, 21H).

5-ethynyl-1,3-difluoro-2-(phenylethynyl)benzene (2.4)

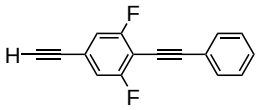

((3,5-difluoro-4-(phenylethynyl)phenyl)ethynyl)triisopropylsilane (510 mg, 1.29 mmol) was deprotected according to the general deprotection procedure C. Chromatography on silica gel (hexanes) yielded **2.4** (272 mg, 89% yield) as a colorless oil that solidified upon standing. ^{1}H-NMR (400 MHz, chloroform-*d*) δ 7.60 (dd, J = 6.3, 2.7 Hz, 2H), 7.41 – 7.36 (m, 3H), 7.10 – 7.03 (m, 2H), 3.25 (s, 1H). ^{13}C-NMR (101 MHz, chloroform-*d*) δ 165.04 (dd, J = 253.8, 6.4 Hz), 134.51 , 131.82 , 131.07 , 124.95 , 117.78 , 117.71 , 117.58 , 117.51 , 103.54 , 83.47 , 78.52.

1-(S-Acetylthiomethyl)-4-iodobenzene

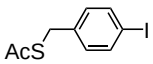

A three neck flask equipped with a magnetic stirring bar and a reflux condenser was charged with 4-iodobenzyl bromide (4 g, 13.5 mmol), KSAc (1.71 g, 15 mmol) and THF. The reaction mixture was refluxed overnight. After completion, the reaction mixture was cooled to room temperature, concentrated in vacuo and extracted with DCM. Chromatography on silica gel (hexanes) yielded the target compound (3.65 g, 93 % yield) as a pinkish solid. ^{1}H-NMR (400 MHz, chloroform-*d*) δ 7.61 (d, J = 8.4 Hz, 2H), 7.03 (d, J = 8.4 Hz, 2H), 4.04 (s, 2H), 2.34 (s, 3H).

4-Acetylthio-1-iodobenzene

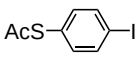

A solution of pipsyl chloride (5 g, 16.6 mmol) and N, N-dimethyl scetamide (4.6 mL, 49 mmol) in 1,2-dichloroethane was added to a suspension of zinc powder (3.85 g, 58.9 mmol) and dichlorodimethylsilane (7 mL, 58 mmol) in 1,2-dichloroethane (130 mL). The gray suspension was stirred for 2.5 hours at 70 °C to give a yellow-green solution. The reaction mixture was cooled to 50 °C and acetyl chloride (1.52 mL, 21.4 mmol) was added. The mixture was stirred for 30 minutes at 45 °C, colled to 40 °C, filtered and poured into H_2O (300 mL). The aqueous layer was extracted with DCM (3 x 200 mL) and the combined organic layers were dried over Na_2SO_4. The solvent was removed by rotary evaporation to give a yellow liquid, which was purified by chromatography on silica gel (DCM/hexane 1:4, R_f = 0.25) followed by recrystallization from hexane to give the target compound (4.1 g, 89 % yield) as a white solid. ^{1}H-NMR (400 MHz, chloroform-*d*) δ 7.74 (d, J = 8.3 Hz, 2H),

7.13 (d, J = 8.3 Hz, 2H), 2.42 (s, 3H).

S-(4-((2,6-difluoro-4-(phenylethynyl)phenyl)ethynyl)phenyl) ethanethioate (2.5A)

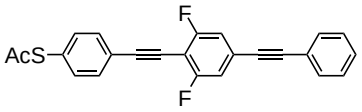

2.2 (290 mg, 1.21 mmol) was reacted with 4-acetylthio-1-iodobenzene (370 mg, 1.33 mmol) according to the general coupling procedure A. Chromatography on silica gel (hexane/ethyl acetate 9:1, R_f = 0.47) followed by recrystallization from hexane yielded **2.5A** (186 mg, 40 % yield) as a yellowish solid. ^{1}H-NMR (400 MHz, chloroform-*d*) δ 7.61 (d, J = 8.3 Hz, 2H), 7.53 (dd, J = 6.5, 3.1 Hz, 2H), 7.42 (d, J = 8.2 Hz, 2H), 7.40 – 7.35 (m, 3H), 7.07 - 7.13 (m, 2H), 2.44 (s, 3H).

S-(4-((2,6-difluoro-4-(phenylethynyl)phenyl)ethynyl)benzyl) ethanethioate (2.5B)

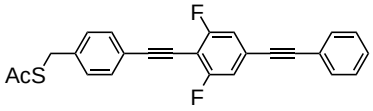

2.2 (170 mg, 0.71 mmol) was reacted with 1-(S-acetylthiomethyl)-4-iodobenzene (230 mg, 0.78 mmol) according to the general coupling procedure A. Chromatography on silica gel (hexane/ethyl acetate 10:1, R_f = 0.44) followed by recrystallization from hexane yielded **2.5B** (148 mg, 52 % yield) as a yellowish solid. ^{1}H-NMR (400 MHz, chloroform-*d*) δ 7.55 – 7.51 (m, 2H), 7.41 (d, J = 8.4 Hz, 2H), 7.35 - 7.39 (m, 3H), 7.16 (d, J = 8.3 Hz, 2H), 7.06 - 7.12 (m, 2H), 4.05 (s, 2H), 2.35 (s, 3H).

S-(4-((3,5-difluoro-4-(phenylethynyl)phenyl)ethynyl)phenyl) ethanethioate (2.5C)

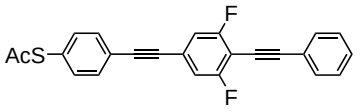

2.4 (130 mg, 0.54 mmol) was reacted with 4-acetylthio-1-iodobenzene (228 mg, 0.81 mmol) according to the general coupling procedure A. Chromatography on silica gel (hexane/ethyl acetate 9:1) followed by recrystallization from hexane yielded **2.5C** (115 mg, 55 % yield) as a white solid. ^{1}H-NMR (400 MHz, chloroform-*d*) δ 7.59 (dd, J = 6.5, 2.8 Hz, 2H), 7.55 (d, J = 8.2 Hz, 2H), 7.42 (d, J = 8.1 Hz, 2H), 7.35 - 7.40 (m, 3H), 7.13 – 7.07 (m, 2H), 2.45 (s, 3H).

S-(4-((3,5-difluoro-4-(phenylethynyl)phenyl)ethynyl)benzyl) ethanethioate (2.5D)

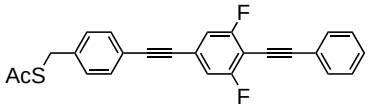

2.4 (250 mg, 1.04 mmol) was reacted with 1-(S-acetylthiomethyl)-4-iodobenzene (368 mg, 1.3 mmol) according to the general coupling procedure A. Chromatography on silica gel (hexane/ethyl acetate 9:1) followed by recrystallization from hexane yielded **2.5B** (200 mg, 48 % yield) as a white solid. ^{1}H-NMR (400 MHz, chloroform-*d*) δ 7.53 (dd, J = 5.9, 2.2 Hz, 2H), 7.51 (d, J = 8.1 Hz, 2H), 7.40 – 7.35 (m, 3H), 7.29 (d, J = 8.2 Hz, 2H), 7.12 – 7.06 (m, 2H), 4.13 (s, 2H), 2.36 (s, 3H).

((3,5-Difluorophenyl)ethynyl)trimethylsilane

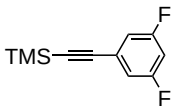

1-Bromo-3,5-difluorobenzene (5 g, 26 mmol) was reacted with (trimethylsilyl)acetylene (4.15 mL, 29 mmol) according to the general coupling procedure A. Chromatography on silica gel (hexane, R_f = 0.73) yielded the target compound (5.4 g, 99 % yield) as a colouless oil. ^{1}H-NMR (400 MHz, chloroform-*d*) δ 6.93 - 6.99 (m, 2H), 6.77 (tt, J = 9.0, 2.4 Hz, 1H), 0.24 (s, 9H).

((3,5-Dimethoxyphenyl)ethynyl)trimethylsilane

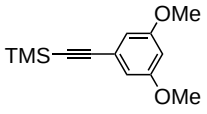

1-Bromo-3,5-dimethoxybenzene (3 g, 13.8 mmol) was reacted with (trimethylsilyl)acetylene (2.1 mL, 15.2 mmol) according to the general coupling procedure A. Chromatography on silica gel (hexane) yielded the target compound (1.95 g, 60 % yield) as a yellowish solid. ^{1}H-NMR (400 MHz, chloroform-*d*) δ 6.62 (d, J = 2.3 Hz, 2H), 6.44 (t, J = 2.3 Hz, 1H), 3.77 (s, 6H), 0.25 (s, 9H).

1-Ethynyl-3,5-difluorobenzene (2.6X)

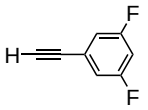

((3,5-difluorophenyl)ethynyl)trimethylsilane (1.2 g, 5.76 mmol) was deprotected according to the general deprotection procedure B. The workup directly yielded **2.6X** (648 mg, 83 % yield) as a white solid. ^{1}H-NMR (400 MHz, chloroform-*d*) δ 7.03 – 6.97 (m, 2H), 6.82 (tt, J = 8.9, 2.2 Hz, 1H), 3.14 (s, 1H).

1-Ethynyl-3,5-dimethoxybenzene (2.6Y)

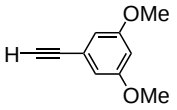

((3,5-dimethoxyphenyl)ethynyl)trimethylsilane (750 mg, 3.67 mmol) was deprotected according to the general deprotection procedure B. The workup directly yielded **2.6Y** (520 mg, 87 % yield) as a white solid. ^{1}H-NMR (400 MHz, chloroform-*d*) δ 6.65 (d, J = 2.3 Hz, 2H), 6.47 (t, J = 2.3 Hz, 1H), 3.78 (s, 6H), 3.04 (s, 1H).

((4-Bromophenyl)ethynyl)triisopropylsilane (2.7)

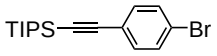

1-Bromo-4-iodobenzene (10 g, 35 mmol) was reacted with (triisopropylsilyl)acetylene (8.6 mL, 38.5 mmol) according to the general coupling procedure A at 30 °C. Chromatography on silica gel (hexane) yielded **2.7** (9.62 g, 81 % yield) as a colorless oil. ^{1}H-NMR (400 MHz, chloroform-*d*) δ 7.43 (d, J = 8.7 Hz, 2H), 7.33 (d, J = 8.7 Hz, 2H), 1.12 (s, 21H).

((4-((3,5-difluorophenyl)ethynyl)phenyl)ethynyl)triisopropylsilane (2.8X)

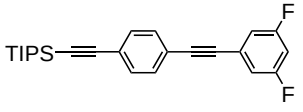

2.6X (600 mg, 4.34 mmol) was reacted with **2.7** (1.76 g, 5.21 mmol) according to the general coupling procedure A. Chromatography on silica gel (hexanes) yielded **2.8X** (1.3 g, 76 % yield) as a yellowish oil that solidified upon standing. ^{1}H-NMR (400 MHz, chloroform-*d*) δ 7.46 (s, 4H), 7.07

– 7.00 (m, 2H), 6.81 (tt, J = 9.0, 2.3 Hz, 1H), 1.13 (s, 21H).

((4-((3,5-dimethoxyphenyl)ethynyl)phenyl)ethynyl)triisopropylsilane (2.8Y)

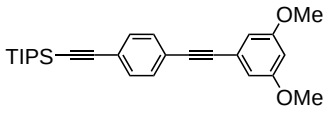

2.6Y (550 mg, 3.4 mmol) was reacted with **2.7** (1.26 g, 3.74 mmol) according to the general coupling procedure A. Chromatography on silica gel (hexane/ethyl acetate 9:1, R_f = 0.67) yielded **2.8Y** (1.01 g, 71 % yield) as a white solid. ^{1}H-NMR (400 MHz, chloroform-*d*) δ 7.45 (s, 4H), 6.69 (d, J = 2.3 Hz, 2H), 6.47 (t, J = 2.3 Hz, 1H), 3.81 (s, 6H), 1.13 (s, 21H).

1-((4-ethynylphenyl)ethynyl)-3,5-difluorobenzene

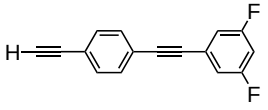

2.8X (650 mg, 1.64 mmol) was deprotected according to the general deprotection procedure C. Chromatography on silica gel (hexane) yielded the target compound (297 mg, 76 % yield) as a white solid. ^{1}H-NMR (400 MHz, chloroform-*d*) δ 7.48 (s, 4H), 7.07 – 7.00 (m, 2H), 6.82 (tt, J = 8.9, 2.3 Hz, 1H), 3.19 (s, 1H).

1-((4-ethynylphenyl)ethynyl)-3,5-dimethoxybenzene

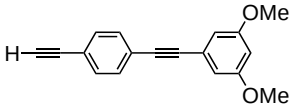

2.8Y (1 g, 2.39 mmol) was deprotected according to the general deprotection procedure C. Chromatography on silica gel (hexane) yielded the target compound (615 mg, 98 % yield) as a white solid. ^{1}H-NMR (400 MHz, chloroform-*d*) δ 7.47 (s, 4H), 6.68 (d, J = 2.3 Hz, 2H), 6.47 (t, J = 2.3 Hz, 1H), 3.81 (s, 6H), 3.17 (s, 1H).

S-(4-((4-((3,5-difluorophenyl)ethynyl)phenyl)ethynyl)phenyl) ethanethioate (2.9XA)

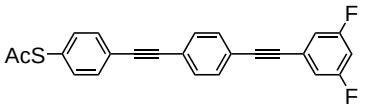

1-((4-ethynylphenyl)ethynyl)-3,5-difluorobenzene (88 mg, 0.37 mmol) was reacted with 4-acetylthio-1-iodobenzene (114 mg, 0.41 mmol) according to the general coupling procedure A. Chromatography on silica gel (hexane/chloroform 1:1, R_f = 0.68) followed by recrystallization from hexane yielded **2.9XA** (80 mg, 56 % yield) as an off white solid. ^{1}H-NMR (400 MHz, chloroform-*d*) δ 7.56 (d, J = 8.3 Hz, 2H), 7.52 (s, 4H), 7.41 (d, J = 8.3 Hz, 2H), 7.08 – 7.01 (m, 2H), 6.82 (tt, J = 8.9, 2.3 Hz, 1H), 2.44 (s, 3H).

S-(4-((4-((3,5-difluorophenyl)ethynyl)phenyl)ethynyl)benzyl) ethanethioate (2.9XB)

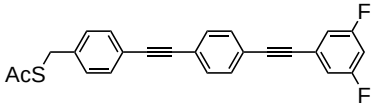

1-((4-ethynylphenyl)ethynyl)-3,5-difluorobenzene (300 mg, 1.26 mmol) was reacted with 1-(S-acetylthiomethyl)-4-iodobenzene (400 mg, 1.4 mmol) according to the general coupling procedure A. Chromatography on silica gel (hexane/ethyl acetate 10:1, R_f = 0.64) followed by recrystallization

from hexane yielded **2.9XB** (201 mg, 40 % yield) as a white solid. ^{1}H-NMR (400 MHz, chloroform-*d*) δ 7.50 (s, 4H), 7.46 (d, J = 8.2 Hz, 2H), 7.28 (d, J = 8.2 Hz, 2H), 7.08 – 7.01 (m, 2H), 6.81 (tt, J = 8.8, 2.3 Hz, 1H), 4.12 (s, 2H), 2.36 (s, 3H).

S-(4-((4-((3,5-dimethoxyphenyl)ethynyl)phenyl)ethynyl)phenyl)ethanethioate(2.9YA)

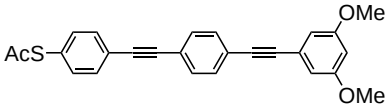

1-((4-ethynylphenyl)ethynyl)-3,5-dimethoxybenzene (470 mg, 1.8 mmol) was reacted with 4-acetylthio-1-iodobenzene (560 mg, 2 mmol) according to the general coupling procedure A over 2 days. Chromatography on silica gel (hexane/ethyl acetate 4:1, R_f = 0.44) followed by recrystallization from hexane yielded **2.9YA** (460 mg, 62 % yield) as a white solid. ^{1}H-NMR (400 MHz, chloroform-*d*) δ 7.55 (d, J = 8.3 Hz, 2H), 7.51 (s, 4H), 7.40 (d, J = 8.2 Hz, 2H), 6.69 (d, J = 2.3 Hz, 2H), 6.48 (t, J = 2.3 Hz, 1H), 3.81 (s, 6H), 2.44 (s, 3H).

S-(4-((4-((3,5-dimethoxyphenyl)ethynyl)phenyl)ethynyl)benzyl)ethanethioate(2.9YB)

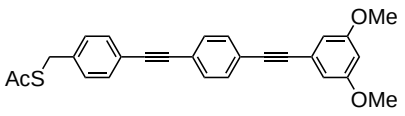

1-((4-ethynylphenyl)ethynyl)-3,5-dimethoxybenzene (470 mg, 1.8 mmol) was reacted with 1-(S-acetylthiomethyl)-4-iodobenzene (584 mg, 2 mmol) according to the general coupling procedure A over 2 days. Chromatography on silica gel (hexane/ethyl acetate 4:1, R_f = 0.43) followed by recrystallization from hexane yielded **2.9YB** (436 mg, 57 % yield) as a white solid. ^{1}H-NMR (400 MHz, chloroform-*d*) δ 7.50 (s, 4H), 7.46 (d, J = 8.1 Hz, 2H), 7.28 (d, J = 8.3 Hz, 2H), 6.69 (d, J = 2.3 Hz, 2H), 6.47 (t, J = 2.3 Hz, 1H), 4.12 (s, 2H), 3.81 (s, 6H), 2.36 (s, 3H).

BIBLIOGRAPHY

[1] Mickael L. Perrin, Riccardo Frisenda, Max Koole, Johannes S. Seldenthuis, GilJose A. Celis, Hennie Valkenier, Jan C. Hummelen, Nicolas Renaud, Ferdinand C. Grozema, Joseph M. Thijssen, Diana Dulić, and van der ZantHerre S. J. Large negative differential conductance in single-molecule break junctions. *Nat. Nanotechnol.*, 9(10): 830–834, 2014.

[2] Davide Fracasso, Hennie Valkenier, Jan Cornelis Hummelen, Gemma Clare Solomon, and Ryan Chiechi. Evidence for quantum interference in SAMs of arylethynylene thiolates in tunneling junctions with eutectic Ga-In (EGaIn) top-contacts. *J. Am. Chem. Soc.*, 133(24):9556–9563, 2011.

[3] Hyo Jae Yoon, Nathan D. Shapiro, Kyeng Min Park, Martin M. Thuo, Siowling Soh, and George M. Whitesides. The rate of charge tunneling through self-assembled monolayers is insensitive to many functional group substitutions. *Angew. Chem. Int. Ed.*, 51(19):4658–4661, 2012.

[4] Hyo Jae Yoon, Carleen M. Bowers, Mostafa Baghbanzadeh, and George M. Whitesides. The rate of charge tunneling is insensitive to polar terminal groups in

self-assembled monolayers in $Ag^{TS}S(CH_2)_nM(CH_2)_mT//Ga_2O_3$/EGaIn junctions. *J. Am. Chem. Soc.*, 136(1):16–19, jan 2014.

[5] Marco Carlotti, Maarten Degen, Yanxi Zhang, and Ryan C. Chiechi. Pronounced environmental effects on injection currents in EGaIn tunneling junctions comprising self-assembled monolayers. *J. Phys. Chem. C*, 120(36):20437–20445, 2016.

[6] Ryan C. Chiechi, Emily A. Weiss, Michael D. Dickey, and George M. Whitesides. Eutectic Gallium–Indium (EGaIn): a moldable liquid metal for electrical characterization of self-assembled monolayers. *Angew. Chem. Intl. Ed.*, 47(1):142–144, 2008.

[7] Andrii Kovalchuk, Tarek Abu-Husein, Davide Fracasso, David A. Egger, Egbert Zojer, Michael Zharnikov, Andreas Terfort, and Ryan C. Chiechi. Transition voltages respond to synthetic reorientation of embedded dipoles in self-assembled monolayers. *Chem. Sci.*, 7(1):781–787, 2016.

[8] Davide Fracasso, Mutlu Iskender Muglali, Michael Rohwerder, Andreas Terfort, and Ryan C. Chiechi. Influence of an atom in EGaIn/Ga_2O_3 tunneling junctions comprising self-assembled monolayers. *J. Phys. Chem. C*, 117(21):11367–11376, 2013.

[9] Li Yuan, Nisachol Nerngchamnong, Liang Cao, Hicham Hamoudi, Enrique del Barco, Max Roemer, Ravi K. Sriramula, Damien Thompson, and Christian A. Nijhuis. Controlling the direction of rectification in a molecular diode. *Nat. Commun.*, 6:6324, 2015.

[10] Chuancheng Jia and Xuefeng Guo. Molecule-electrode interfaces in molecular electronic devices. *Chem. Soc. Rev.*, 42:5642–5660, 2013.

[11] Veerabhadrarao Kaliginedi, Alexander V. Rudnev, Pavel Moreno-Garcia, Masoud Baghernejad, Cancan Huang, Wenjing Hong, and Thomas Wandlowski. Promising anchoring groups for single-molecule conductance measurements. *Phys. Chem. Chem. Phys.*, 16:23529–23539, 2014.

SUMMARY

This thesis is aimed to expand the understanding of the properties of large-area molecular junctions comprising SAMs with EGaIn as the top electrode. In the **Chapter 2** and **3** we study the effects of embedded dipoles on the charge transport. We designed three molecules based on a *p*-terphenyl structure in which the central aromatic ring is either phenyl or a dipole-inducing pyrimidyl in one of two different orientations. All three molecules form well-defined SAMs with similar thickness, packing density and tilt angle, with dipole moments embedded in the SAM, isolated from either interface. This series perfectly isolates the effects of dipole moments from other variables that are known to influence charge transport, *e.g.*, length of the molecules, position of the frontier orbitals, etc. We address these SAMs with EGaIn electrode, which allows us to obtain big sets of data and analyze the statistical significance of the effects. An immediate consequence of the collective effect of SAMs of polar pyrimidyl groups is the modification of the electrostatic potential profile, which shifts the vacuum level and the energy separation between E_F and frontier molecular orbitals. Our experimental approach is to vary an internal, molecular property—in this case dipole moments—and measure the effect in a SAM supported by a bottom electrode before the top contact is installed—work function shift. After we perform EGaIn measurements, we extract transition voltages (V_T) from I/V curves. V_T is known to be related to the energetic separation of the frontier orbitals from the Fermi level ($E-E_F$). Consequently, we find a good correlation between V_T and $E-E_F$. This result demonstrates that V_T can be manipulated synthetically in a predictable manner and changes to V_T can be ascribed to an intrinsic property of the molecules inside the tunneling junction. It also provides a handle to manipulate the energy level alignment inside the junction without altering any other characteristic of the SAM. A more detailed analysis of the I/V curves of the pyrimidyl-containing members of the series reveals statistically significant asymmetry. The cause of this asymmetry is likely the result of the electrostatic profile of the SAMs arising from the collective effects of aligned dipoles affecting the de/localization of the frontier states. This mechanism is distinct from the other known mechanisms and is solely attributable to the supramolecular structure of the SAM.

Utilization of SAMs in large-area molecular junctions gives the opportunity to chemically address the top interface and test its effects on the charge transport. In **Chapter 4** we describe reversible in-place switching of molecular tunneling junctions comprising SAMs of terminal aliphatic carboxylic acids between rectifying and non-rectifying states. In its pristine state these SAMs are non-rectifying and exhibit symmetrical J/V characteristic. The switching is achieved via partial protonation of the interface containing acid groups. A weak acid, such as H_2O, is sufficient to protonate the interface and induce rectifying behavior. Consequently, the SAM is treated with a water scavenger which restores the initial state of the SAM and reverses the effect. The switching process can be coupled to the external stimulus, such as light, if a photo-acid is used. We perform the

switching with a photo-acid in dry solvent, which points to the protonation as a necessary condition to induce the effect. We support these findings with XPS spectra, which demonstrate that the switching process is driven by protonation. The ability to switch the function of a tunneling junction reversibly between resistor and diode creates the possibility of fabricating molecular-electronic devices that exhibit unique functions.

In the last **Chapter 5** we perform a systematic study of the effects of different substituents on the charge transport. We take OPE3 as a parent structure and functionalize it with −F and −OMe groups in varying patterns with two types of anchoring groups. This approach allows us to change the energy positions of the frontier orbitals, dipole moments of SAMs and the strength of the coupling to the bottom electrode while keeping other properties of the SAMs comparable (packing density, tilt angle, thickness, etc.). We found that neither the position of the frontier orbitals, nor the direction of the dipole moment has a measurable effect on the current-voltage characteristic. Yet, a single methylene unit is enough to change the strength of the coupling to the bottom electrode, which we observe as asymmetry in the J/V output. This finding provides a valuable synthetic tool for tuning the properties of the large-area molecular junctions.

NEDERLANDSE SAMENVATTING

Dit proefschrift richt zich op het uitbreiden van het begrip van de eigenschappen van moleculaire aansluitingen met een groot oppervlak, welke SAMs bevatten en met EGaIn als top elektrode. In **Hoofdstukken 2** en **3** bestuderen wij het effect van ingebedde dipolen op de ladingstransport. We hebben drie moleculen ontworpen, gebaseerd op een *p*-terphenyl structuur, waarin de centrale aromatische ring dan wel een phenyl is, dan wel een dipoolinducerende pyrimidyl in een van twee verschillende oriëntaties. Alle drie de moleculen vormen goed gedefiniëerde SAMs met gelijke diktes, pakkingsdichtheid en hellingsgraad, met dipoolmomenten ingebed in de SAM, geïsoleerd van beide grensvlakken met de elektrodes. Deze serie moleculen isoleert perfect het effect van dipoolmomenten van andere variabelen, waarvan bekend is dat zij ladingstransport beïnvloeden, zoals bijvoorbeeld de lengte van moleculen, de positie van de grensorbitalen, enz. We maken contact met deze SAMs met een EGaIn elektrode, welke ons in staat stelt om grote sets van data te verkrijgen en de statistische significantie van de effecten te analyseren. Een direct gevolg van het collectieve effect van SAMs van polaire pyrimidyl groepen is de aanpassing van het elektrostatische potentiaal profiel, waarin het vacuüm niveau en het energieverschil tussen E_F en de grensorbitalen verschuiven. Onze experimentele benadering is om een interne moleculaire eigenschap—in dit geval dipoolmomenten—te variëren en het effect te meten in een SAM gevormd op een bodemelektrode voordat de topelektrode geïnstalleerd wordt. Na EGaIn meting uitgevoerd te hebben, leiden we transitievoltages (V_T) af van I/V curves. Van V_T is het bekend dat het in verband staat met de energetische scheiding tussen de grensorbitalen en het Ferminiveau ($E - E_F$). Als gevolg vinden we een goede correlatie tussen V_T en $E - E_F$. Dit resultaat laat zien dat V_T synthetisch gemanipuleerd kan worden in een voorspelbare manier en dat veranderingen in V_T toegedicht kunnen worden aan intrinsieke eigenschappen van moleculen in de tunneling aansluiting. Het biedt ook een handvat om de energieniveau uitlijning in de aansluiting te beïnvloeden zonder andere karakteristieke eigenschappen van de SAM aan te passen. Een gedetailleerdere analyse van de I/V curves van de pyrimidyl bevattende leden van de serie laat een statistisch significante asymmetrie zien. Deze asymmetrie is waarschijnlijk het resultaat van het elektrostatische profiel van de SAMs, voortkomend uit het collectieve effect van uitgelijnde dipolen welke de (de)lokalisatie van grensorbitalen beïnvloedt. Dit mechanisme is verschillend van andere bekende mechanismes en is enkel toe te schrijven aan de supramoleculaire structuur van de SAM.

Het gebruik van SAMs in moleculaire aansluitingen met grote oppervlakken geeft de mogelijkheid om het top grensvlak chemisch aan te spreken en zijn effect op ladingstransport te testen. In **Hoofdstuk 4** beschrijven we omkeerbare schakeling van moleculaire tunneling aansluitingen, bestaande uit SAMs van eindstandig alifatisch carbonzuur, tussen een rectificerende en niet-rectificerende staat. In hun ongerepte staat zijn deze SAMs niet-rectificerend en laten ze symmetrische J/V karakteristieken zien. Het schakelen wordt bereikt via gedeeltelijke protonering van het grensvlak dat de zuur-

groepen bevat. Een zwak zuur, zoals water, is genoeg om het grensvlak te protoneren en rectificerend gedrag te induceren. Vervolgens wordt de SAM behandeld met een water scavenger, welke de SAM terugbrengt naar zijn orspronkelijke staat en het effect terugdraait. Het schakelproces kan worden gekoppeld aan een externe stimulus, zoals licht, als een fotozuur wordt gebruikt. We voeren deze schakeling uit met een fotozuur in droog oplosmiddel, wat er op wijst dat protonering een noodzakelijke voorwaarde is om het effect teweeg te brengen. Wij ondersteunen deze vindingen met XPS-spectra, welken laten zien dat het schakelproces gedreven wordt door protonering. The mogelijkheid om de functie van een tunneling aansluiting reversibel te kunnen schakelen tussen een weerstand en een diode creëert de mogelijkheid tot het fabriceren van moleculaire elektronica met unieke functies.

In het laatste hoofdstuk, **Hoofdstuk 5**, voeren we een systematisch onderzoek uit naar het effect van verschillende substituanten op ladingstransport. We nemen OPE3 als kernstructuur en functionaliseren het met −F en −OMe groepen in verscheidene patronen met twee verschillende ankergroepen. Deze benadering stelt ons in staat om de energetische positie van de grensorbitalen, dipoolmomenten van de SAMs en de sterkte van de koppeling met de onderste elektrode te veranderen, terwijl de andere eigenschappen van de SAMs vergelijkbaar blijven (pakkingsdichtheid, hellingsgraad, dikte, enz.). We vonden dat noch de positie van de grensorbitalen, noch de richting van het dipoolmoment een meetbaar effect heeft op de stroom-voltage karakteristiek. Daarentegen, een enkele methyleen groep is voldoende om de sterkte van de koppeling met de onderste elektrode te veranderen, wat we waarnemen als asymmetrie in de J/V functie. Deze vondsten bieden een kostbaar synthetisch middel voor het bijstellen van eigenschappen van groot-oppervlakkige moleculaire aansluiting.

ACKNOWLEDGEMENTS

A successful completion of a PhD project requires a lot of perseverance, knowledge and some luck. However, most of all, this thesis wouldn't exist, if not for a number of great people who accompanied my journey. I am tremendously happy to have met and worked with all of you!

First and foremost, I would like to thank immensely my supervisor Prof. Dr. Ryan C. Chiechi. Your guidance, motivation and friendly, open attitude put me in the position to work and enjoy working every day. Our numerous discussions on topics ranging from philosophy and science to life experience helped me to grow not only professionally but, more importantly, personally. All my friends who did not have the privilege to meet Ryan in person can't believe the amazing stories I tell them about my boss. Endless source of motivation—check; tremendous knowledge and experience and willingness to share it freely—check; little pressure, lots of freedom, patience and trust—check; openness and honesty about any topic—check. Is there anything else you can ask for in your supervisor?

I would like to thank Prof. Dr. Kess Hummelen for his support and assistance during the four years of my PhD. Your useful discussions during the group meetings were always helpful and gave me new perspectives on many things.

A big thank you to the members of the reading committee Prof. Dr. M. Stöhr, Prof. Dr. S. Faraji and Prof. Dr. F. Grozema for the time and effort to strengthen this dissertation.

I would like to express my sincere gratitude to Dr. Thomas P. Voortman who introduced me to the synthetic lab and helped me to get up to speed with organic synthesis. Your friendliness and willingness to help made me feel at home and encouraged me to learn and deepen my knowledge and skills of synthesis.

I would like to thank all the members of the "RCC-self-assemble + Thijs" group. We helped each other all the way and created a truly remarkable atmosphere in the group. Our lunch breaks filled with various discussions, sometimes humorous, sometimes serious, gave me a much needed reboot in the middle of the working day. As much as science is abstract and strict, it is the people who bring it to life. And our research group was an excellent place to work and flourish.

Renate, thank you for taking care of all the office related issues and making the lives of all the PhD students much easier. Reinder and Rick, you are the "magicians" of engineering and building stuff from scratch, thank you for all the help around the lab.

Finally, I'm grateful for the support of my family. A special thanks to Xinkai Qiu for designing the cover of this thesis.

CURRICULUM VITÆ

Andrii Viktorovich Kovalchuk was born in Dniprodzerzhinsk, Ukraine on January 3, 1990. After graduating in 2007 from the Gymnasium 11, he continued to study Chemistry at National Taras Shevchenko University of Kyiv. He defended his qualifying thesis on the topic of "3-[5-amino-4-hetaryl-3-azolyl]-1-propanol based heterocyclizations" at the faculty of Chemistry of Natural Compounds and received his Bachelor's degree diploma with honors in 2011. Kovalchuk then went on to study High Technologies at the Institute of High Technologies, Kyiv. He carried out his research project in computational physics, studying frustrated spin-1 atomic systems in optical lattices. In 2013 he received his Master's degree in High Technologies. In 2014 Kovalchuk moved to The Netherlands to perform research in the University of Groningen as a PhD student in the group of prof. R.C. Chiechi. His field of interest was Molecular Electronics.